Comparison of Switching Behaviours Between Vacuum and SF_6 Technologies at 145kV Network

Von der Fakultät für Maschinenbau, Elektrotechnik und Wirtschaftsingenieurwesen der Brandenburgischen Technischen Universität Cottbus zur Erlangung des akademischen Grades eines Doktors der Ingenieurwissenschaften genehmigte Dissertation

vorgelegt von

Master of Science

Ruoyu XU

geboren am 15. März 1985 in Chongqing, VR China

Vorsitzender:	Prof. Dr.-Ing. Harald Fien
Gutachter:	Prof. Dr.-Ing. Dr. h. c. Heinz-Helmut Schramm
Gutachter:	Prof. Dr.-Ing Harald Schwarz

Tag der Mündlichen Prüfung: 1st October 2015

Abstract

This PhD project started from one basic question: whether vacuum technology can be applied to $145kV$ electrical power system networks as a potential substitution to SF_6 technology which has been utilised for decades of practice, due to environment and economic concerns. Possible threats and challenges, which might cause problems for the proposed replacement, are identified mainly in three areas: (1) small inductive current switching, (2) capacitive load current switching and (3) short-line fault switching. Three circuit-breaker programming models, therefore, have been developed based on statistic data provided by breaker manufactures: (1) a maximum $^{di}/_{dt}$ fixed model which has been utilised for small inductive current switching tests and capacitive load current de-energising tests; (2) a dynamic $^{di}/_{dt}$ model adopting from Mayr's classic arc model for SF_6 circuit-breakers which has been utilised for short-line fault tests; and (3) a current making model for capacitive load current energising tests. In a general conclusion, vacuum technology shows its superiority in most of the switching duties although in some rare cases, SF_6 technology still stands a chance to break it even. But if we take the environment and economic factors into consideration, vacuum is definitely worth investigating in the future market.

Key words: vacuum, SF_6, ATP, simulation, dielectric breakdown, thermal breakdown, high-frequency current quenching, TRV, inductive current, capacitive current, SLF

Abstrakt

Diese Doktorarbeit basiert auf einer grundlegenden Frage: Ob die Vakuum-Schalttechnik als potentieller Ersatz für die in Energieverteilungsnetzenbis $145kV$ in jahrzehntelanger Praxis verwendete SF_6-Technoligie geeignet ist, da gegen letztere Bedenken bezüglich der Umweltverträglichkeit bestehen. Die potenziellen Probleme für das vorgeschlagene Ersetzen sind vor allem in drei Bereichen identifiziert: (1) Schalten kleiner induktiver Ströme, (2) Schalten kapazitiver Lasten, und (3) Kurzschlüsse auf Freileitungen. Daher wurden drei Programmiermodelle für Leistungsschalter, basierend auf statistischen Angaben von Leistungsschalter-Herstellern, entwickelt: (1) ein auf maximales $^{di}/_{dt}$ festgelegtes Modell, das für das Schalten kleiner induktiver Ströme und das Abschalten kapazitiver Ströme verwendet worden ist; (2) ein dynamisches $^{di}/_{dt}$-Modell, das vom klassischen Lichtbogenmodell nach Mayr übernommen worden ist; (3) ein Strommodell für das Einschalten kapazitiver Lasten. Daraus resultiert eine allgemeine Schlussfolgerung, dass die Vakuum-Schalttechnik in den meisten Schaltaufgaben überlegen ist. Jedoch hat auch die SF_6-Schalttechnologie unter einigen seltenen Umstnden eine Chance überlegen zu sein. Aber, wenn wir Umweltprobleme und wirtschaftliche Faktoren berücksichtigen, lohnt es sich auf jeden Fall, die Vakuum-Schalttechnik im Hinblick auf den zukünftigen Markt weiter zu untersuchen.

Schlüsselwörter: vacuum, SF_6, ATP, simulation, dielectric breakdown, thermal breakdown, high-frequency current quenching, TRV, inductive current, capacitive current, SLF

Acknowledgements

I would like to express my sincere gratitude to:

- Professor Dr.-Ing. Dr. h.c. Heinz-Helmut Schramm for his precious guidance, patient explanations and valuable suggestions in the past four years. His profound knowledge, rigorous scholarship and diligent enthusiasm inspired me from conquering one challenge to another.

- Mr Frank Richter and other experts from Siemens AG for their guidance, supports and data information.

- Professor Harald Schwarz for participating in my dissertation committee.

- Last but not least, special thanks to my beloved parents for their deepest love.

Contents

List of Tables

List of Figures

Chapter 1

Introduction

1.1 Overview

Circuit Breakers can be classified in terms of interruption media. In modern electrical power systems, vacuum and SF_6 technologies are predominant in the Medium Voltage (MV) and High Voltage (HV) networks respectively. Although SF_6 demonstrates outstanding performances in all range of its switching duties, yet some merits held by vacuum, such as smaller size and lower maintenance costs, have not been covered. Besides, because of the rising concerns over environmental issues, it is intended to apply the vacuum technology into higher ratings (i.e. $145kV$) to replace SF_6 breakers in the near future. Since we have already had decades of experiences on the SF_6 breakers working on the HV levels, it is a good approaching to illustrate the difference between these two technologies before further steps. On the other hand, there exist a number of differences between MV and HV networks from the aspects of network topology, earthing arrangements and load types, etc. The aim of this project is comparing SF_6 and vacuum circuit-breakers in terms of switching performances under various operation scenarios. Hence, prove the feasibility of adopting vacuum technology in $145kV$ networks.

1.2 Motivation

To figure out the suitability of adopting vacuum circuit breakers in sub-transmission grids, two generic networks from Scottish Power and E-On Central Network, have been selected as a reality instance. In Great Britain, voltage levels higher than $145kV$ are classified as transmission Network, running by National Grid. Voltage level at 145kV is considered as sub-transmission network, $72.5kV$ and $36kV$ are primary distribution networks. Lower than $36kV$ are secondary distribution networks. $72.5kV$ is considerably rare which can only be found in the west part of the Central Network of E-On. Although the vast majority of customers are connected at $12kV$ and below, there are a few major customers connected directly to the primary networks.

Based on the information provided by the Scottish Power, its distribution system consists of approximately 25 circuit kilometres of $145kV$, $36kV$ and lower voltage networks (i.e. $12kV$, $7.2kV$) overhead lines and underground cables as detailed in Table 1.1. On the other hand, Central Network West operated by E-On holds another profile. A comparison between these two distribution networks has been presented as following.

Table 1.1: Overhead Line vs. Cables in real Networks

Voltage Lv(kV)	Line length (km)				Percentage of OHL	
	Overhead line		Underground Cable			
	SP	E-On	SP	E-On	SP	E-On
145	1,316	1,328	233	328	85.0%	80.1%
72.5	NA	760	NA	27	NA	96.5%
36	1,977	1,021	1,702	365	53.7%	73.7%
≤ 36	12,639	14,972	7,166	12,400	63.8%	51.7%

The above table indicates that the total length of both types of line increases following the downstream of the voltage level. The percentage of the overhead line goes down meanwhile. At the level of our interests, i.e. $145kV$, overhead lines are absolutely predominant. With a large number of overhead lines involved, concerns

regarding to fault current switching duties, especially short-line fault switching duties rise.

Generally speaking, power consumers are not directly connected to $145kV$ networks. The switching duties can be classified into four categories, namely normal load switching, fault switching, small inductive current switching and capacitive current switching. Basically, no major concerns are related to normal load switching duty. In terms of fault switching, three-phase terminal fault has the highest overvoltage magnitude. The severity depends on earthing arrangement. Unearthed systems demonstrate higher overvoltage. Under certain circumstances, say $145kV$ overhead line connected sub-transmission networks, special attention should be addressed on short-line fault which is not a problem in medium voltage cable connected networks.

For small inductive current switching duty, reactor switching is more severe than unloaded transformers due to its lower surge impedance. Multiple re-ignitions with high-frequency oscillation can potentially cause damaging to the system devices. However, they are designed to be connected to the tertiary winding of the transformers and are unlikely to be deployed in $145kV$ terminals. As a result, for small inductive current switching, efforts should be made on reactor switching.

Capacitor and capacitor banks are not likely to be deployed in $145kV$ systems. However, if circuit-breakers are subjected to capacitive current switching tasks overvoltage due to re-strike and high magnitude inrush current due to pre-strike could be very severe.

In a short conclusion, the motivation of this project is that vacuum technology so far has never been rated in $145kV$ voltage level. Its merits and drawbacks are basically unknown to manufactures. Before actual development of this product, it is motivated to identify any threats and challenges which may encounter in practice.

1.3 Project Objectives

To achieve the aim of this project, it is designed to spite the main objective into the following sub-objectives:

1. Development computer simulation models for SF_6 and vacuum circuit-breakers which have the capability to simulate energising and de-energising processes for various testing purposes.

2. Implementing the simulation models into inductive load test circuits. Carrying out a set of comparisons of switching performance between SF_6 and vacuum circuit-breakers in terms of overvoltage magnitude and heat energy production

3. Implementing the simulation models into capacitive load test circuits. Carrying out a set of comparisons in terms of overvoltage and heat energy production when considering energising and de-energising operations.

4. Implementing the simulation models into short-line fault test circuits. Carrying out a set of comparisons between different parameter setups for SF_6 circuit-breaker when subjecting to thermal stress. Carrying out another set of comparisons between SF_6 and vacuum circuit-breakers when subjecting to dielectric breakdowns.

1.4 Thesis Organisation

In Chapter 2, general technique backgrounds regarding to SF_6 and vacuum technologies will be introduced from the perspectives of physical process during arc interrupting and mechanic mechanism. Important physical phenomena with great influence on the outcome of the tests are also included in this chapter.

In Chapter 3, programming environment and strategies for different circuit-breaker types (SF_6 and vacuum) and for different operating purposes (opening and closing) will be explained in detail with the help of flowcharts.

In the next three chapters, they have similar structures. Simulation tests will be designed into several test groups based on a IEC standard study. Each one of the test groups is for achieving a specific objective. Then test results and data analysis will follow. As for Chapter 4, discussion will be focusing on small inductive current switching and the sub-objective two will be achieved. Chapter 5 is for capacitive current switching and sub-objective three. Chapter 6 is for short-line fault switching and sub-objective four.

In the final chapter, conclusions will be made to sum up the achievements which have been made in this PhD thesis at first. Limits and other factors that have not been included in the thesis will also be mentioned in this chapter. Finally, words will be given to the future work.

Chapter 2

General Background

2.1 Chapter Introduction

The most time-economic effective approach to compare the switching behaviours between SF_6 and vacuum technologies is to put them into computer simulation. It involves several steps, such as parameters identification, physical process analysis, programming and so on. In this chapter, as a part of the simulation pre-work, electrical discharges in SF_6 and vacuum quenching media will be studied in detail to help have a deep understanding of what happens in the switching process from the physical perspective.

A general description of electric arc will be introduced first. Followed by that, properties of SF_6 and vacuum arcs will be discussed separately from the point view of their arc characteristics, dynamic arc equation and quenching mechanisms. Phenomena observed in the switching process such as current chopping, transient recovery voltage, thermal breakdown, dielectric breakdown, and, hence, the high-frequency re-ignition current burning between the contacts gap shall be examined. Then, a comparison regarding to the arc interrupting capability between these two technologies will be carried out qualitatively. Finally, a summary will be given to conclude this chapter.

2.2 SF_6 and Vacuum Arcs

2.2.1 General Concept of Arcs

Basically, the term "electrical discharge" can be divided into two board categories: "The non-self-sustaining discharge" and "The self-sustaining discharge". The electric arc is a self-sustained discharge that exhibits a low voltage drop, that is capable of sustaining large currents and that it behaves like a non-linear resistor.[1]

Arcs used in circuit-breakers can be divided into high pressure arcs, with pressure between one and some hundreds of atmospheres, and low pressure (vacuum) arcs, with ambient pressure below $10^{-4} torr$.[2] Introduced by F. Paschen in 1889, Paschen's Law states that, "at higher pressure (above a few *torr*) the breakdown characteristics of a gap are a function of the product of the gas pressure and the gap length, usually written as $V = f(pd)$, where p is the pressure and d is the gap distance; as the pressure is reduced below $1 torr$ the curve of breakdown voltage versus pressure reaches a minimum, and then, as pressure is further reduced, rises steeply again." Figure 2.1 is a typical Paschen Curve.

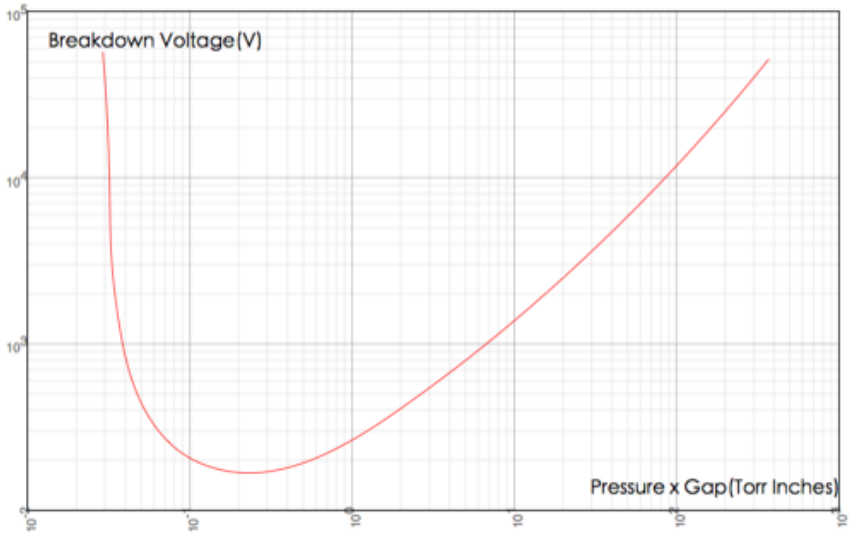

Figure 2.1: Typical Paschen curve

2.2.2 High Pressure Arcs

Arcs which exist at or above one atmospheric pressure are classified as "high pressure arc". It has a bright column characterised by a small highly, brightly burning core consisting of ionised gases that convey the electric current.[1] Without external cooling, the core temperature is normally around $6,000K$. If external cooling applies, temperature as high as $20,000K$ or even higher can be observed. The higher temperature is the result of a reduction in the arc diameter that produces an increase in the current density of the plasma and consequently leads to the observed temperature increase.

The magnetic phenomenon in arcs is one of the factors drawing concerns. Basically, there are two types of magnetic field existing in the arcing process: circumferential field and transverse field. On the one hand, axial current flow produces the circumferential field. A pressure on the ionised plasma acting radially inwards is observed as a result of the interacting between this axial current flow and the field. The pressure is given, approximately, by $P = JI \times 10^{-8}$ atmospheres, where J is the current density. If the cross-section of an arc changes along the length of the arc, J changes and therefore the pressure at the axis changes, and an axial pressure gradient changes. On the other hand, the transverse field comes from two sources: the current flowing in the arc itself and in its associated metallic circuit, and thus an initially straight arc will almost always bow under the influence of its self-magnetic field.[2] Generally speaking, neither of the magnetic phenomena plays an important role in blast-type circuit-breakers. Therefore, in the computer simulation programme, no particular consideration will be put regarding to the magnetic factor.

Electrode material also plays an important role in determination of the current density of the arc. Experiment results show that materials with high boiling point produce a relatively fixed cathode spot. Mainly caused by thermionic emission, the current density near the cathode spot is in the order of 10^3 Amps per cm^2. Materials with low boiling point, on the other hand, lead to highly mobile cathode spots. The

current density is much higher at this circumstance: 10^6 to 10^7 Amps per cm^2. In spite of this difference affects the behaviour of the arc, in the actual programming no particular material will be specified. The current density factor will be treated identically as a constant value.

What happens in the arcing process is actually the establishing and breaking of the thermal equilibrium. When the arc is burning at the steady-state, the thermal equilibrium is established and maintained because the power losses from the arc column are balanced by the power input from the driving source. However, due to the energy storage capacity of the arc, there is a time lag between the instantaneous power loss and the steady-state losses and therefore at any given instant the power input to the arc, plus the power stored in the arc is equal to the power loss from the arc.[1] This time lag is very important to the arc interruption and it will be discussed further in the following chapters. At the near current zero region, the input energy is reducing and approaching to zero, which, at some point, makes the power loss greater than the input. The thermal equilibrium cannot be kept further and hence it leads to an arc extinguishing.

2.2.3 SF_6 Arc Quenching Mechanism

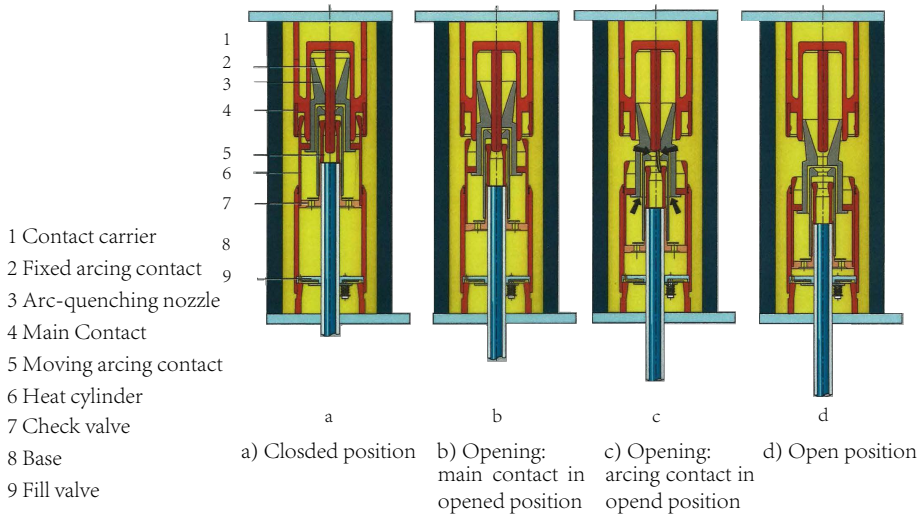

Figure 2.2: Schematic Diagram of the Self-Compression Principle

To be more specific to our topic, arcs in the SF_6 quenching media, a typical high pressure arc, is about to be discussed in this section. From the arc quenching mechanism point of view, self-compression principle designed switching unit, which uses the thermal energy of the arc, is predominate in the high voltage circuit-breaker market.

The current conducting path of the interrupter unit consists of the contact carrier(1), the base (8) and the heat cylinder (6). In the closed position, the current flows via the main contact (4) and the heat cylinder. (See position a)

During the opening operation, the main contact opens first, and the current commutates to the still closed arcing contact. (See position b) During the further course of opening, the moving arcing contact (5) opens up and an arc is drawn between the contacts. (See position c) With large short-circuit current, the quenching gas surrounding the moving contact in the arcing chamber is heated by the arc's energy and driven into the heat cylinder at high pressure. When the current passes through zero, the gas flows back from the heat cylinder into the nozzle and quenches the arc. When this happens, the check valve (7) in the heat cylinder prevents the high pressure from entering the compression chamber between check valve and the fill valve (9). In the dynamic variation, the moving contact is moved against the direction of movement of the tube contact by the connected components of heat cylinder, nozzle (3), connecting rod, pin, control lever.[3]

The moved pin is also pushed in the opposite direction of the heat cylinder. Thus, the speed of creating the contact gap is increased. During the continued course of the opening operation, the arcing contact opens, creating an arc. At the same time, the heat cylinder moves to the downwards and compresses the quenching gas between check valve and the fill valve.

Therefore, interrupt small currents the arc energy is not sufficiently high. The contact cylinder moves into the base and compresses the SF_6 gas located there. This gas compression creates a gas flow through the contact cylinder and the nozzle

to the arcing contact, extinguishing the arc.

2.2.4 Mayr's Arc Model

To make the physic process programmable, a mathematic model, which precisely describes the dynamic arc state, especially, at its extinction phase is required. During the recent almost 100 years, numerous studies have been put into this topic. Cassie (1939) is the first one who developed the arc model based on energy-balance perspective. It assumes that the current arc is governed mainly by convection losses. Experiments proved that this model works perfectly at high current conditions. The original Cassie's equation is given below:

$$\begin{aligned} R\frac{d(1/R)}{dt} &= \frac{1}{\theta}\left[\left(\frac{v}{v_0}\right)^2 - 1\right] \\ \theta &= \frac{Q}{N} \end{aligned} \tag{2.1}$$

where R is the arc resistance, v_0 is the voltage at steady-state, v is the arc voltage at any time instant, θ is the arc time constant which is governed by Q (the energy storage) and N (the finite rate of energy losses).

Later in 1943, Mayr proposed an improved model.[4] He considered an arc column where the arc diameter is constant and where the arc temperature varies as a function of time, and of the radial dimension. He further assumed that the decay of the temperature of the arc was due to thermal conduction and that the electrical conductivity of the arc was dependent on temperature.[1] The Mayr's equation is given by:

$$\frac{1}{R}\frac{dR}{dt} = \frac{1}{\theta}\left(1 - \frac{V \cdot i}{N_0}\right) \tag{2.2}$$

where N_0 is a constant which represents the power loss in his assumption; V and i are the momentary arc voltage and current respectively.

Mayr's equation is particularly useful for describing the arc resistance characteristic

in the near current zero region. Based on Mayr's equation, a programmable mathematic expression has been developed in this PhD work:

$$R = \frac{prevval(R)}{1 - \frac{\Delta t}{\theta}\left(1 - \frac{V \cdot i}{N_0}\right)} \tag{2.3}$$

where $prevval(R)$ is the arc resistance value obtained in the previous time step of simulation, Δt is the width of each time step, and R is the present resistance value. More details of how this adopted equation works in the simulation will be explained in the next chapter.

2.2.5 Low Pressure Arcs

In terms of "low pressure arcs", it actually means "vacuum arcs" in which the ambient pressure is way lower than one atmosphere. Technically speaking, the name "vacuum arc' is incorrect. "Vacuum" and "arc" cannot exist at the same place at the same time. According to A. Greenwood[5], a more exact name would be " metal vapour arc", since the arc which forms when current-carrying contacts separate in a vacuum "burns" in the metal vapour of the contacts. Although an ideal vacuum enclosure does not exist either, a tiny amount of gas arcs are mixed with metal vapour and the name vacuum arc is now so pervasive and so uniformly accepted that it will be preserved in the following chapters as meaning a metal vapour arc.

The low pressure arc shares most of the common characteristics as described in high pressure arcs. However, there are three major differences:

(a) Average voltage drop across a vacuum arc is only a few volts, which is much lower than the arc voltage observed in a high pressure arc.

(b) The composition of the positive column of these two arcs are different: in high pressure arcs, the positive column is made up of ionised gas from the arc's surrounding ambient while in the vacuum arcs it is composed of metal vapours

that have been boiled off from the electrodes, which makes the electrode material the major influencing factor.

(c) The last, but most important difference is arcs in vacuum can transfer its form from diffuse mode to constricted mode. The mode depends on the magnetic field and that in turn depends on the current level and to a significant extent on the size and shape of the contacts.[5]

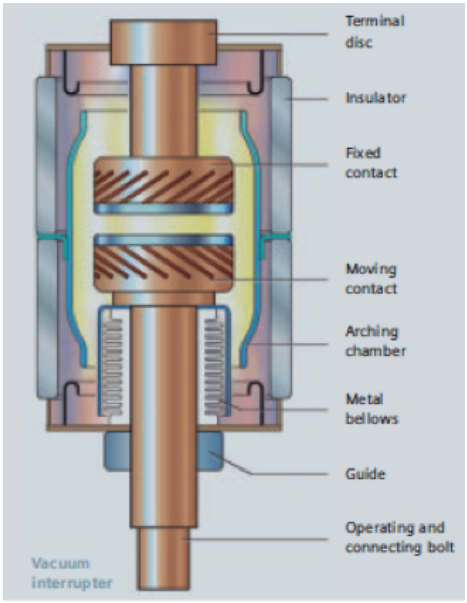

Figure 2.3: Cross-section of a typical Vacuum Circuit-Breaker

At low current levels, the diffuse mode applies. Single or multiple cathode spot(s) appear(s), each with the diameter around about $20\mu s$, on the cathode surface. They are in constant motion with variable lifespan. New ones have been created to replace the old ones. These spots heat up locally that evaporate the electrode metal as well as electrons through the acceleration zone to the ionisation zone. The ionisation zone is such a space where positive ions, electrons and neutral atoms interact and collide together. New particles are generated inside of this zone and plasma, which contains electrons and ions, flows out in both directions in different velocities: electrons move much faster. The velocity of the main stream of the plasma is very high, in the order of $10^4 m/s \sim 10^5 m/s$. Electrons move towards the anode violently with high velocity, which produces a large amount of heat. They are absorbed and

condensed on the anode and the wall of the chamber when they hit them. Each cathode spot (on copper) carries $\leq 100A$ of current and the overall current level determines the total number of spots. As the power frequency current approaches current zero, the number of spots reduces as well until the last one. At the moment of current chopping occurs, which will be discussed later, the last cathode spot vanishes. The metal evaporation and condensation take the arc energy away, which makes the cathode spot cool down rapidly after extinguishing. No further particles are emitted afterwards in most of the circumstances. Therefore, the vacuum arc has two important characteristics from the perspective of capability of arc extinguishing: 1) it can interrupt current with very high $^{di}/_{dt}$ at current zero point; and 2) the dielectric strength in the contacts gap can be built up quickly after current zero.

If the arc current flows at a higher level, on the other hand, the diffuse mode will possibly change to another form: the constricted mode. The plasma, instead of bathing the anode in the manner just described, becomes focused on a small area of that electrode.[5] Besides the current level, contact size and material also determine at which pace the transition from diffuse mode to constricted mode takes place. In practice, a constricted vacuum arc produces exceeding heat that consequently would cause damage to the electrode surface and should be avoided at all cost. As a result, in this PhD work, all simulation results and discussions are based on the assumption that the arc is burning at a diffuse mode.

A mathematic expression for the vacuum arc, like the Mayr's equation for gas arcs, is unavailable. From the programming perspective, the vacuum model will be developed according to its statistic behaviour in different load conditions.

2.2.6 Magnetic Field in Vacuum Technology

To keep the arc burning at diffuse mode, magnetic field is applied to the modern designed vacuum circuit-breakers. This technology enables the current interrupting

capacity of a vacuum breaker to stand at a higher level. Basically, there are two types of contacts design that produces radial magnetic field and axial magnetic field.

- **In radial magnetic field contact**

In Figure 2.4, the arc burns diffusely until approximately $10kA$ (momentary value). Higher currents burn across a constricted arc. In this case, local overheating of the contacts must be avoided. Contacts are shaped to build an additional magnetic field to produce a force (Figure 2.4) which makes the arc rotate on the arcing rings of the contacts. Thus, contact erosion at the base point of the arc is distributed over the entire ring surface.

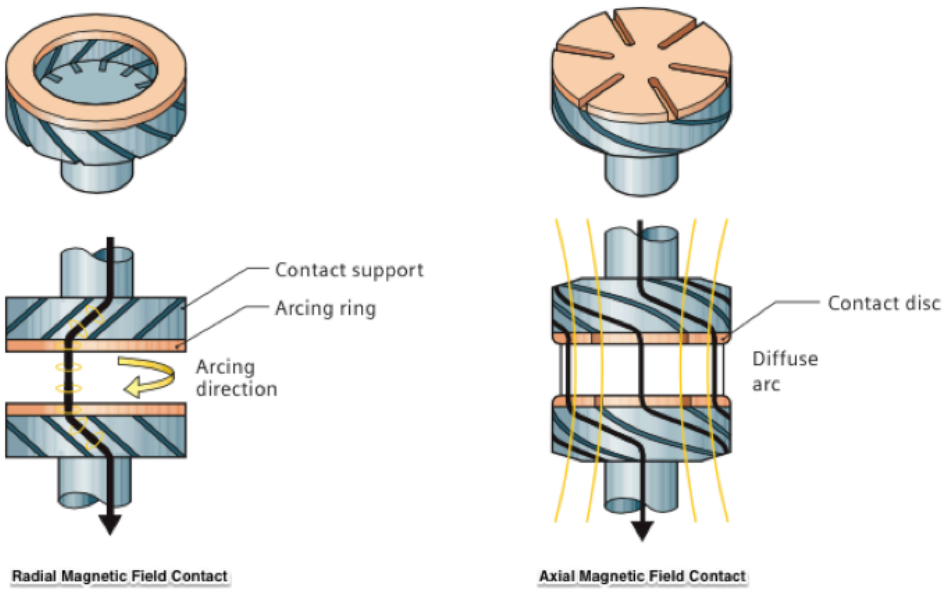

Figure 2.4: Radial and Axial magnetic Field Contacts

- **In axial magnetic field contact**

The arc remains diffuse even with high currents due to the axial magnetic field. The disc-type contact surfaces are uniformly stressed, and local melting is reduced.

The performances of these two types contacts design do not show a significant difference from the point of view of current quenching capability in practice. As a result, no distinguishing will be given to this factor in the simulation work.

2.3 AC Current Interruption and its Phenomena

Generally speaking, current interrupting is mainly caused by either one of three different processes: forced arc extinguishing, current chopping and current zero extinguishing.

- **Forced arc extinguishing**

Under this circumstance, the arc voltage becomes so high that the source voltage cannot sustain. Thus, the current decays to zero quickly and leads to extinguishing as a result. This approach is more applied on fuse and low voltage systems and is less relative to this PhD topic.

- **Current chopping**

This phenomenon is observed in small current interrupting, mainly caused by arc instability.

- **Current zero extinguishing**

In most of high voltage circuit-breaker interrupting cases, the arc voltage is way lower than the source voltage, which means the power source is able to provide enough energy to sustain the burning of the arc. Then the arc extinguishing can be achieved by proper contact configurations.

Phenomena associated with the latter two arc extinguishing mechanisms should be examined with great concerns.

2.3.1 Current Chopping

Current chopping is a phenomenon that the power frequency current is prematurely interrupted before natural zero due to instability of the arc. At an earlier stage of this research topic, it was commonly believed that this phenomenon is much more pronounced in vacuum type circuit-breakers[6][7], but later has been proven incorrect. All types of breaker can chop, but in different ways. For vacuum

circuit-breakers the chopping is largely associated with instability of the last cathode spot, while for other circuit-breaker types, oil, air-blast and SF_6 , current chopping is generally the result of an unstable interaction between the circuit-breaker arc and the circuit.[7]

Current chopping is one of the major factors that causes overvoltages in an interrupting process. A typical inductive current switching equivalent circuit has been illustrated in Figure 2.5:

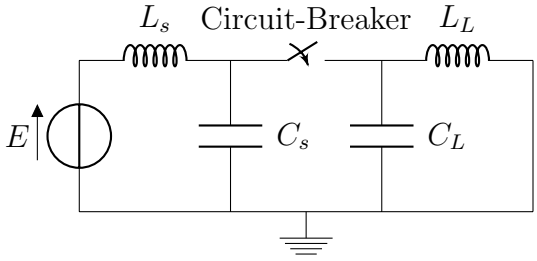

Figure 2.5: Typical Equivalent Circuit for small Inductive Current Switching

Referring to the energy balance equation at the moment of current chopping, we have:

$$\frac{1}{2}C_L E_m^2 = \frac{1}{2}C_L E_c^2 + \frac{1}{2}L_L I_{ch}^2 \tag{2.4}$$

The overvoltage factor K, therefore, can be defined as following:

$$K = \frac{E_m}{E_s} = \sqrt{\left(\frac{I_{ch}}{E_s}\right)^2 \left(\frac{L_L}{C_L}\right) + \frac{E_c}{E_s}} \tag{2.5}$$

where E_m is the overvoltage peak after chopping, E_s is the peak voltage at the source side, E_c is the voltage across the load capacitor at the instant of current chopping, I_{ch} is the chopping current.

From the above, it is clear that the chopping level is the key factor which determines the overvoltage factor.

- **Current Chopping in Circuit-Breakers other than Vacuum**

For all types of traditional circuit-breakers, the system capacitance plays a critical

role in determining the arc instability. Figure 2.6[1] shows the chopping level vs. load capacitance in different quenching media. It is clear that for all types of breakers except vacuum, the chopping level (chopping current) increases with larger capacitance. On the other hand, the chopping level in vacuum is almost a constant value.

An approximate mathematic expression based on test results concludes the relationship between the chopping level and load capacitance:

$$I_{ch} = \lambda\sqrt{C_L} \tag{2.6}$$

where λ is a coefficient meaning "chopping number", it varies in different types of circuit-breaker.

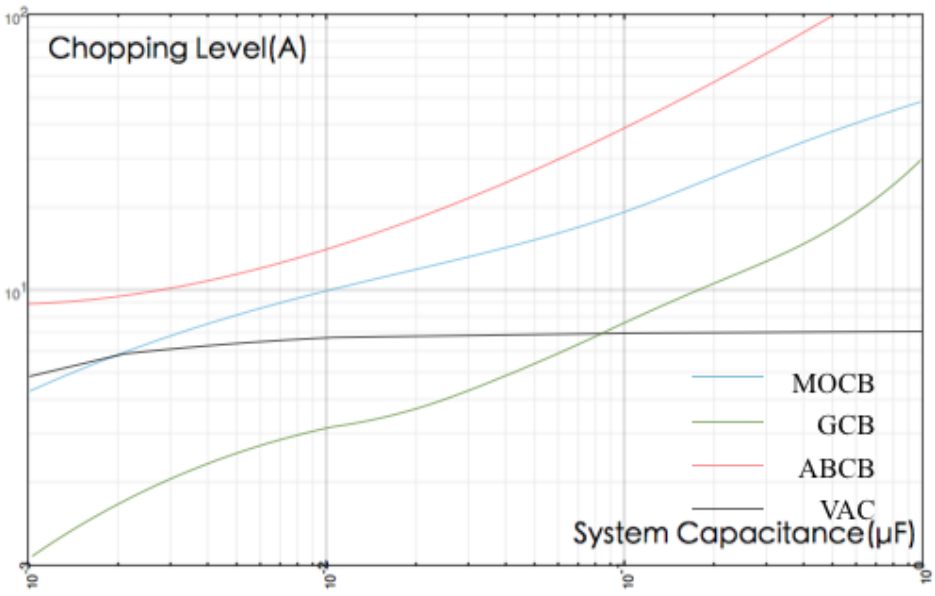

Figure 2.6: Current Chopping Level as Function of Capacitance[1]

Particularly for SF_6 puffer circuit-breakers, their λ value is ranged from 4 to 17×10^4; its system capacitance is assumed as $10nF$. Therefore, a typical current chopping level for an SF_6 breaker is 4 to $17A$ in old times of designing. Nowadays, this value has be restrained within $3A$.

[1]MOCB: Oil Circuit-Breaker; GCB: Gas Circuit-Breaker (SF_6); ABAC: Ari Blast Circuit-Breaker; VAC: Vacuum Circuit-Breaker

• **Current Chopping in Vacuum Circuit-Breakers**

Like what has been found in all traditional types of circuit-breakers, current chopping can also be observed in vacuum circuit-breakers when switching off small current. However the principle in vacuum is different. Contact material, which in turn, is the key factor that determines the chopping level. The characteristic impedance and the parallel branch capacitance of the breaker, however, have little influence.

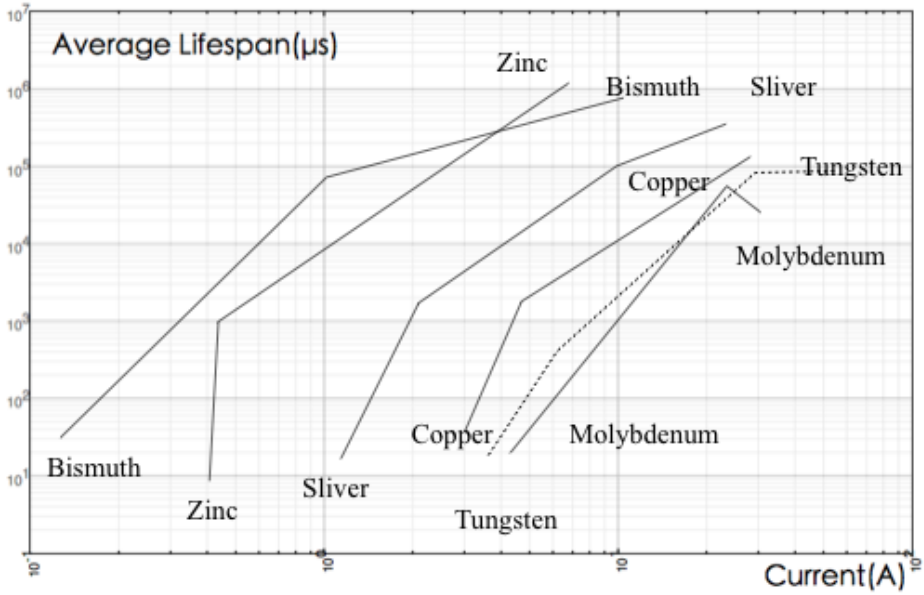

Figure 2.7: Arc Lifespan for different Contact Materials at different Current Levels[8]

As it has been discussed earlier, each cathode spot has a finite lifespan. Likewise, electric arc also has its lifespan. After sustained for a while, a DC vacuum arc with small current level extinguishes automatically because of instability. A massive amount of repeated test results shown that only N trails of arcs could survive after a time duration t, if N_0 is the initial number of trials of arcs at any given time instance, we have:

$$N = N_0 \cdot e^{-t/\tau} \tag{2.7}$$

where τ is the average lifespan of a vacuum arc. Figure 2.7 shows the relationship between arc current level and its lifespan for different contact materials. It is clear

that the arc lifespan increases with larger arc current level.

When the vacuum arcs are burning at the near current zero zone, their lifespan reduces along with the decaying current that approaches natural zero. At the instance $t_r = \frac{1}{2}T - t$, (where T is the power frequency cycle) the momentary current i reaches the critical value I_{ch} whose corresponding lifespan is exactly t_r. The arc instantaneously chops because of the instability and this critical current value is called chopping level. Figure 2.8 shows a schematic diagram of this process:

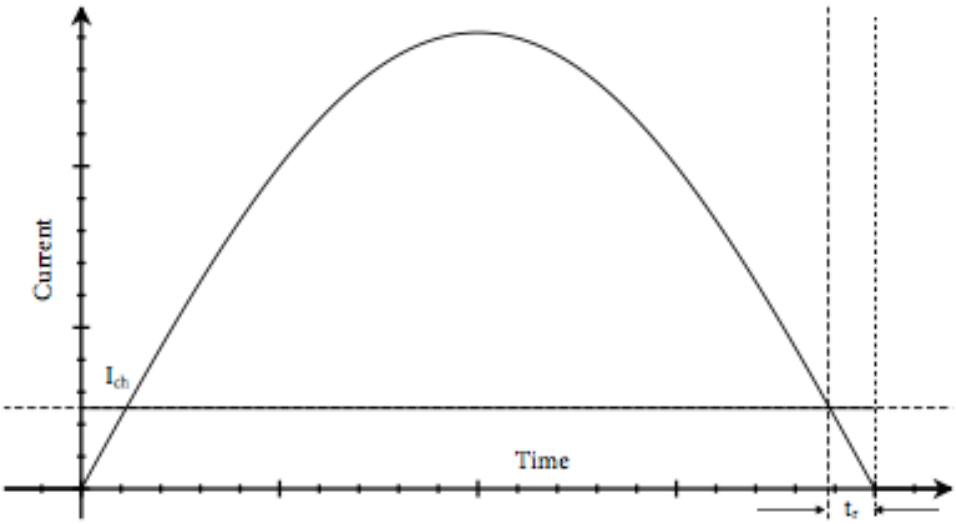

Figure 2.8: Schematic Representation of Instability at end of AC Half Cycle using the DC Lifespan Analog[9]

From the analysis above, it is clear that a shorter average arc lifespan leads to lower chopping level. There are three major factors that have great influence on the arc's average lifespan and the chopping level:

1) **The vapour pressure of the electrode material**

In most cases, materials with higher vapour pressure produce larger amount of vapour, which can help maintaining the stability of the arc and, hence, shorten the lifespan of the arc.

2) **The product of the boiling temperature and the thermal conductivity**

A higher product of T_b and τ usually leads to a higher chopping level. Table 2.1

shown below gives the relationship between the product and chopping level of some common metal materials. Electrode material made of alloys is more complicated: it

Table 2.1: Chopping Level of different Metal Materials

Material	Mo	W	Ag	Cu	Al	Sn
$\lambda \cdot T_b(cal \cdot cm^{-1} \cdot s)$	1,280	2,820	1,150	2,140	935	350
$I_{ch}(A)$	$5.7 \sim 6.7$	$12 \sim 21$	$7 \sim 7.5$	$16 \sim 18$	$12 \sim 13$	$1 \sim 2.3$

is not simply the average value of the blended two materials corresponding chopping level, but, in most cases, lower than each of the element playing solely. For example, alloy W80%-Cu20% has its chopping level ranged in $5A$ to $6A$, lower than Tungsten and Copper respectively; alloy Cu50%-Cr50% has it chopping level ranged in $4A$ to $5A$, also lower than Copper and Chrome's corresponding chopping level.

3) **The peak value of the load current**

By referring to Figure 2.8, it can be found that if the peak value of the load current is higher than a certain threshold, the average lifespan of the arc is longer than 10 ms, which means longer than half-cycle of the power frequency in $50Hz$ (also longer than in $60Hz$), No current chopping can be observed at such circumstance.

The most state of the art of the manufacturing technology now can provide high voltage circuit breakers with very low chopping for both SF_6 and vacuum. Detailed value specification will be assigned to each of them in the later chapters.

2.3.2 Thermal Breakdown and Post-Arc

Breakdown can possibly take place in two phases when performing a switch-off operation: thermal breakdown and dielectric breakdown. Thermal breakdown phase occurs immediately after current zero, mainly caused by the limitation of circuit-breaker's current quenching capability. The dielectric breakdown phase, on the other hand, happens later if the transient recovery voltage between the contacts

gap is higher than the dielectric strength. Both of them are critical factors which can significantly influence the performance of a circuit-breaker.

The mechanisms of thermal breakdown in SF_6 and vacuum are different. The following section will discuss them separately.

1) **Thermal breakdown in SF_6 and other traditional circuit-breakers**

Generally, when switching off a high current, the quenching medium between the contacts gap stays at a very high temperature: higher than the temperature at which the metal vapour continues to dissociate, after current zero. At this circumstance, the quenching medium still has conductivity. The current lags the conductivity with a time of θ which has been defined as arc time constant in the section of Mayr's equation. This constant is a quenching media dependent factor. Specifically for SF_6, the arc time constant is approximately in the range of $0.2\mu s \sim 0.5\mu s$.

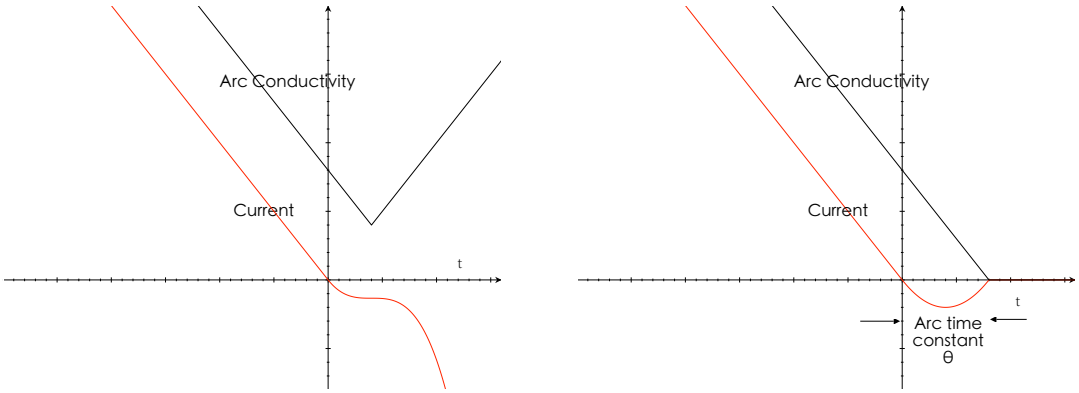

Figure 2.9: Post-arc with and without Thermal Breakdown

When recovery voltage applies across the gap, a small current, which is known as the post-arc current, follows through (right side, Figure 2.9). Meanwhile, there are two processes proceeding at the same time: on the one hand, the electrical source drives energy to the gap; on the other hand, the gap passes the energy to the ambient media. If the energy provided by the source is larger than that which has been passed over to the ambient media, the temperature of the gap will keep rising and finally leads to a thermal breakdown (left side, Figure 2.9). Contrarily, the temperature

will decrease and the conductivity of the contacts gap will be reduced to zero as a result.

If the gap is at a thermal equilibrium, we have:

$$u_{tr} = \sqrt{r_a N}, \tag{2.8}$$

where u_{tr} is the recovery voltage across the gap, N is the heat dissipation power and r_a is the arc resistance.

At this circumstance, it is believed that the gap has a certain level of dielectric strength, which is:

$$u_d = \sqrt{r_a N} \tag{2.9}$$

Apparently, at the thermal breakdown phase, if the dielectric strength of the gap u_d is stronger than the recovery voltage u_{tr}, the thermal re-ignition will not happen. As a result, at the thermal breakdown phase, the arc extinguishing condition is:

$$\sqrt{r_a N} > u_{tr} \tag{2.10}$$

Consequently, the principle to reduce the possibility of thermal breakdown of gas blast circuit-breakers is to reinforce the cooling of the breaker and ensure the heat dissipation is large enough.

2) **Thermal Breakdown in Vacuum Circuit-Breakers**

The mechanism of thermal breakdown in vacuum is quite different from any other traditional circuit-breakers as discussed above. Basically, the vacuum circuit-breaker does not blow gas to the contacts gaps for cooling. The vacuum arcs cool down by the means of condensation of the metal vapour on the contacts and the wall of the vacuum chamber.

By referring to Greenwood's theory[5], as the current commences to decline there are typically a number of cathode spots pouring plasma into the interelectrode gap.

As the current falls, these will extinguish one-by-one until only one remains. Most of the current is carried by electrons but some fraction is carried by ions. Before current zero, the electron stream travels faster than the ion stream. As the current in the last cathode spot continues its decline following the dictate of the external circuit, the electron stream decelerates and at the instant of current zero these two streams have the same speed. The polarity of the two involved electrodes swaps at this very moment, which means the original cathode transfers to the new anode and the original anode transfers to the new cathode. The gap remains bridged by low impedance plasma, so current continues to flow. Because ions have much larger inertia, they keep travelling towards to the former anode while the electrons continue decelerate and travel slower than the ions. The overall current then is negative. This is the post-arc current in the vacuum.

Shortly after current zero, the speed of the electrons stream decelerates to zero and the net current reverse by that point. It creates a region adjacent to the former anode which is depleted of electrons. It is at this instant when a positive ion sheath forms, that the TRV commences to build up and concentrate across the ion sheath.

Because the metal vapour condenses on the contacts and the wall of the vacuum chamber very quickly, its cooling efficiency is much higher than other technologies. As a result, the post-arc current in a vacuum circuit-breaker has a much shorter time duration and current amplitude. On the other hand, Mayr's equation is not applicable in a vacuum environment and there are no mathematical expressions which can accurately describe what happens in the post-arc process. Therefore, in the following simulation work, instead of building an arc model, the factor "current quenching capability" will be used to evaluate the performance of a vacuum circuit-breaker.

2.3.3 Dielectric Breakdown and TRV

When the temperature declines to $3,000K \sim 4,000K$, the process of thermal dissociation stops and the contacts gap transfers to dielectric strength. At this phase, if an re-ignition takes place, it is a dielectric breakdown.

If a circuit-breaker can interrupt a current at one of its current zero points, which means the post-arc current does not develop to another current cycle, a competition starts between the rebuilt of the dielectric strength and the development of the recovery voltage. From the point of view of the dielectric strength, it is generally proportional to the distance of the gap. For SF_6 , it needs a longer space to rebuild the same strength as it requires in a vacuum. The contacts separating velocity could be adjusted to any specific circuit-breaker design. But generally speaking, the rate of dielectric strength rising in a vacuum is faster than in an SF_6 breaker at the same voltage level.

From the point view of the recovery voltage, things are more complicated. It is mainly determined by the structure and parameters of the external circuit. Case-specific recovery voltage will be discussed in detail in the later chapters.

If the rebuilt of the dielectric strength wins the competition at any given time instant, it is a successful interrupting; otherwise, dielectric breakdown happens and it leads to one or multiple re-ignitions as a consequence.

2.3.4 Multi-Frequency Oscillations

Using an inductive load circuit as a typical example, the voltage across the inductive load starts to oscillate after current interruption. Figure 2.10 shows a simplified single-phase equivalent circuit diagram in which all network elements are regarded lumped and linear.

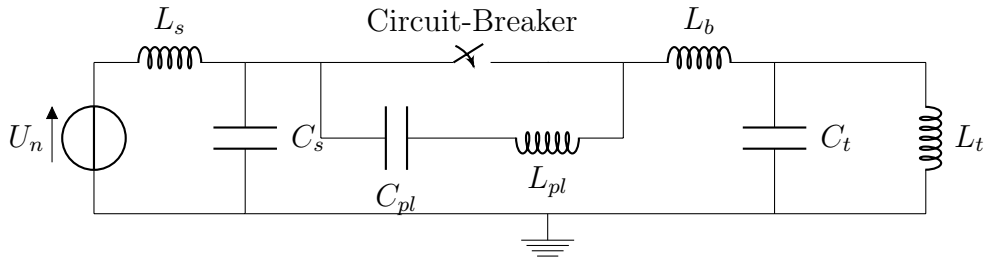

Figure 2.10: Simplified Single-Phase Equivalent Circuit Diagram

All resistance elements have been neglected at this stage to make things easier to understand. However, they are very important in practice as they provide damping in the real case. When no current flows through the circuit-breaker, i.e. after a current interruption with or without chopping, the source side and the load side oscillate practically independently with oscillation frequencies, respectively:

$$f_s = \frac{1}{2\pi\sqrt{L_s C_s}} \text{ and } f_t = \frac{1}{2\pi\sqrt{L_t C_t}} [7] \tag{2.11}$$

Because of the difference of these two frequencies, a voltage is stressed across the circuit-breaker contacts gap. There are three types of oscillation which could be involved if a dielectric breakdown happens.

1) **First parallel Oscillation**

The first parallel oscillation just involves the circuit-breaker and its parallel branch, namely C_{pl} and L_{pl} shown in Figure 2.10. As these are particularly small, the fist parallel oscillation has a very high-frequency:

$$f_{pl} = \frac{1}{2\pi\sqrt{L_{pl} C_{pl}}} \tag{2.12}$$

This frequency is normally ranged in a few MHz and the amplitude of the re-ignition current is higher than $100A$. Since no circuit-breaker, vacuum nor SF_6 , can interrupt such kind of current with its extremely high $^{di}/_{dt}$, it is often been disregarded.

2) **Second parallel Oscillation**

A potential difference between the source side and the load side causes the second parallel oscillation to equalise these voltages. The flux-linkages in the inductances L_s and L_t remain nearly constant and the oscillation frequency therefore is:

$$f_{p2} = \frac{1}{2\pi}\sqrt{\frac{C_t + C_s}{L_b C_s C_t}} \tag{2.13}$$

This frequency is ranged in the order of kHz and often can be interrupted by vacuum and SF_6 circuit-breakers, depending on the actual $^{di}/_{dt}$ passing through the current zero and the current interrupting capability of the case-specific circuit-breaker.

3) **Main Circuit Oscillation**

If the second parallel oscillation cannot be interrupted, the main circuit oscillation takes place. This oscillation involves all elements of the circuit. At this scenario, the voltage cross C_t and C_s are assumed equal. After interrupting the frequency of the main circuit oscillation is:

$$f_m = \frac{1}{2\pi}\sqrt{\frac{L_s + L_t}{L_s L_t (C_s + C_t)}} \tag{2.14}$$

Normally, if a re-ignition process develops to this stage, the current will not be able to cross the zero anymore and another power frequency current loop will be needed to attempt the second chance for interrupting.

2.4 Interrupting Capacity Comparison

There is a universal criterion for all types of interrupting devices as a figure of merit:

$$\xi = \left[\frac{dI}{dt}\right]_1 \times \left[\frac{dV}{dt}\right]_2 \tag{2.15}$$

$\left[\frac{dI}{dt}\right]_1$ is the maximum current slope at a current zero the circuit-breaker is able to interrupt without thermal re-ignition. $\left[\frac{dV}{dt}\right]_2$ is the rate of rise dielectric strength

that the contacts gap can rebuild. Higher value of the product value means better interrupting capacity the breaker has. From this point of view, the vacuum technology is way superior than any other traditional ones.

2.4.1 Maximum Current Slope at Current Zero

There are basically two approaches to determine the quenching capability. Proposed by M. Glinkowski[10], the mean value with a normal distribution can be expressed in a linear equation as following:

$$\overline{di/dt} = C_c(t - t_0) + D_D \tag{2.16}$$

The values of the constants used in the above equation are given in Table 2.2: While other authors suggest that the high-frequency current quenching capability

Table 2.2: High-frequency Current Quenching Capacity Constants

DW Type	$C_C(A \cdot \mu s^{-2})$	$D_D(A \cdot \mu s^{-1})$
High	-0.034	255
Medium	0.31	155
Low	1	190

characteristic $\overline{di/dt}$ is constant, varying between $100A/\mu s$ to $600A/\mu s$[11], it is assumed in a higher voltage rating the vacuum circuit-breaker has a higher current quenching capability. In my simulation, $1000A/\mu s$ and $150A/\mu s$ will be assigned to vacuum and SF_6 models respectively as a first assumption. These values can be changed from test to test to evaluate the performance in a variety of different cases.

2.4.2 Dielectric Recovery Curve

As it has been mentioned earlier in this chapter, the re-establishment of the dialectic strength of the contacts gap is proportional to the separating distance. That

means for a specific case, the dialectic strength is the product of the momentary gap distance and a certain coefficient. SF_6 and vacuum have different coefficients: vacuum has a much higher one because of it special recovery mechanism. However, the separating velocity is a very case dependent factor that makes the overall dielectric strength vs. time curve more complicated:

$$dielectric(t) = coefficient \times \int_{t=t_0}^{t=t} v(t)\, dt \tag{2.17}$$

where $v(t)$ is the momentary velocity of the separating contacts.

To simplify this issue the aforementioned coefficient will not be included in the following simulation work. Instead, the overall dielectric strength vs. time curve will be adopted based on real test results.

For vacuum circuit-breaker, table 2.3 listed below shows one of test results. Putting

Table 2.3: Test Result of Dielectric Strength vs. Time

Time after contact separation (ms)	Dielectric strength (kV)
0.1	47.91
1	135
2	200.2
3	254.9
4	303.7
5	348.6
6	390.5
7	430.2
8	468
9	504.3
10	539.4
20	680
30	725
40	740
50	750

the data acquired from the test result to ATP computer program, it converts the discrete dots to a following successive curve:

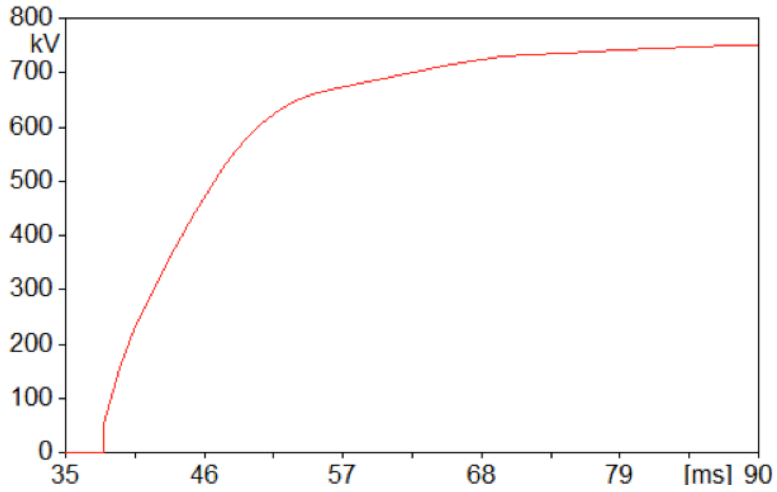

Figure 2.11: Typical Dielectric Strength Recovery Curve of a $145kV$ Vacuum Circuit-Breaker

It is clear that at the shortly after contacts separation, a small amount of dielectric strength has been re-established almost immediately. Then it increases steeply along with the time during the following $10ms$. The approximate average rate of rise, therefore, is starting with $50kV/ms$. After that, the rate of rising decreases and finally it approaches to $750kV$ slowly as a steady-state.

In terms of SF_6 breakers, similar tests have been made. The results show considerable varieties. To make the SF_6 and vacuum comparable, the curve obtained in the vacuum will be set-up as a reference and the curve for SF_6 varies from 50% to 80% according to the reference.

2.5 Chapter Summary

In this chapter, SF_6 and vacuum technologies have been compared in all aspects that are related in the further simulation work. The outcome of this chapter presents a general vision of the differences existing between vacuum and other traditional power interrupting devices. In conclusion,

1. vacuum circuit-breaker has a better post-arc control capability which enables it to interrupt current with much higher $^{di}/_{dt}$ at current zero;

2. vacuum circuit-breaker also has faster dielectric recovery rate after current interrupting;

3. new designed contacts material and structure relieve the current chopping presented in vacuum, which makes the difference between the vacuum and other types of device is relatively small.

Chapter 3

Methodology

3.1 Chapter Introduction

In this chapter, discussion will be focusing on the simulation software environment itself. A brief introduction of the ATP Draw programming interface will be presented at the beginning. Boundary conditions and other setups will be specified later. Detailed programming strategy, then, will be explained in three perspectives: current breaking and making model for vacuum circuit-breaker and current breaking model for SF_6 circuit-breaker. Following by that, a serial of general result will be illustrated to give a basic concept of the outcome of the simulation. At last, a brief summary will be given to conclude this chapter.

3.2 Brief to ATP Draw Simulation Environment

The programming tool which has been utilised in this PhD work is called Alternative Transients Program (ATP). It is a universal program system for digital simulation of transient phenomena of electromagnetic as well as electromechanical nature. With this digital program, complex network and control system of arbitrary structure can

be simulated. ATP has extensive modelling capabilities and additional important features besides the computation of transients.

3.2.1 Programming User Interface

ATP Draw, as a sub-branch of the original ATP program, uses graphical interface instead of pure coding environment which makes programming much easier. Users can simply drag and drop elements from tools bar to the canvas and wire them up via mouse linking. Parameters for each element do not need to be specified via coding. Instead, they can be directly entered to the data box. Figure 3.1 shown below illustrates a sample of the UI environment.

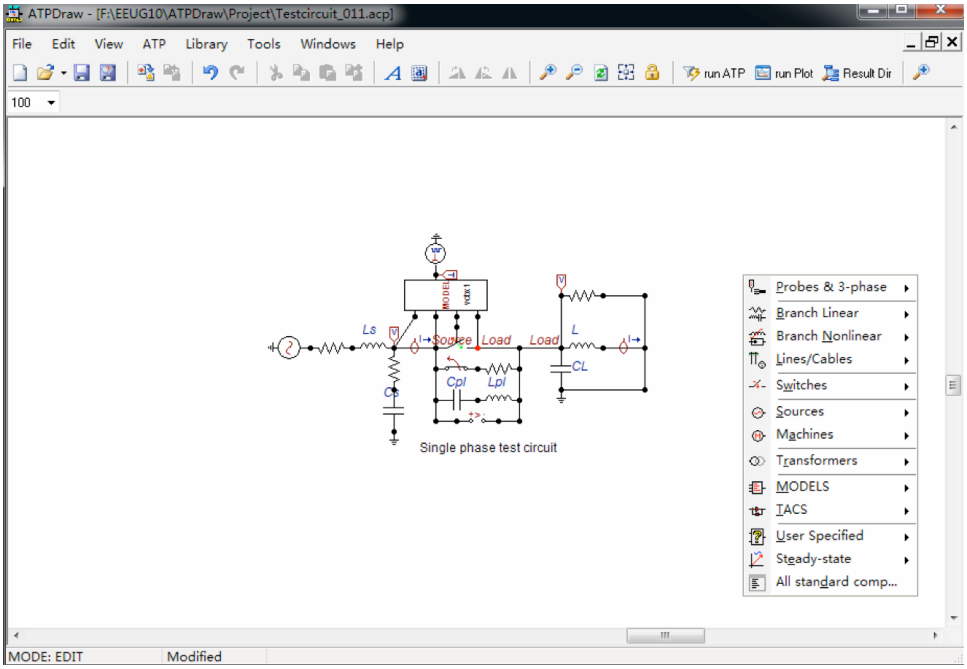

Figure 3.1: Example of ATPDraw UI

After all circuit elements stalled, click the “run ATP” button on top of the menu bar and the program will do the rest calculations. When it is done, clicking “run plot” can present the result of the simulation.

3.2.2 Basic Elements

ATP Draw provides large number of standardised electrical elements whose physical properties have been kept as in the real world. Specifications for those are relevantly simpler. Basic impedance elements like resistor, inductor and capacitor are classified as linear and non-linear categories. In this PhD work, only linear impedance elements have been used. Some other important circuit elements, which have been adopted in my simulations, need to be emphasised in the following paragraph:

1. **Voltage source**

ATP Draw provides two kinds of voltage source: three phase source and single phase source. A voltage source will be considered as an ideal power supply feeding from the power system. Users need to specify its amplitude, frequency, phase angle and earthing condition.

2. **TAC/Model controlled switch**

A TAC/Model controlled switch acts as an ideal circuit-breaker. It has three ports: two ports for connections with source side and load side of the circuit and the other one for receiving control signals. Users need to specify whether its initial status is closed or open.

3. **TAC/Model controlled resistor**

To simulate an arcing model for SF_6 type circuit-breaker in a short-line fault situation, an ideal circuit-breaker is not enough. Alternatively, a TAC/Model controlled resistor has been adopted, acting as the arcing resistance in reality. Its value is controlled by an external Model (which will be introduced later). Users need to specify its initial value.

4. **Impulse generator**

An impulse generator is adopted to generate triggering signal, like a man pushing a bottom in reality to switch the circuit-breaker on and off. It generates 0 and 1 signals periodically. Users need to specify the period and width for the pulse.

3.2.3 Model Elements

In order to enable the circuit performing more complex actions, ATP Draw also provides user-defined Models as a resolution. Users have full control of the behaviour of the Model they defined. Meanwhile it involves massive coding techniques. To define a Model, users first need to specify how many ports it has. Then, define the constants and variables. After that, and most importantly, the internal logic, which actually gives the order how this Model would behave, needs to be programmed. In Section 3.3, 3.4 and 3.5 detailed programming strategies will be explained.

3.3 Fixed di/dt Current Breaking Model

In the fixed $^{di}/_{dt}$ circuit-breaker model, it has three major factors which have significant influences on the performance. These factors are: current chopping level, dielectric recovery rate in the gap and high-frequency current quenching capability. The programming strategy is listed as following:

Phase 0 An ideal circuit-breaker will be used as a linkage to connect the source side and load side of the circuit. A Model is attached on the ideal circuit-breaker, acting as a control box, which gives order to open or close. At the initial status, the ideal breaker is kept closed.

Phase 1 The model waits for the triggering signal for the impulse generator from time to time. If no signal has been received at the present time-step of simulation, the Model does nothing but just moves to the next time-step.

Phase 2 In case at time instance t_0, the Model received a triggering signal it activates immediately. The dielectric strength starts to increase in each of the following time-step according to the data introduced in Section 2.4.2, Chapter 2, until it reaches its maximum value.

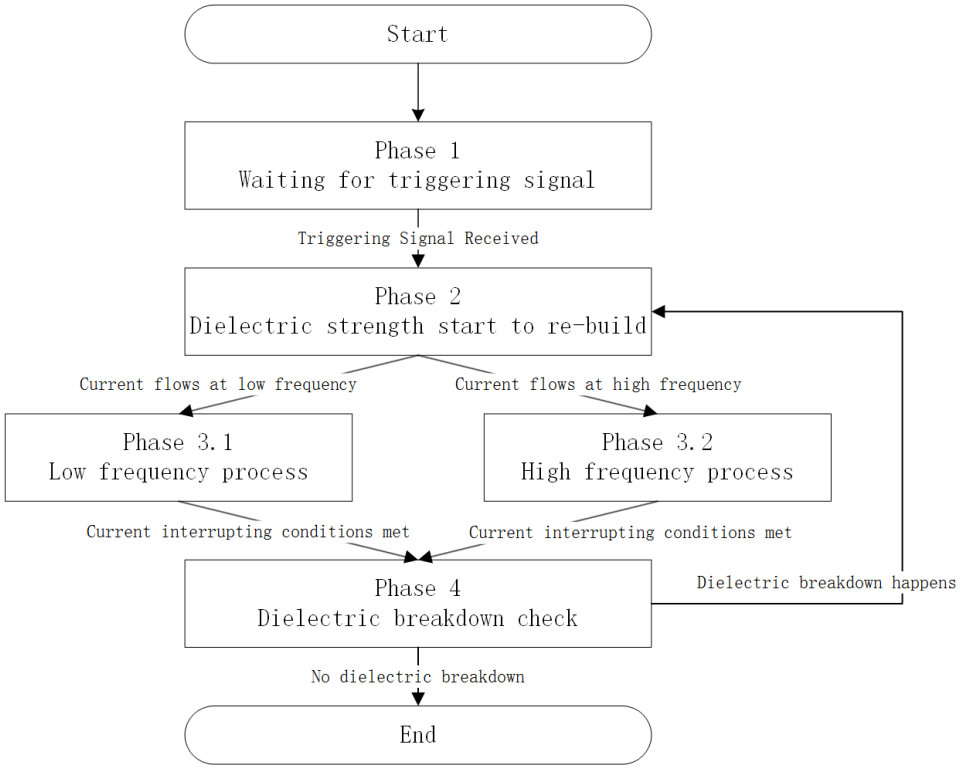

Figure 3.2: Simplified Schematic Flowchart for Fixed $^{di}/_{dt}$ Breakers

Phase 3.1 If the current passing through the ideal breaker is at lower frequencies (namely $50Hz$ or $60Hz$), the model reads the present current value until it reaches the chopping level. Then it gives the order "open" to the ideal breaker. The breaker opens immediately in the next time-step.

Phase 3.2 If the current passing through the ideal breaker is at a high-frequency, the behaviour of the Model changes: when two conditions have met, namely a) the product of the present current value and the previous current value is negative (which makes sure the present current is at a zero crossing point) and b)$\frac{\Delta i}{timestep}$is smaller than the given value Q (which means the present $^{di}/_{dt}$ is lower than the high-frequency quenching capability of the breaker), it gives the order "open" to the ideal breaker. The breaker opens immediately in the next time-step.

Phase 4 In any case (high-frequency or low-frequency), if the ideal breaker is at "open" status, the Model keeps comparing the voltage across the breaker and

the value obtained from Phase 2. If the dielectric strength is larger than the gap voltage all the time, it means a successful interruption. Otherwise, dielectric breakdown happens and the process backs to Phase 3.2 again.

Figure 3.2 presents a simplified flowchart for fixed $^{di}/_{dt}$ circuit-breaker model.

3.4 Dynamic di/dt Current Breaking Model

In the dynamic $^{di}/_{dt}$ circuit-breaker model programming, a much different strategy has been adopted in order to simulate the arcing process during contacts separating. Generally speaking, the statistic "high-frequency quenching capability" Q which has been adopted in the previous model will no longer be a constant but governed by Mayr's dynamic arc equation. The programming strategy is listed as following:

Phase 0 A Model-controlled resistor R_{arc} will be used in the new circuit to replace the ideal circuit-breaker. At the initial stage (before contact separating) its value is set to be $0.1\mu\Omega$. (acting as a pure conductor with no resistance)

Phase 1 The model waits for the triggering signal for the impulse generator from time to time. If no signal has been received at the present time-step of simulation, the Model does nothing but just moves to the next time-step.

Phase 2 In case at time instance t_0, the Model received a triggering signal, an internal counter t_1, with an initial value of 0, actives. It accumulates to itself each time-step afterwards until its value reaches $10ms$. This step is designed to simulate, in the reality, SF_6 breaker do take a short time of period to rebuild its dielectric strength. Any current zero happens during that period leads to an immediate breakdown. Meanwhile, starting from t_0, the arcing resistance R_{arc} shifts from $0.1\mu\Omega$ to $20m\Omega$.

Phase 3 The Model starts to monitor the current passing through the arcing resistor since the beginning of Phase 3. When two conditions have met, namely a) the absolute value of the current in the present time-step is lower than the absolute value in the last time-step and b) the absolute current value in this present time-step is lower than $100A$, the Mayr's equation takes over the control of the arcing resistor. The reason for this arrangement is Mayr's equation is only applicable in lower current values. As it has been explained in Section 2.2.4, Chapter 2, the Mayr's equation is transformed as the following format:

$$\begin{aligned} &\frac{1}{R}\frac{dR}{dt} = \frac{1}{R}\left(1 - \frac{V \cdot i}{N_0}\right) \\ \Rightarrow &\frac{1}{R}\frac{R - prevval(R)}{timestep} = \frac{1}{\theta}\left(1 - \frac{V \cdot i}{N_0}\right) \\ \Rightarrow &R = \frac{prevval(R)}{1 - \frac{timestep}{\theta}\left(1 - \frac{V \cdot i}{N_0}\right)} \end{aligned} \tag{3.1}$$

From the above equation, it is clear that the present arcing resistance value is based on the previous R value obtained from the last calculation. Meanwhile, the dielectric strength between the gap starts to build up.

Phase 4.1 If at any time-step afterwards, the product of the gap voltage V and the post-arc current i gets larger than the heat removal factor N_0, the factor $\frac{V \cdot i}{N_0}$ becomes larger than 1 which make the part $-\frac{timestep}{\theta}\left(1 - \frac{V \cdot i}{N_0}\right)$ positive and hence makes the denominator $1 - \frac{timestep}{\theta}\left(1 - \frac{V \cdot i}{N_0}\right)$ go larger than 1. As a result, the present arcing resistance would be smaller than the previous value in the last time-step. In the next time-step, the product of V and i becomes even larger because of the smaller R.

The process keeps going until R equals to $20m\Omega$. Then it returns to Phase 3 and start over again. (Thermal breakdown)

Phase 4.2 In case the thermal breaking down does not happen, which means the

arcing resistance is continually increasing, it leads to an extinguishing of the post-arc current. Mayr's equation cease when the absolute current value goes less than $100A$ and the arcing resistance holds the same value since then till the next event.

The Model compares the gap voltage to the dielectric strength from the beginning of Phase 4 (also applied in Phase 4.1). If at any time instance the gap voltage goes larger than the dielectric strength, dielectric breakdown happens. In that case, arcing resistance suddenly shifts from whatever value it holds previously to $20m\Omega$ and whole process enters the next phase. Otherwise, it means a successful interruption.

Phase 5 In case dielectric breakdown happens in Phase 4.2, high-frequency resignation(s) would be expected. Likewise what happened in Phase 3, when condition a) and b) have been met, Mayr's equation takes over the governing of the arcing resistance at each sequel near current zero zone.

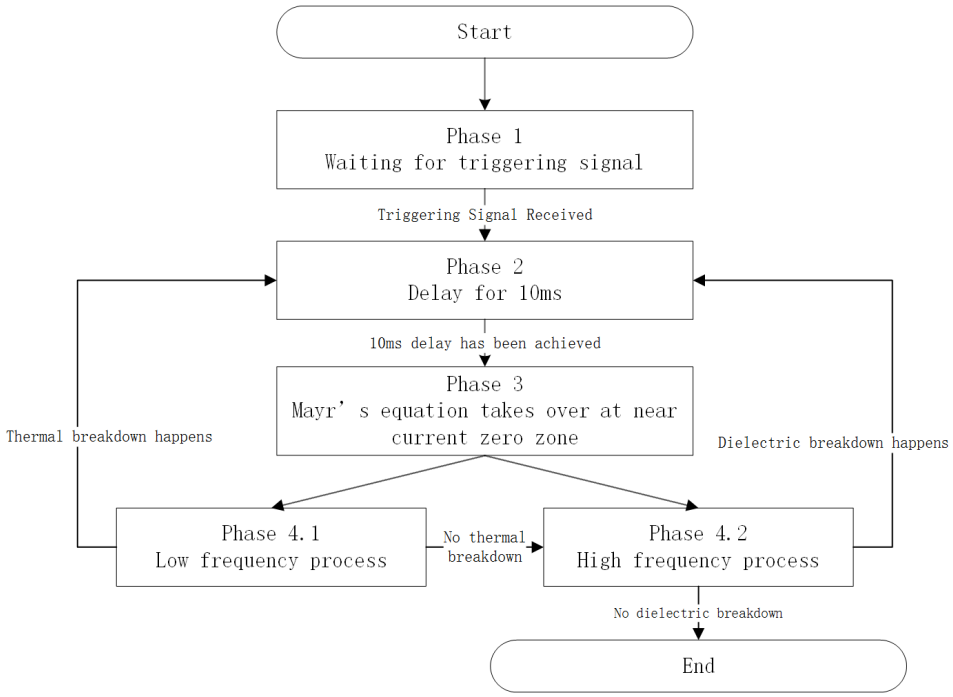

Figure 3.3: Simplified Schematic Flowchart for Dynamic $^{di}/_{dt}$ Breakers

3.5 Current Making Model

When considering capacitive load circuit switching, current making is of particular interests. It basically reverses the breaking process.

Phase 0 Use the ideal circuit-breaker, as introduced in current breaking model, to the current making circuit. The initial dielectric strength is set-up as the maximum value.

Phase 1 The model waits for the triggering signal for the impulse generator from time to time. If no signal has been received at the present time-step of simulation, the Model does nothing but just moves to the next time-step.

Phase 2 In case the triggering signal has been received at time instance t_0, the dielectric strength start to decrease step by step following its designed profile. Meanwhile, the ideal circuit-breaker stays at "open" state which blocks the current passing through as usual until next event.

Phase 3 The Model compares the voltage across the gap and the momentary dielectric strength in each time-step. If the dielectric strength is lower than the gap voltage in a particular time instance t_1, the ideal beaker instantaneously gets the order to switch to "close" position. As a result, dielectric breakdown happens and high-frequency current flows through. Depends on the instance of triggering signal received, the time duration between t_0 and t_1 could vary from 0 up to $10ms$.

Phase 4 The Model compares the current slope $^{di}/_{dt}$ measured at each current zero point with the fixed high-frequency current quenching capability Q. If any $^{di}/_{dt}$ is lower than Q, it gives the order "open" to the ideal breaker and the pre-strike process ceases immediately. In case the Q is not strong enough to interrupt the current at any current zero point, the arc keeps burning until Phase 6.

Phase 5 The Model compares the gap voltage to the dielectric strength curve after the ceasing of the pre-strike. If at any time instance, the gap voltage is higher than the voltage withstand strength a new pre-strike happens. Then the process repeats from Phase 4 again.

Phase 6 If the momentary dielectric decreases to zero, it represents a physical touch of the contact in reality. The ideal breaker then keeps at "close" position no matter what current is passing through or what voltage is crossing the gap. The whole process ends at this point.

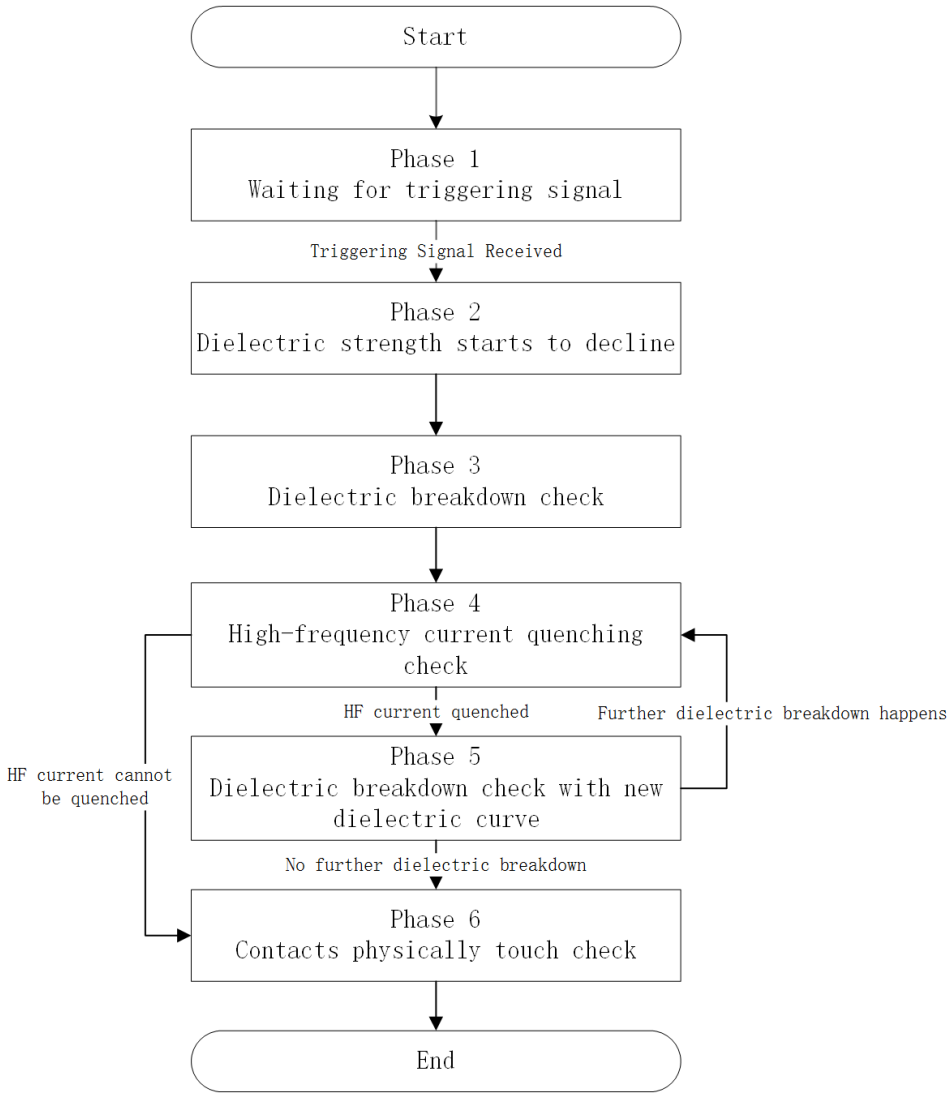

Figure 3.4: Simplified Schematic Flowchart for Current Making

3.6 General Simulation Results Illustration

In this section, a serial of simulation results will be demonstrated in a general circuit setup. In this occasion only, no actual circuit parameters related to real situation will be included. Instead, simulation results, by the means of current and voltage curves, will be presented to give a basic concept of the phenomena which have been mentioned in Chapter 2.

3.6.1 Current Chopping

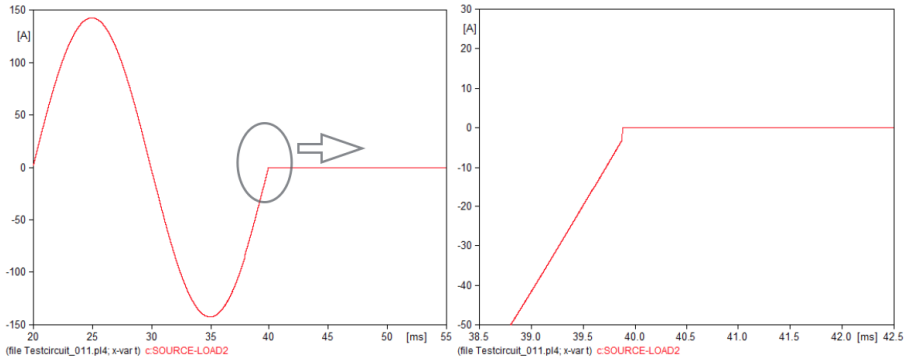

Figure 3.5: Current Chopping

In Figure 3.5, it shows a successful current interrupting (left hand side) with a clear current chopping (right hand side).

3.6.2 Dielectric Breakdown

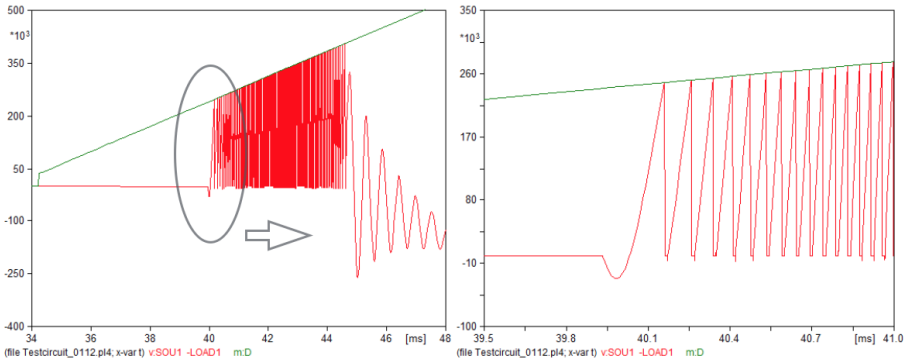

Figure 3.6: Dielectric Breakdown

The green curves in Figure 3.6 represent the dielectric strength during contacts separating while the red curves represent the actual voltage across the contacts gap. The simulation result shows that when the gap voltage reaches the momentary dielectric strength at any time instance, a dielectric breakdown happens.

3.6.3 High-Frequency Current Quenching

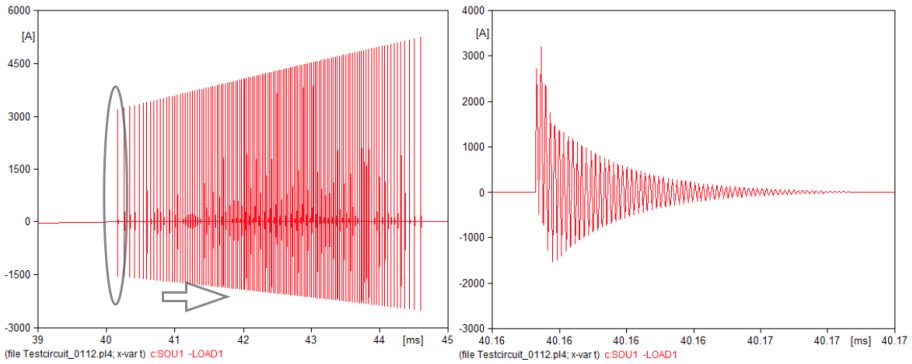

Figure 3.7: High-Frequency Current Quenching

When dielectric breakdown happens, high-frequency current re-ignition follows as a consequence. Figure 3.7 shows this switching phenomenon in detail. In this specific case, the high-frequency re-ignition current involves both first parallel and second parallel oscillations. The arc keeps burning while its slope at current zero crossing point is higher than the breaker's quenching capability.

3.6.4 Thermal Breakdown and Post-Arc

The upper trace of Figure 3.8 shows an unsuccessful current interrupting with thermal breakdown. At the circulated area, the circuit-breaker tries to interrupt the short-circuit current (green curve) at its natural current point. Unfortunately, its heat-removal factor is not large enough at this circumstance. Arc resistance (red curve) drops down and the post-arc finally develops to a new loop of power frequency current.

The lower trace of Figure 3.8, on the other hand, shows a successful interrupting. With large enough heat-removal factor, the arc resistance keeps increasing to an infinite level which suppresses the post-arc from further developing.

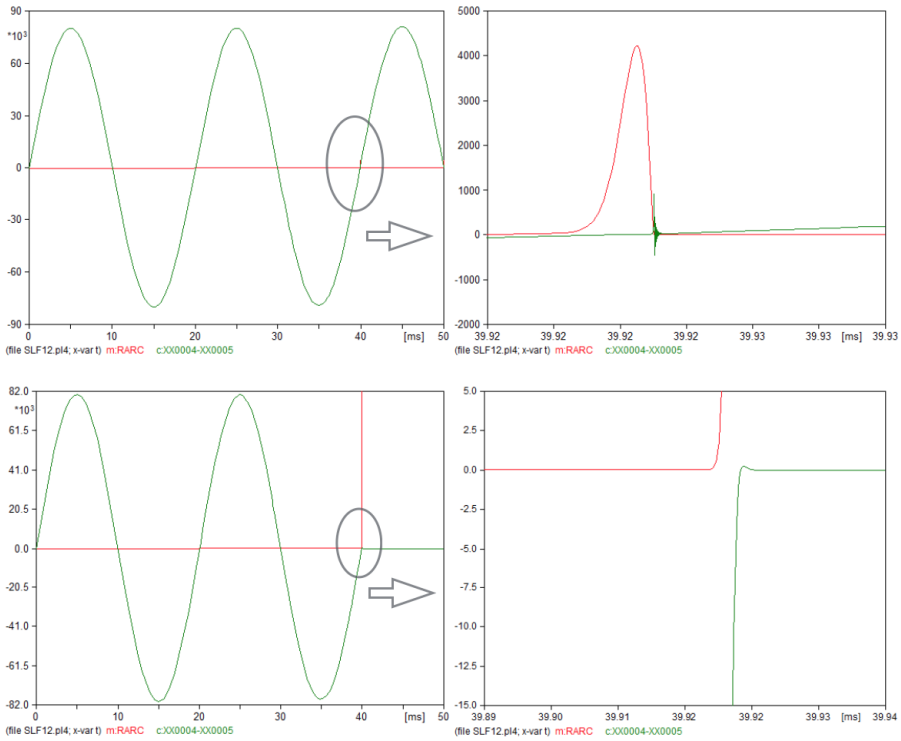

Figure 3.8: Thermal Breakdown

3.6.5 Pre-Strike

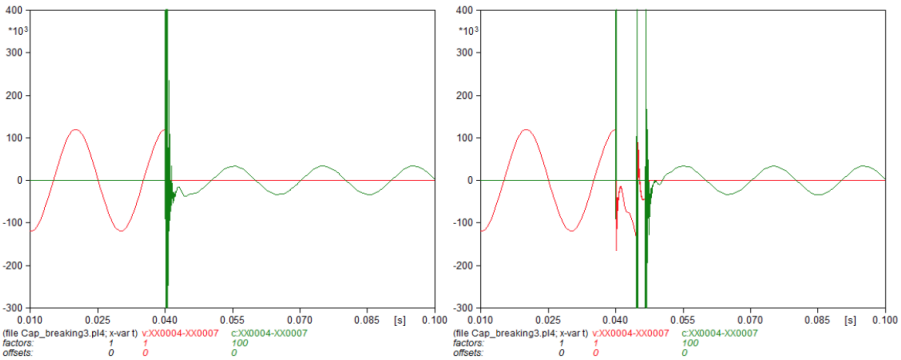

Figure 3.9: Pre-Strike

Pre-strike is a switching phenomenon which is virtually inevitable in circuit-breaker closing operation. What really matters is the behaviour of the pre-strike current

(green curve) during this process. With poorer high-frequency quenching capability, pre-strike arc keeps burning once dielectric breakdown happens (red curve indicates the gap voltage). It damps out to power frequency current eventually. (Shows in the left hand figure) With strong enough high-frequency quenching capability, on the other hand, pre-strike can happen several times during a single closing operation. Which scenario causes more damage? This question will be answered in Chapter 6.

3.7 Chapter Summary

In this chapter, programming environment in ATP Draw simulation software has been introduced from the point of views of important basic elements to complex control Models. Internal logics of the models have been described with the help of flowcharts. A set of general simulation results also have been included. In conclusion, in order to simulate both vacuum and SF_6 circuit-breaker models in various switching phenomena, three different models have been programmed in good structure and are capable of performing complex simulations with proper configured circuit parameters.

Chapter 4

Small Inductive Current Switching

4.1 Chapter Introduction

The implementation of vacuum circuit-breakers in medium voltage level electrical networks in decades of practice shows that they might have difficulties in interrupting small inductive current under some circumstances. Overvoltage, especially voltage escalation caused by multiple re-ignitions, is identified as the major negative impact which damages both the circuit-breaker itself and other network applicants. Therefore, before applying this technology into higher voltage levels its feasibility needs to be studied by the means of computer simulation. The aims of the study of this chapter include two major points:

1. Compare the performances of the proposed vacuum circuit-breaker under different load current conditions.

2. Compare the performances of the proposed vacuum circuit-breaker and SF_6 breaker under the aforementioned load current conditions.

IEC standard 62271-110 (2009) Inductive load switching provided detailed testing requirements. In the first section of this chapter, requirements related to the

following simulation work will be studied in advance. Based on the requirements specified, the testing circuit will be arranged and its parameters will be calculated next. To achieve the outlined aims of the study, simulations with different circuit setups are designed into several groups to test each of the individual objectives. Simulation results, then, will be presented in terms of curves and tables. Analysis will be conducted following each group of simulation. Finally, conclusions, together with recommendations, will be made to summarise this chapter.

4.2 IEC Standard Study

4.2.1 Load Type Requirements

In general, circuit-breakers with voltage level higher than $52kV$ for shunt reactor switching purpose should be considered. High-voltage motor switching is also included in the standard. However, in my case, circuit-breakers with rated voltage at $145kV$ are rarely used for motors or generators switching purposes. Motor/generator switching will not be included. In terms of transformers, because they have much higher surge impedance, high-frequency re-ignitions do not present significant issues in such scenario. Therefore, in conclusion, for circuit-breakers designed for rated voltage level at $145kV$, only the shunt reactor switching will be considered in this PhD work.

4.2.2 Frequency Requirement

According to the statements in sub-clause 6.115.1, both $50Hz$ and $60Hz$ with a relative tolerance of $\pm 10\%$ are covered in this standard. Tests performed at either frequency shall be considered as valid for the other frequency. Because $50Hz$ is used in European countries, this frequency with no diversity will be adopted.

4.2.3 Supply Circuit Requirements

The source inductance L_s shall be ranged between the value which provides the corresponding to the rated short-circuit current of the circuit-breaker and 10% of the inductance of the load circuit L. The source capacitance C_s, on the other hand, shall be at least 10 times the load capacitance C_L. [12]

4.2.4 Test Voltage Requirements

For single-phase laboratory tests, the test voltage measured at the circuit-breaker location immediately before the opening shall, as near as possible, be equal to the product of $U_r/\sqrt{3}$ and the following factor:

1. 1.0 for full pole tests of circuit breakers rated $245kV$ and above;
2. 1.5 for full pole tests of circuit breakers rated $170kV$ and below.[12]

Consequently, in this PhD thesis the factor 1.5 is applied.

4.2.5 Load Circuit Requirements

In sub-clause 6.115.6.2 and 6.115.6.3 of IEC 62271-110, two different load circuits are given with current based on the rated voltage of the circuit-breaker.

Table 4.1: Test Current for Load Circuit #1 & #2

Rated Voltage	**Test Current for Circuit 1**	**Test Current for Circuit 2**
$52 \sim 72.5kV$	$630A$	$200A$
$\geq 100kV$	$315A$	$100A$

The inductance on the load side then can be calculated based on voltage requirements and load circuit requirements. Detailed calculation procedure will be presented in the next section of this chapter.

4.2.6 Successful Testing Criteria

The criteria for successful testing are as follows:

1. the circuit-breaker shall consistently interrupt the current with re-ignitions at one current zero crossing only;

2. re-ignitions shall always occur between the arcing contacts.

In the following simulation work, point 2) will be considered as a fixed condition while point 1) will be guaranteed in each simulation result.

4.3 Simplifications and Assumptions

There are some simplifications and assumptions which need to be specified ahead of the rest parts of the dissertation.

1. For both VCB and SF_6 models, there is a constant initial dielectric withstand strength as $3.5kV$ at the moment of contacts separating. In reality, the initial strength varies from each time of testing even if all other conditions keep at the same value. On the other hand, it never increases linearly since the velocity of the contacts separating is not constant (an acceleration and a deceleration process must be involved based on Newtown's Second Law).

2. The current chopping level in this simulation is set to be as constant at $2.5A$. In reality, the value also changes from time to time and is related to the load current and the moment of contacts separating. This setup is just for simplification reason.

3. For the same reason, the high-frequency current quenching capability is also set up as constant, $1kA/\mu$s for VCB and $150A/\mu$s for SF_6.

4. The arcing voltage has been considered as zero for both two circuit-breaker models.

5. Particularly for SF_6 model, the current chopping process is simplified as to the VCB model. The actual process involves high-frequency oscillation but it has less influence on the overall performance.

4.4 Circuit Arrangement

4.4.1 Circuit Parameters Determination

The object circuit-breaker unit is rated at $145kV$. Therefore, according to Section 4.2.4, the voltage measured at the circuit-breaker immediately before the opening location is the product of the factor 1.5 and $^{145}/\sqrt{3}$. The voltage injected at the source side of the breaker is calculated as:

$$V_{source} = \frac{145}{\sqrt{3}} \times 1.5 = 124.57kV \tag{4.1}$$

The inductance L of the load circuit shall be adjusted to give the breaking current as 315A or 100A for breakers with rated voltage higher than $100kV$ in our case. As a result, the inductance chosen for test circuit 1 is:

$$X_L = \frac{V_{source}}{I_{load}} = \frac{125.57kV}{315A} = 398.64\Omega \tag{4.2}$$

$$L = \frac{X_L}{2\pi f} = \frac{398.64\Omega}{100\pi} = 1268.9mH \tag{4.3}$$

The rated short-circuit current of the subject circuit-breaker is $31.5kA$. Therefore, the driving voltage of the ideal power source and the source impedance can be obtained by solving the following equations:

$$\frac{V_{drive}}{X_{source} + X_L} = I_{load} \tag{4.4}$$

$$\frac{V_{drive}}{X_{source}} = I_{sc} \tag{4.5}$$

Substituting $I_{load} = 315A$, $I_{sc} = 31.5kA$ and $X_L = 398.64\Omega$ to the equations above, we have:

$$L_s = 12.817mH \tag{4.6}$$

$$V_{drive} = 126.83kV \tag{4.7}$$

To satisfy the required d.c. current constant $45ms$,

$$R_s = \frac{L_s}{\tau} = \frac{12.817mH}{45ms} = 0.2848\Omega \tag{4.8}$$

To satisfy the required TRV frequency of $2.1kHz$ [12],

$$\omega_{TRV} = \sqrt{\frac{1}{L_s C_0}} \Rightarrow C_0 = \frac{1}{(2\pi f_{TRV})^2 L_s} = 0.45\mu F \tag{4.9}$$

$$R_0 = \sqrt{\frac{L_s}{C_0}} \cdot \frac{1}{k_{af}} = 112.7\Omega \tag{4.10}$$

(Parameter f_{TRV} , the TRV frequency and k_{af}, amplitude factor are required by IEC 62271-100)

For test circuit 2, repeating the same procedure we have:

$L = 3997mH$, $L_s = 12.73mH$, $R_s = 0.2829\Omega$, $C_0 = 0.45\mu F$

$R_0 = 111.97\Omega$, $V_{drive} = 125.97kV$

Table 4.2 concludes all circuit parameters for both test circuit 1 and 2 for rated voltage $U \geq 100kV$.

Table 4.2: Test Circuit Parameters

Load Side Parameters						
$I_{load}(A)$	$L(mH)$		$C_L(nF)$		$R(\Omega)$	
315	1269		1.75		$400k$	
100	3997		1.75		$400k$	
Source Side Parameters						
$I_{load}(A)$	$L_s(mH)$	$R_s(\Omega)$	$C_0(\mu F)$	$R_0(\Omega)$	$V_{source}(kV)$	$V_{drive}(kV)$
315	12.82	0.28	0.45	112.7	125.57	126.84
100	12.73	0.28	0.45	112.7	125.57	135.97

4.4.2 Circuit-Breaker Parameters Specification

For vacuum circuit-breaker model rated at $145kV$, The final gap distance: $d = 60mm$;

Contacts separating velocity: $v = 4m/s$;

Therefore, the time duration for the total opening process:

$$t = d/v = \frac{60mm}{4m/s} = 0.015s = 15ms \tag{4.11}$$

The initial dielectric strength at the moment of contacts separating: $V_0 = 3.5kV$

The final dielectric strength of the gap: $V_{final} = 750kV$; (This value is quoted form Siemens technique brochure)

Therefore, the average dielectric strength recovery rate is:

$$\overline{\frac{du}{dt}} = \frac{\Delta V}{t} = \frac{V_{final} - V_0}{t} = \frac{750kV - 3.5kV}{15ms} \approx 50kV/ms \tag{4.12}$$

For SF_6 breaker which is rated at the same voltage level, its final gap distance has been increased to $120mm$ with a constant velocity of $5m/s$. As a result, the dielectric recovery rate turns to $31kV/ms$. Table 4.3 concludes circuit-breaker parameters for both of these two technologies.

Table 4.3: Circuit-Breaker Parameters

Breaker Type	Gap Distance (mm)	Velocity (m/s)	Ave. Dielectric Recovery Rate (kV/ms)	Chopping Lv.(A)	HF Current Quenching Capability ($A/\mu s$)
VCB	60	4	50	3	1000
SF_6	120	5	31	3	150

4.4.3 Circuit Layout

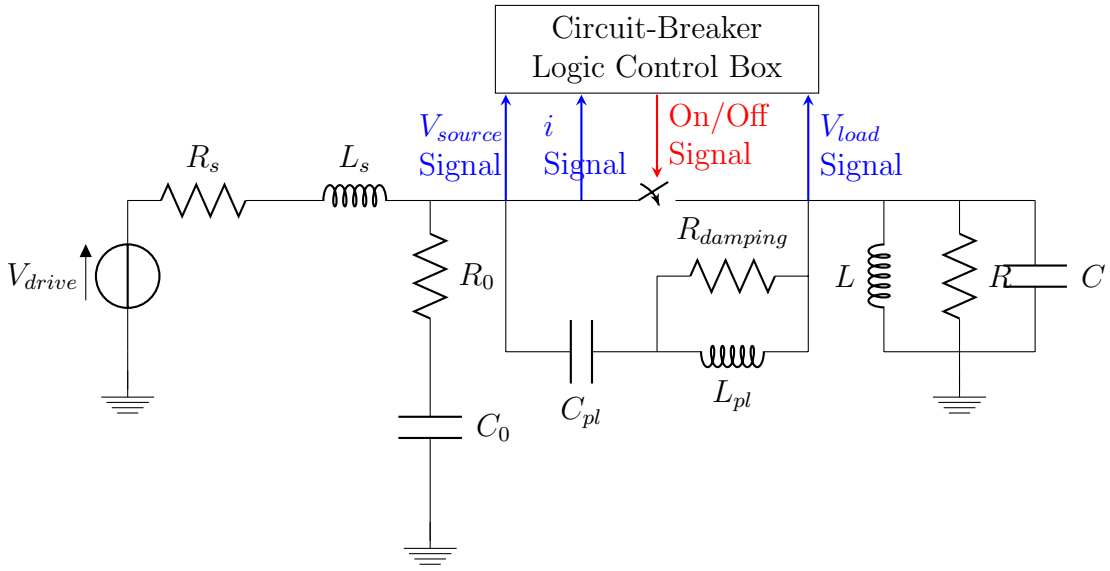

Figure 4.1: Test Circuit Layout

Figure 4.1 shows the layout of test circuit. Voltage source, source resistor (R_s), source inductor (L_s), source capacitor (C_0) and its associated resistor (R_0) on the left hand side of the circuit form the source side circuit. The ideal circuit-breaker, stray capacitor (C_{pl}), stray inductor (L_{pl}) and its associated damping resistor form the circuit-breaker model. The circuit-breaker logical control box does not physically exist in the real case, yet it controls the behaviour of the ideal breaker via reading voltage and current signals and feeding control signals back in the computer simulation programme. Load inductor (L) acts as the shunt reactor in the real case. R and C are its associated resistor and capacitor.

4.5 Test Objectives and Grouping

Due to the completely different breaker characteristics shown in Table 4.3, four groups of tests are to be carried out. In Test Group One, circuit-breaker model acts as the proposed vacuum breaker; in Test Group Four, it acts as the existing

SF_6 breaker; in Test Group Two and Three, the breaker models are not physically realistic but have been introduced as intermediate assumptions for comparison purposes only.

- **Test Group One**

Dielectric recovery rate (D), high-frequency current quenching capability (Q) and chopping level (I_{ch}) are assigned to the circuit-breaker logical control box according to the proposed VCB designs. Arcing time (time interval between contacts separating and current chop), load side voltage peak value, peak voltage value across the contacts and the accumulated heat energy generated during re-ignitions at the load current $315A$, $100A$ and $10A$ will be recorded. The objective to the Test Group One is setting up a reference line for further comparisons.

- **Test Group Two**

Reduce Q to 15% of its original value while maintaining D and I_{ch}. Repeat testing procedures at $315A$, $100A$ and $10A$ load current. The objective to the Test Group Two is figuring out the solo influence caused by changing high-frequency current quenching capability.

- **Test Group Three**

In Test Group Three, dielectric recovery rate D of the circuit-breaker will be reduced to 60% of its original value while maintain Q and I_{ch} as the setups in Test Group One. Test procedures will be repeated at $315A$, $100A$ and $10A$ load current. The objective to the Test Group Three is figuring out the solo influence caused by changing dielectric recovery rate.

- **Test Group Four**

In the last test group, Q will be reduced to 15%, D will be reduced to 60% of its original value respectively. The objective is figuring out the overall influences caused by all three circuit-breaker parameters.

4.6 Test Results and Analysis

4.6.1 Test Group One

In Test Group One, original vacuum circuit-breaker parameter set-ups will be tested under $315A$, $100A$ and $10A$ load current conditions. Test results will be recorded for those who meet the successful testing criteria which has been required by IEC 62271-110: the circuit-breaker shall consistently interrupt the current with re-ignitions at one current zero crossing only. To be more specific, the contact separating time will be adjusted to find out the minimum arcing time that leads to a successful current interrupting within one natural current zero crossing. Then, it will be shifted backwards one by $1ms$ until the breaker can interrupt the current with at least one re-ignition.

(1) **Test results undertaken at** $315A$ **load current**

When the proposed vacuum circuit-breaker model works under 315A load current, the minimum arcing time is 4ms. Adjusting the contacts separating time one mini second forwards, it leads to another power frequency current loop for a successful current interruption. $1ms$ backwards, on the other hand, leads to a successful interruption without re-ignition at all.

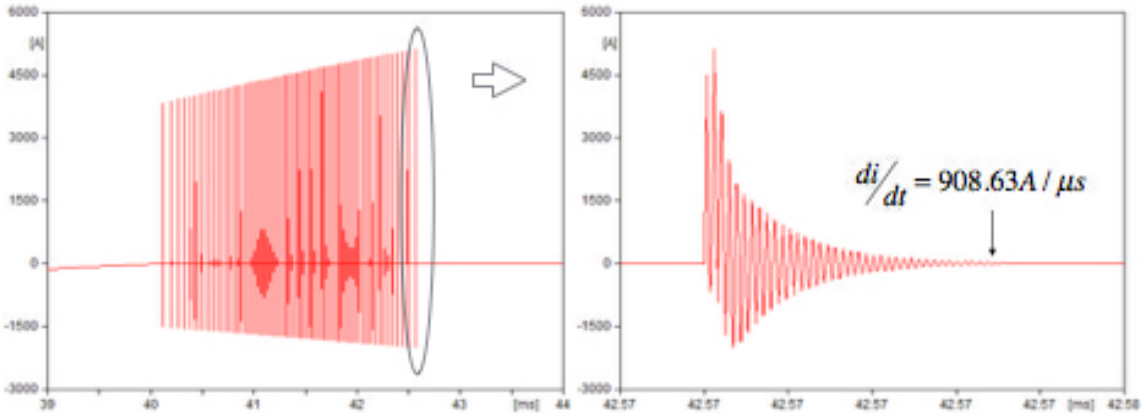

Figure 4.2: High-Frequency Current Quenching

On the left hand side Figure 4.2 shows the high-frequency current flowing through

the circuit-breaker during multiple re-ignitions. On the right hand side, it shows detailed current waveform during the last section of re-ignition. Two different frequencies of oscillation can be easily distinguished: the higher frequency is caused by the first parallel oscillation and the lower frequency is caused by the second parallel oscillation. By checking the slope of the current at its last zero crossing point, it can be found that the current was finally quenched at $908.63A/\mu s$, which is just below the threshold value $1000A/\mu s$, whereas the $^{di}/_{dt}$ at the penultimate current zero is $1123.47A/\mu s$.

Heat energy generated during multiple re-ignitions is one of the most important factors which causes damages to circuit-breaker contacts. The energy of the heat can be calculated with the following formula:

$$P = \int_{t=t_{chop}}^{t=t_{clear}} i^2(t) R \, dt \tag{4.13}$$

where t_{chop} represents the time instant when current chopping happens; t_{clear} represents the time instant when the current is finally cleared by the circuit-breaker; R represents the resistance of the breakers contact material, which, however, is a very case specific value. Therefore, this heat energy is represented by Joule per Ohm. For programming purpose, the aforementioned continuous integral equation has been adapted as the following discrete format:

$$P = R \sum_{t=t_{chop}}^{t=t_{clear}} i^2(t) \Delta t \tag{4.14}$$

Historical experiment results gave us the qualitative idea that, generally, SF_6 breaker produces fewer number of re-ignition sections but each section with relatively longer time duration. On the other hand, vacuum breaker produces larger number of re-ignition sections but each section with shorter time duration. To answer the question that which one of these two causes the more severe scenario, the measurement of heat energy per unit resistance sets up a reference line for comparison.

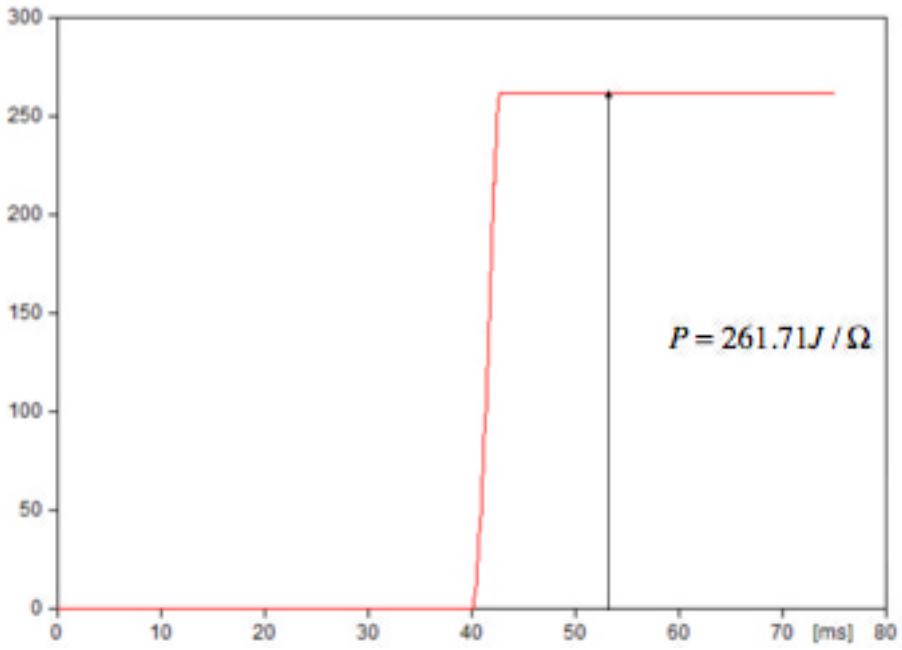

Figure 4.3: Heat Generation

Figure 4.3 shows the cumulative heat energy per ohm produced during the multiple re-ignitions. It can be found that the maximum value is $261.71 J/\Omega$.

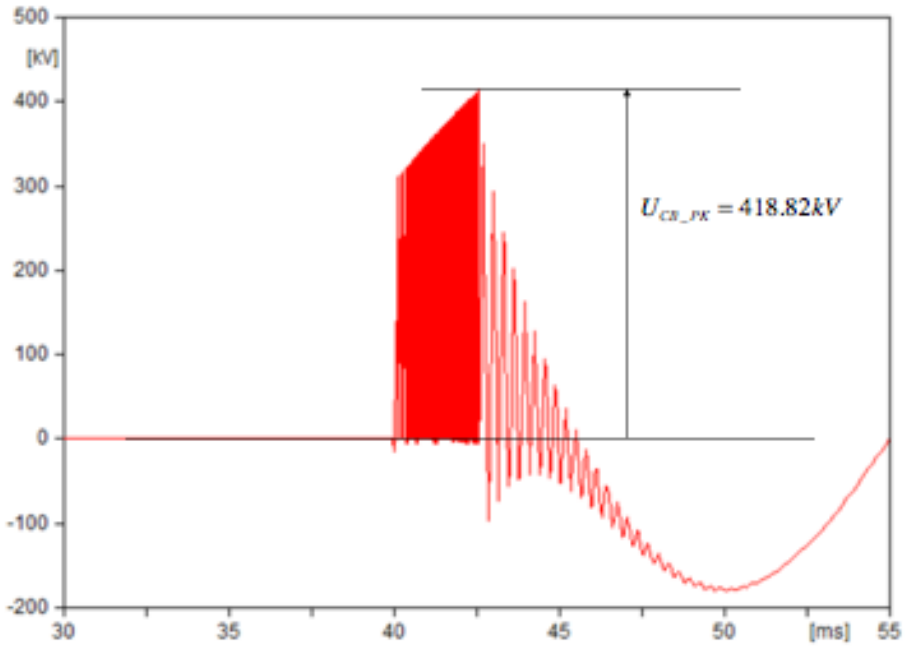

Figure 4.4: Voltage Across the gap During Current Breaking

Figure 4.4 shows the voltage waveform between the breakers contacts during an opening operation. It is clear that the voltage peak value escalated due to multiple

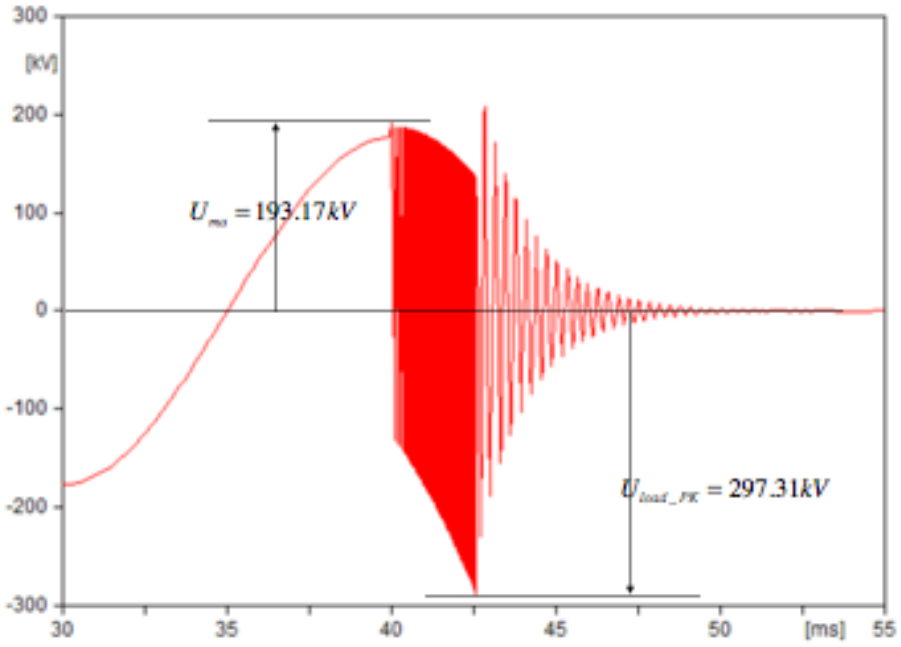

Figure 4.5: Voltage Across the Load During Current Breaking

re-ignitions and it reaches $418.82kV$ as a maximum result. Figure 4.5 presents the result of the voltage across the load circuit. The suppression peak voltage is $193.17kV$ while the maximum peak value of the load peak voltage is measured as $297.31kV$.

(2) **Test results undertaken at** $100A$ **load current**

For $100A$ load current, the minimum arcing time that leads to a successful interrupting without another current loop is $2ms$ while the maximum arcing time that leads to a successful interrupting with at least one re-ignition is $5ms$.

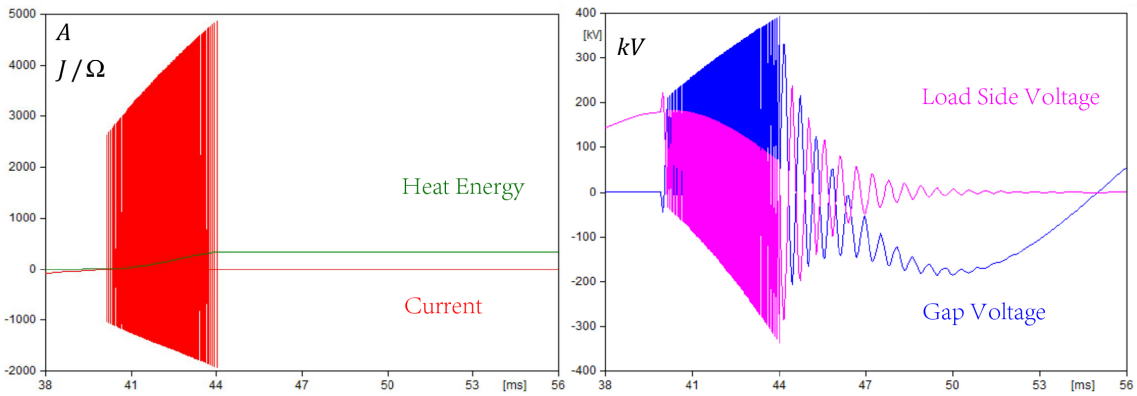

Figure 4.6: Arcing Time equals to $2ms$ at $100A$ Load Current (TG1)

On the left hand side of Figure 4.6 shows the heat energy generated (green curve) and the current waveform (red curve) during a current interrupting process. On the right hand side, it shows the load side voltage (purple curve) and gap voltage (blue curve) waveform. This figure layout arrangement also applies to all the following figures in this chapter.

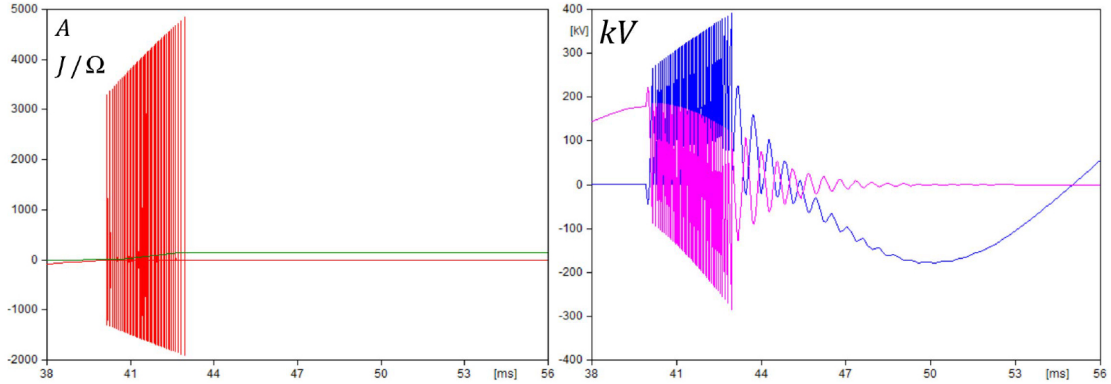

Figure 4.7: Arcing Time equals to $3ms$ at $100A$ Load Current (TG1)

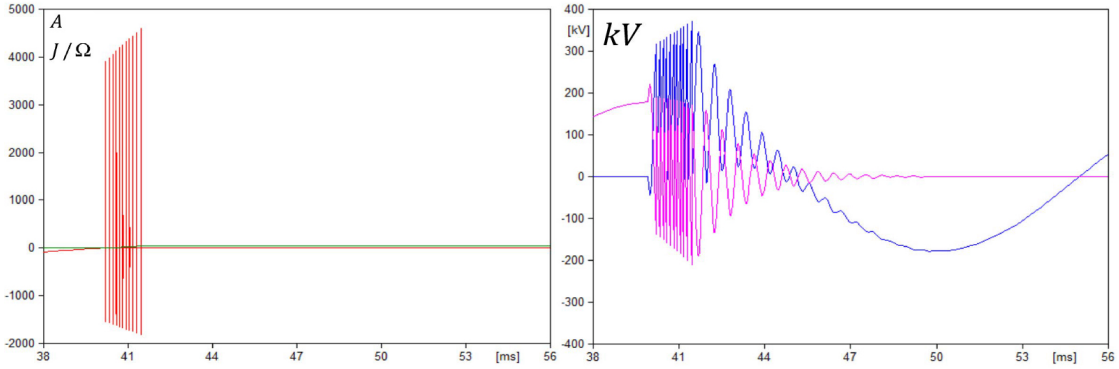

Figure 4.8: Arcing Time equals to $4ms$ at $100A$ Load Current (TG1)

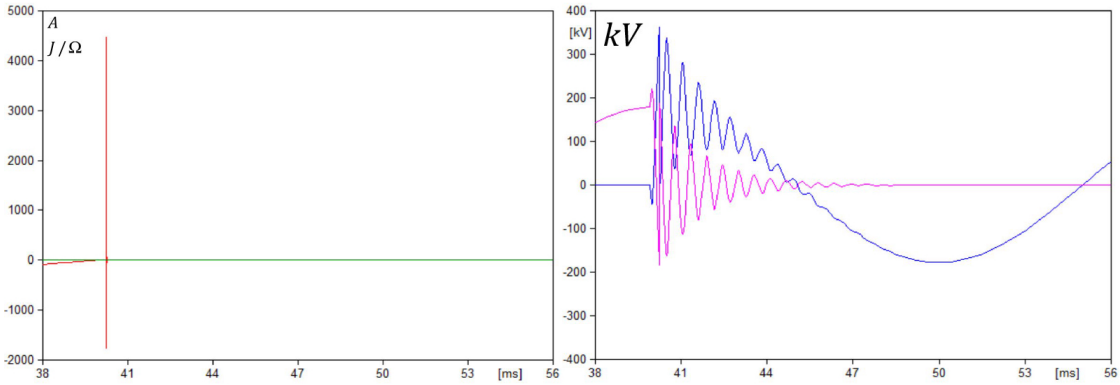

Figure 4.9: Arcing Time equals to $5ms$ at $100A$ Load Current (TG1)

By comparing Figure 4.6 to Figure 4.9 , it can be found that with longer arcing time, the circuit-breaker can interrupt the same inductive load current more effectively. The total number of multiple re-ignitions is reduced.

(3) **Test results undertaken at** $10A$ **load current**

For 10A load current, the minimum arcing time that leads to a successful interrupting without another current loop is $0ms$ while the maximum arcing time that leads to a successful interrupting without multiple re-ignitions is $5ms$.

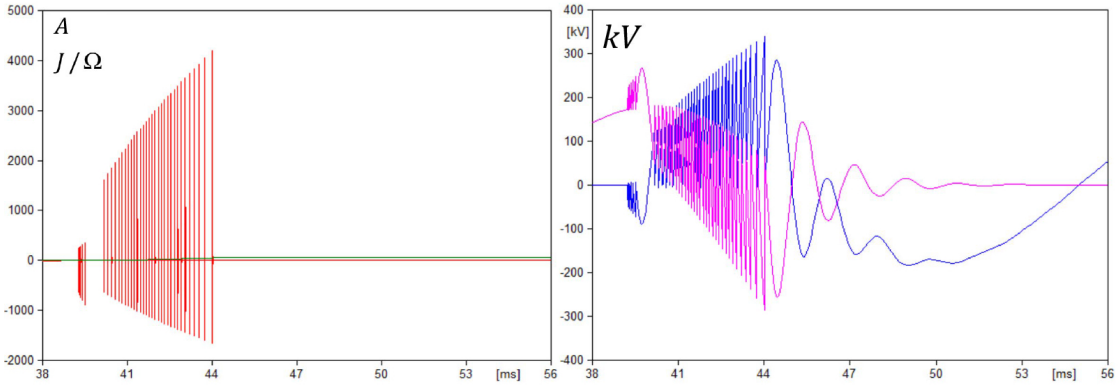

Figure 4.10: Arcing Time equals to $0ms$ at $10A$ Load Current (TG1)

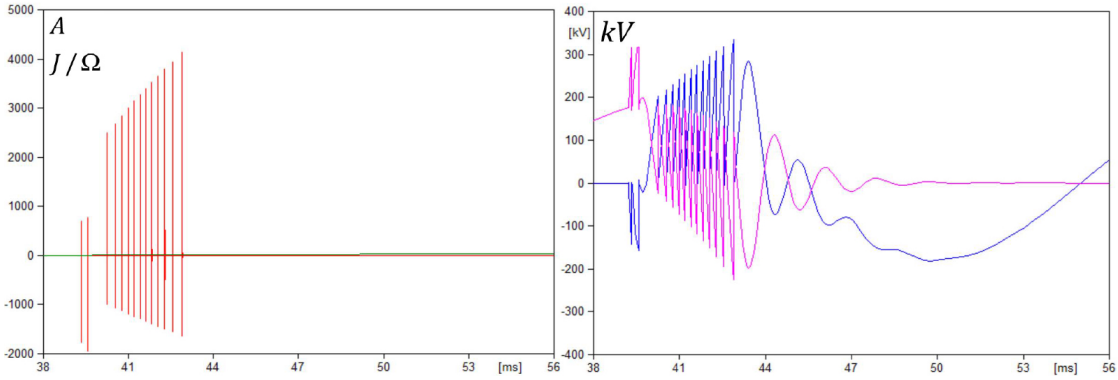

Figure 4.11: Arcing Time equals to $1ms$ at $10A$ Load Current (TG1)

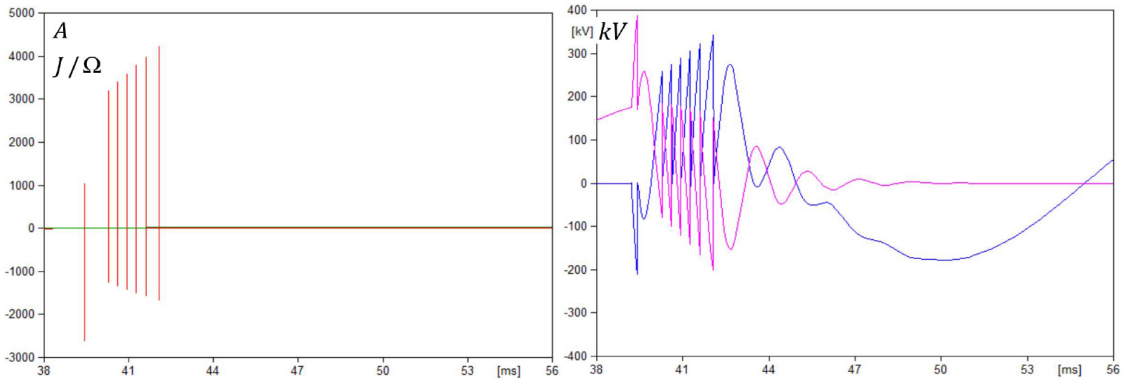

Figure 4.12: Arcing Time equals to $2ms$ at $10A$ Load Current (TG1)

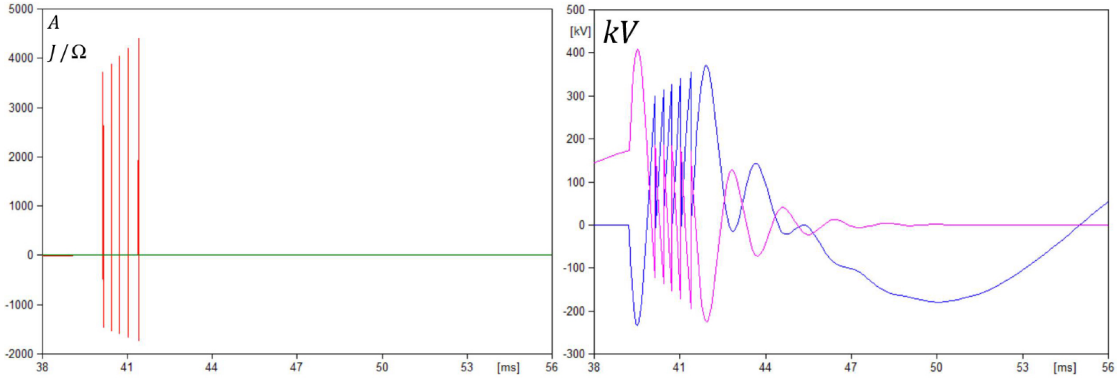

Figure 4.13: Arcing Time equals to $3ms$ at $10A$ Load Current (TG1)

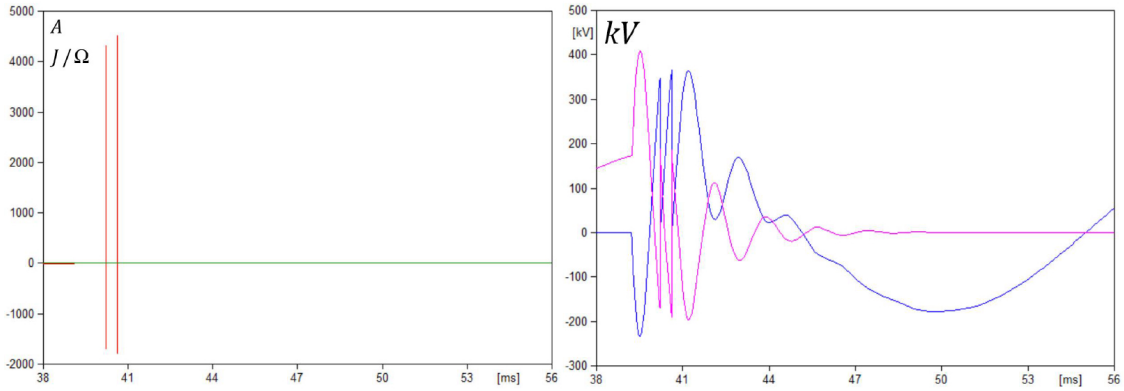

Figure 4.14: Arcing Time equals to $4ms$ at $10A$ Load Current (TG1)

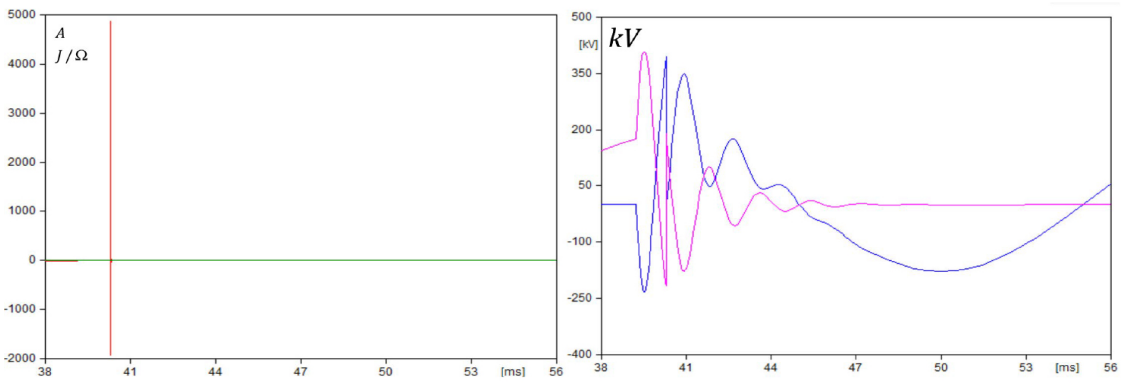

Figure 4.15: Arcing Time equals to $5ms$ at $10A$ Load Current (TG1)

Assembling data from Test 1, 2 and 3, Table 4.4 concludes the results of Test Group One as follows:

Table 4.4: Simulation Results for Test Group One

Load Current (A)	**Arcing time (ms)**	**P (J/Ω)**	**U_{ma} (kV)**	**U_{CB_PK} (kV)**	**U_{load_PK} (kV)**
315	4	261.71	193.17	418.82	297.31
100	2	333.51	221.63	393.79	337.37
	3	148.76	221.63	391.64	283.76
	4	36.6	221.63	371.22	210.95
	5	3.7	221.63	362.09	184.15
10	0	51.618	266.66	339.37	284.80
	1	21.106	344.17	334.02	224.46
	2	16.402	386.65	341.72	199.79
	3	15.08	409.34	355.52	193.64
	4	7.15	409.34	365.45	190.38
	5	4.36	409.34	392.28	188.21

By comparing the contents of this table, it can be found that with the same arcing time, higher load current brings higher load side re-ignition peak as well as heat energy per resistance unit, but lower suppression peak. Especially, when interrupting very small load current (say $10A$), suppression peak could be even higher than the load peak. Evidences also show that if re-ignition happened after the full suppression peak has been reached, load side peak decreases following longer arcing time and this conclusion varies if re-ignition happens beforehand.

4.6.2 Test Group Two

In Test Group Two, the high-frequency current quenching capability will be reduced to 15% of its original level while the original dielectric recovery rate will be kept to test the influence on the breakers current interrupting performance solely caused by this parameter.

(1) **Test results undertaken at** $315A$ **load current**

When the high-frequency current quenching capability reduced model works under $315A$ load current condition, it is impossible to interrupt such current within one power frequency loop with dielectric breakdown involved.If the arcing time is longer than $10ms$, which means longer than a full power frequency loop at $50Hz$, the breaker can interrupt such current without and dielectric breakdowns.

(2) **Test results undertaken at** $100A$ **load current**

For $100A$ load current, the minimum arcing time that leads to a successful interrupting without another current loop is 4ms while the maximum arcing time that leads to a successful interrupting with at least one re-ignition is $5ms$.

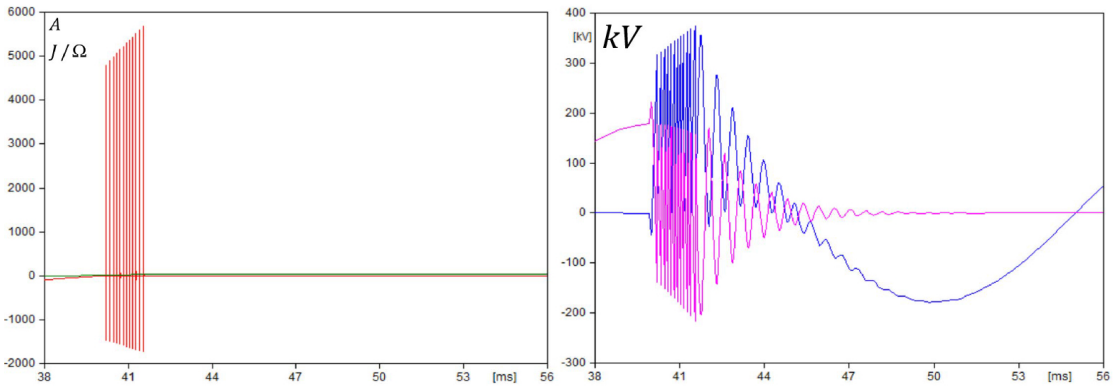

Figure 4.16: Arcing Time equals to $4ms$ at $100A$ Load Current (TG2)

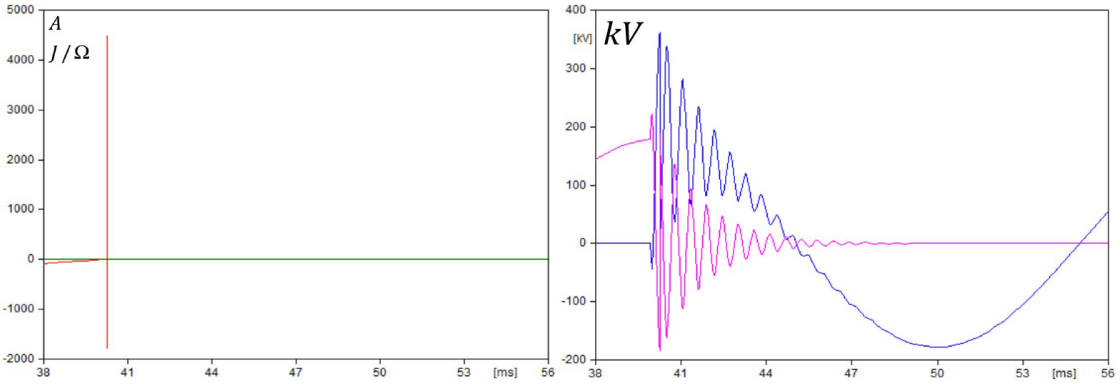

Figure 4.17: Arcing Time equals to $5ms$ at $100A$ Load Current (TG2)

(3) **Test results undertaken at** $10A$ **load current**

For $10A$ load current, the minimum arcing time leads to a successful interrupting without another current loop is $0ms$ while the maximum arcing time that leads to a successful interrupting with at least one re-ignition is $5ms$.

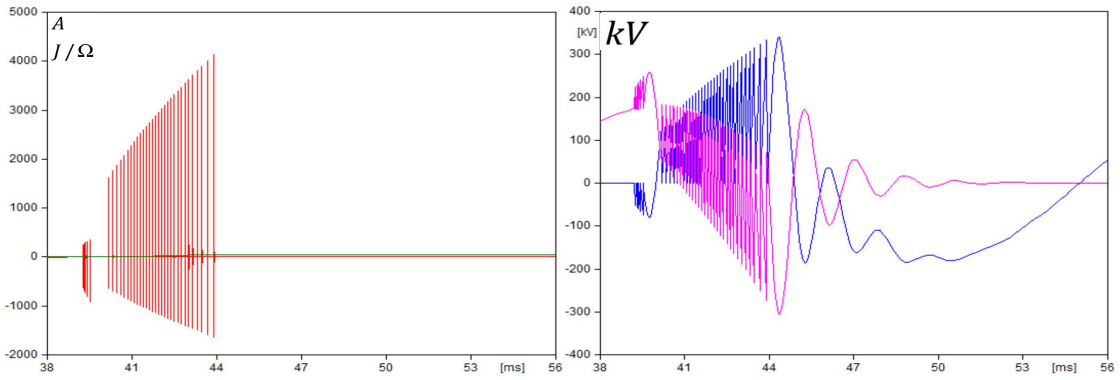

Figure 4.18: Arcing Time equals to $0ms$ at $100A$ Load Current (TG2)

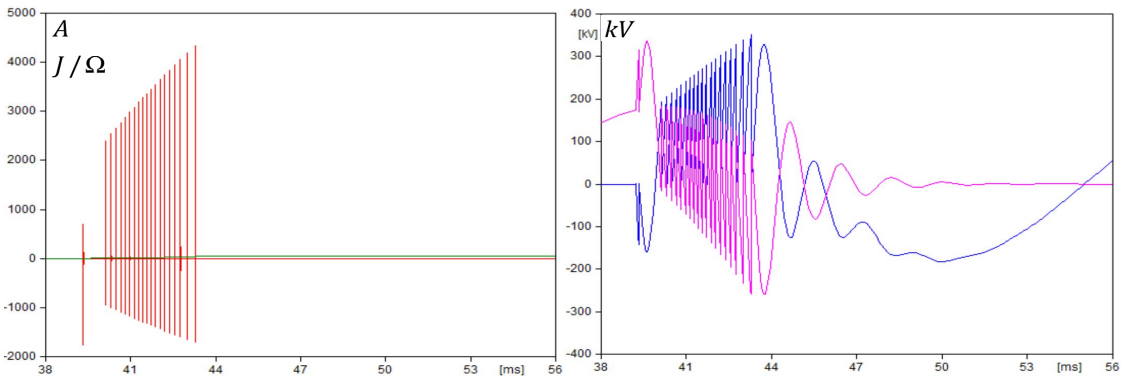

Figure 4.19: Arcing Time equals to $1ms$ at $100A$ Load Current (TG2)

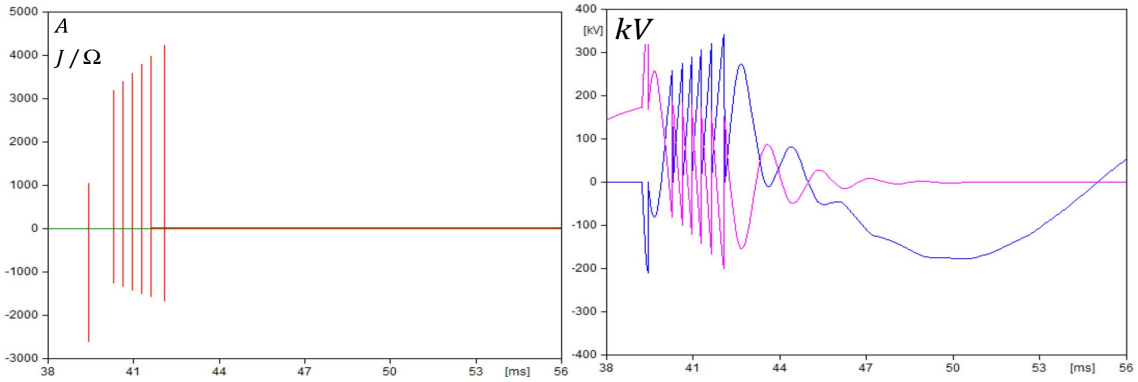

Figure 4.20: Arcing Time equals to $2ms$ at $100A$ Load Current (TG2)

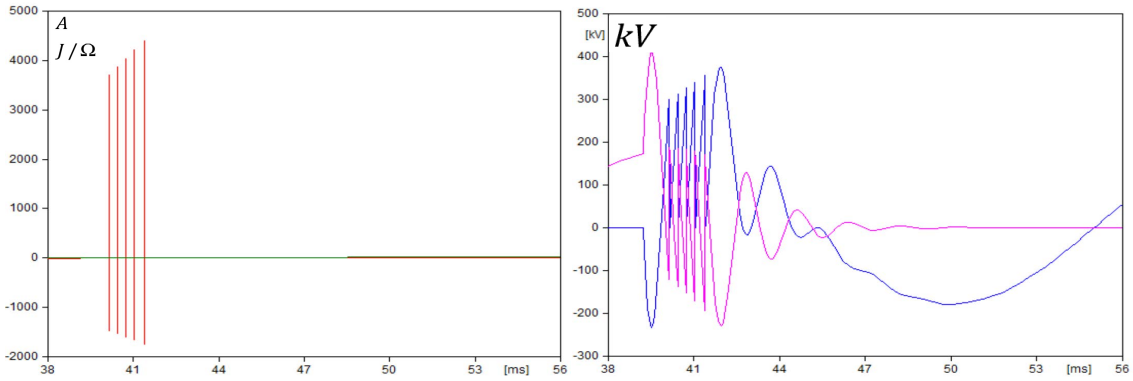

Figure 4.21: Arcing Time equals to $3ms$ at $100A$ Load Current (TG2)

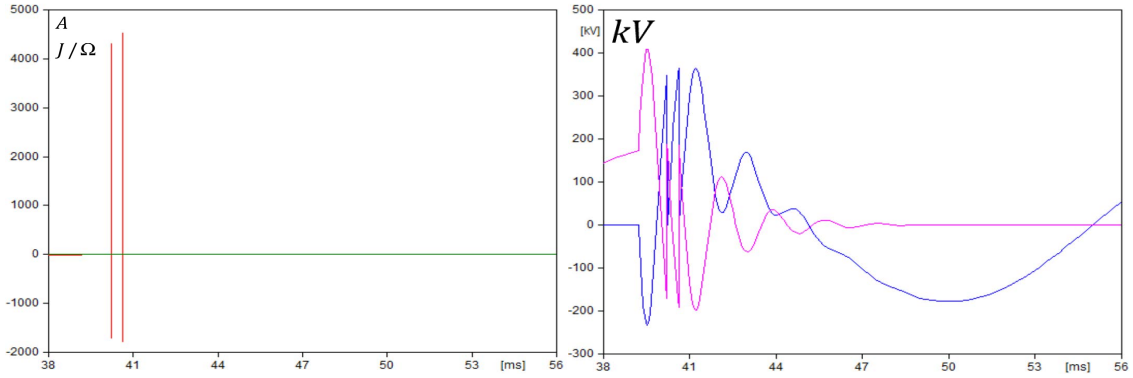

Figure 4.22: Arcing Time equals to $4ms$ at $100A$ Load Current (TG2)

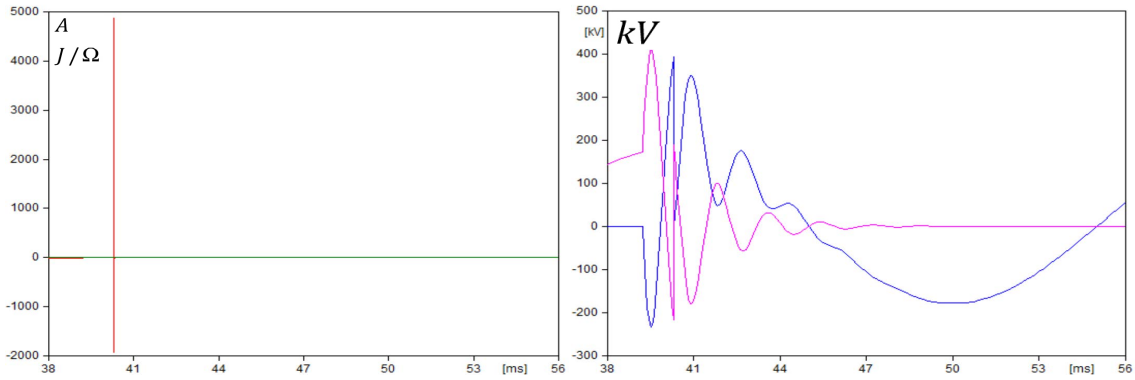

Figure 4.23: Arcing Time equals to $5ms$ at $100A$ Load Current (TG2)

Again, the number of multiple re-ignitions becomes lower at longer arcing time, i.e. at higher interrupting capability. However this holds true for lower load current, only due to reduced quenching capability.

Assembling data from Test 1, 2 and 3, Table 4.5 concludes the results of Test Group Two as follows:

Table 4.5: Simulation Results for Test Group Two

Load Current (A)	**Arcing time (ms)**	**P (J/Ω)**	**U_{ma} (kV)**	**U_{CB_PK} (kV)**	**U_{load_PK} (kV)**
100	4	45.061	221.63	373.76	216.16
	5	3.687	221.63	362.12	181.77
10	0	49.806	266.66	339.37	284.80
	1	21.106	344.17	334.02	224.46
	2	16.402	386.65	341.72	199.79
	3	15.08	409.34	355.52	193.64
	4	7.15	409.34	365.45	190.38
	5	4.36	409.34	392.28	188.21

The above results prove that circuit breaker with lower high-frequency quenching capability would require a longer minimum arcing time when interrupting current at $100A$ and above.

In terms of extremely low current, this is a good example showing that load peak voltage may not reduce following a longer arcing time if the first re-ignition happens before the full built of the suppression peak.

By comparing the $100A$ test result to the same rows in Table 4.4, the reduced Q brings an even higher load side voltage peak at the same arcing time. However, the difference is insignificant.

From the point of view of the heat energy generation, high-frequency current quenching capability does not have strong influence on this factor.

4.6.3 Test Group Three

The influence caused by changing dielectric recovery rate will be figured out in Test Group Three. The high-frequency current quenching capability will be restored back to its original level while its dielectric recovery rate will be reduced by 85%.

(1) **Test results undertaken at** $315A$ **load current**

For 315A load current, it can be interrupted by the circuit-breaker model with reduced dielectric recovery rate with $8ms$ arcing time. One ms shorter leads to another power frequency current loop; one ms longer leads to a successful interrupting without re-ignition.

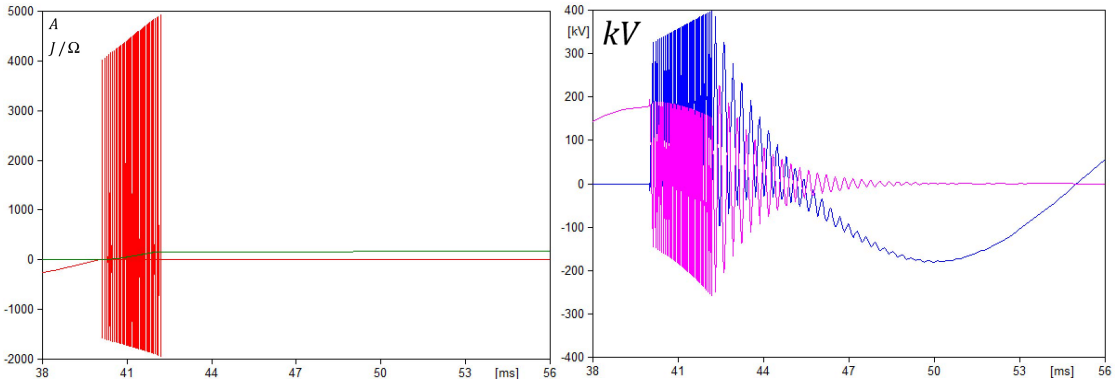

Figure 4.24: Arcing Time equals to $8ms$ at $315A$ Load Current (TG3)

(2) **Test results undertaken at** $100A$ **load current**

For $100A$ load current, the minimum arcing time that leads to a successful interrupting without another current loop is $5ms$ while the maximum arcing time that leads to a successful interrupting with at least one re-ignition is $8ms$.

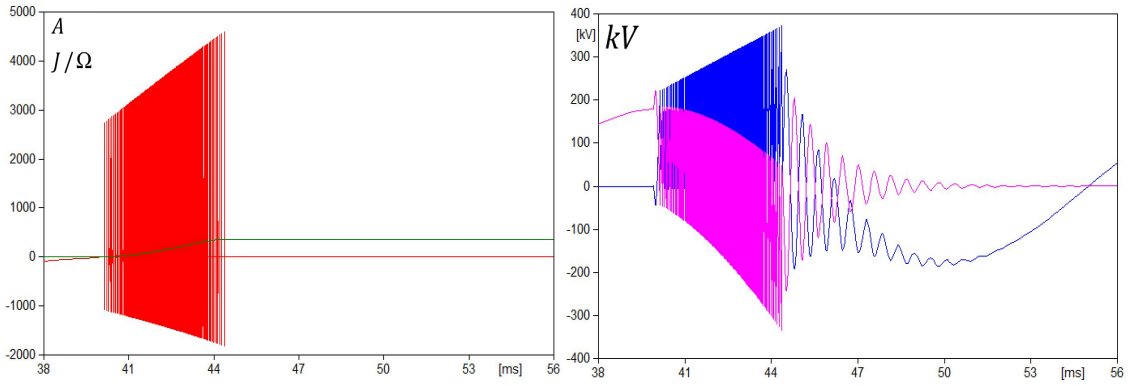

Figure 4.25: Arcing Time equals to $5ms$ at $100A$ Load Current (TG3)

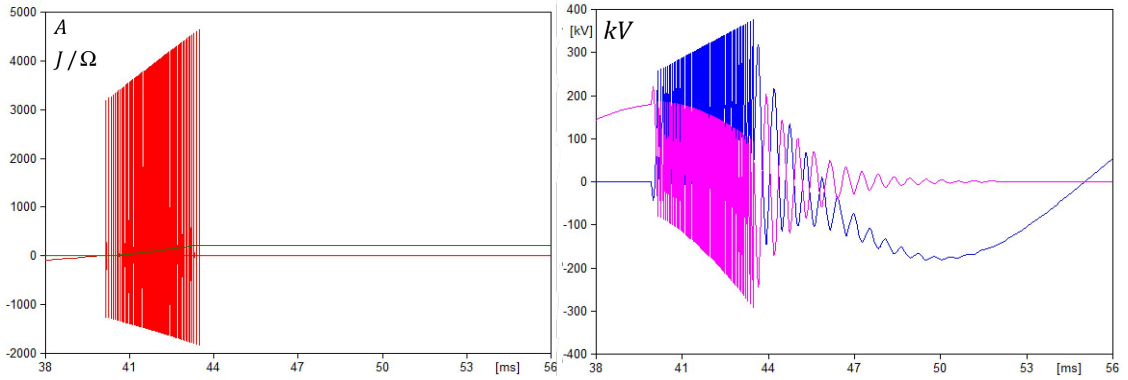

Figure 4.26: Arcing Time equals to $6ms$ at $100A$ Load Current (TG3)

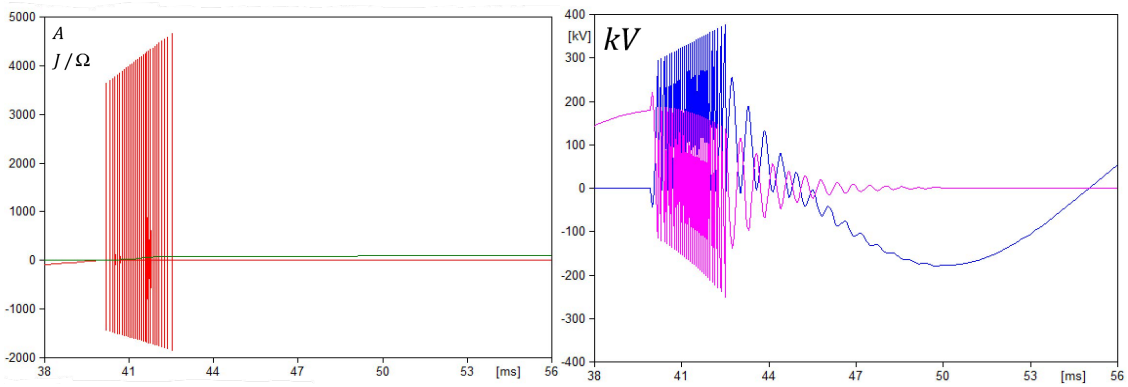

Figure 4.27: Arcing Time equals to $7ms$ at $100A$ Load Current (TG3)

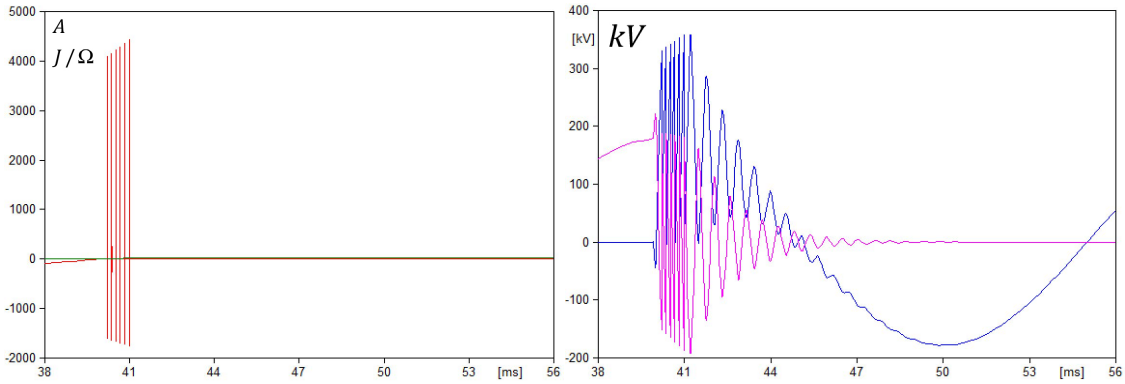

Figure 4.28: Arcing Time equals to $8ms$ at $100A$ Load Current (TG3)

However, the maximum amplitude of the circuit-breaker voltage at multiple re-ignitions is about the same as in TG1, yet at longer arcing time.

(3) **Test results undertaken at** $10A$ **load current**

For $10A$ load current, the minimum arcing time that leads to a successful interrupting without another current loop is $0ms$ while the maximum arcing time that leads to a successful interrupting with at least one re-ignition is $8ms$.

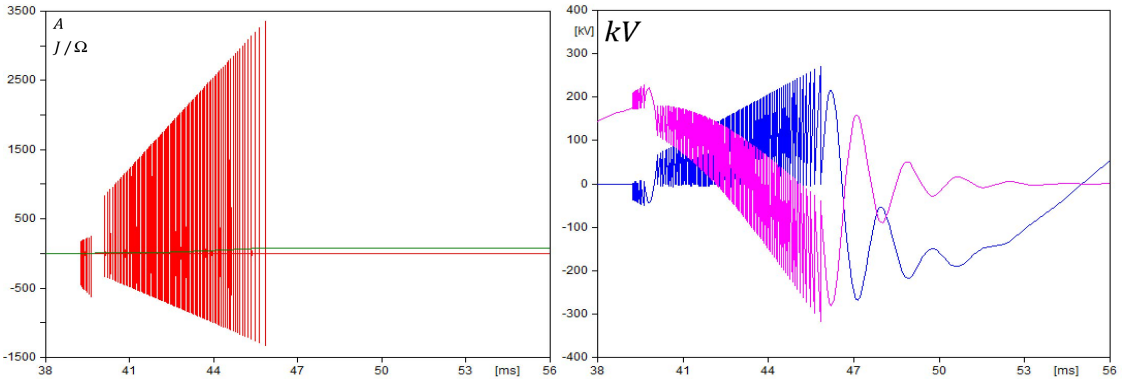

Figure 4.29: Arcing Time equals to $0ms$ at $10A$ Load Current (TG3)

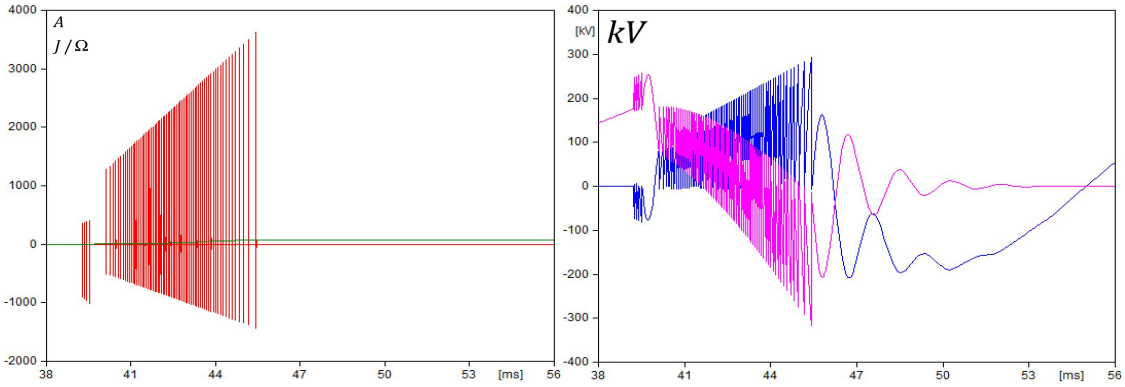

Figure 4.30: Arcing Time equals to $1ms$ at $10A$ Load Current (TG3)

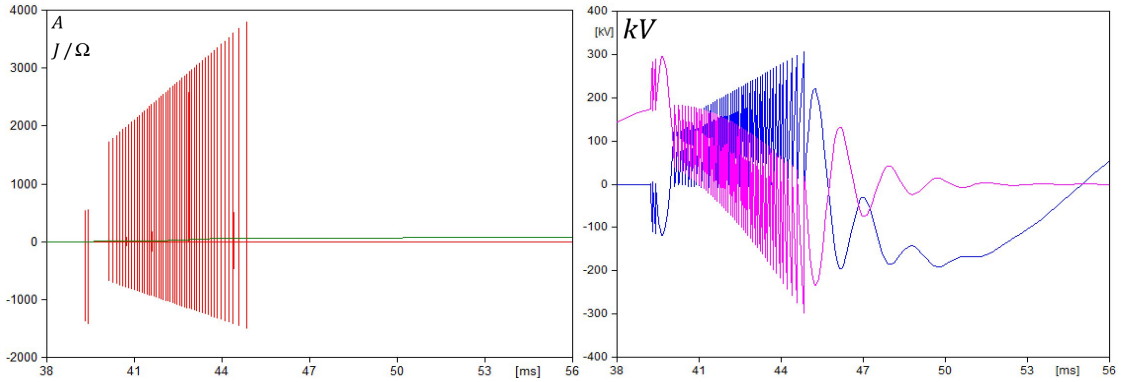

Figure 4.31: Arcing Time equals to $2ms$ at $10A$ Load Current (TG3)

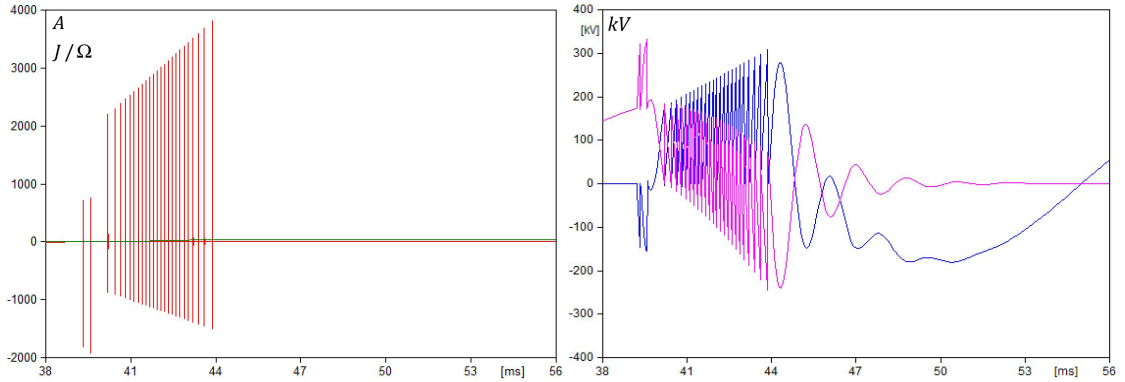

Figure 4.32: Arcing Time equals to $3ms$ at $10A$ Load Current (TG3)

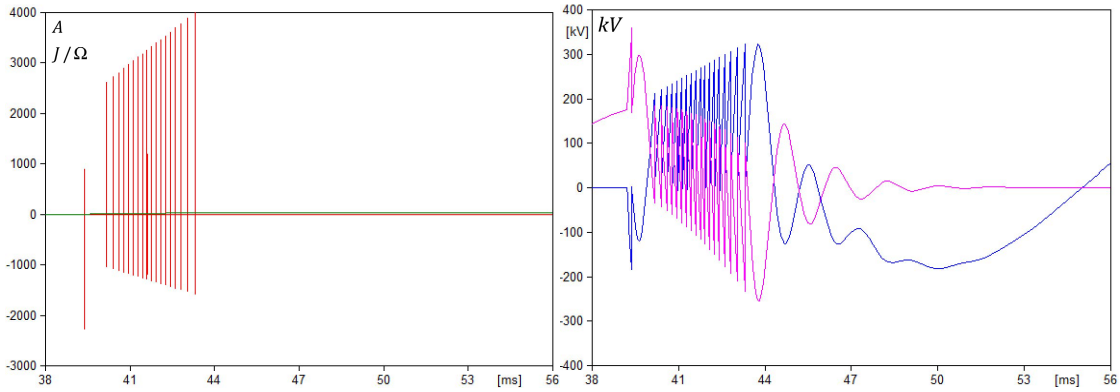

Figure 4.33: Arcing Time equals to $4ms$ at $10A$ Load Current (TG3)

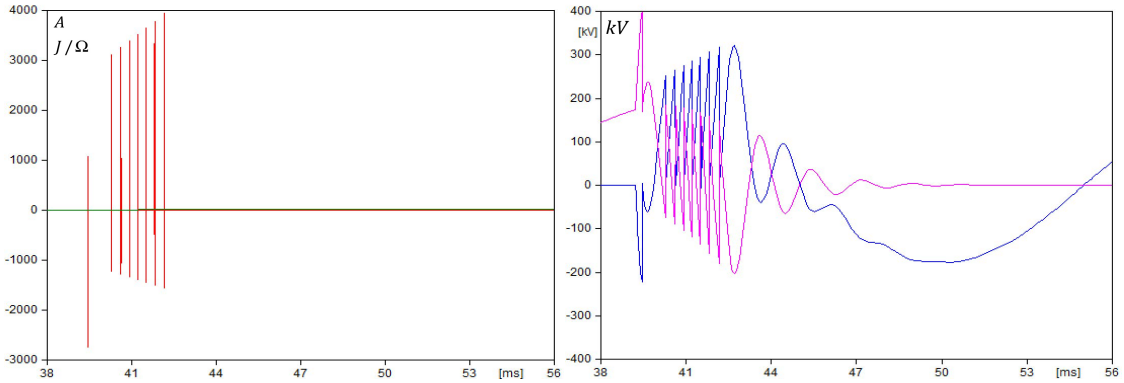

Figure 4.34: Arcing Time equals to $5ms$ at $10A$ Load Current (TG3)

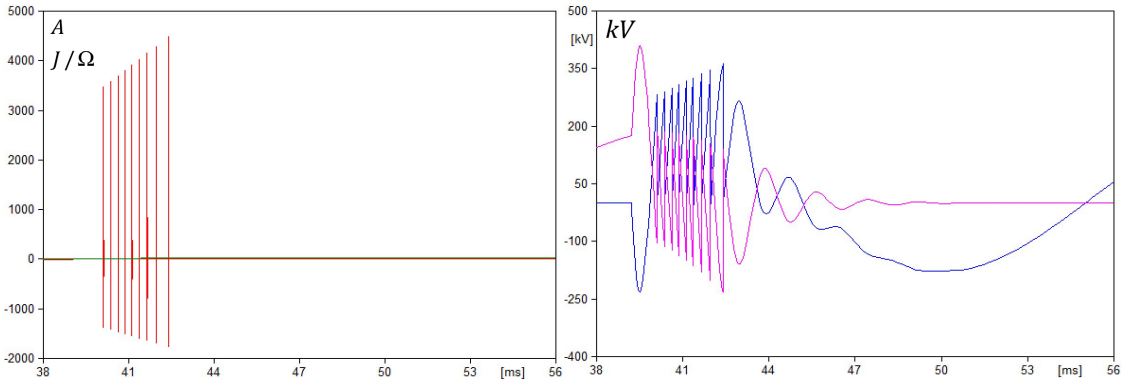

Figure 4.35: Arcing Time equals to $6ms$ at $10A$ Load Current (TG3)

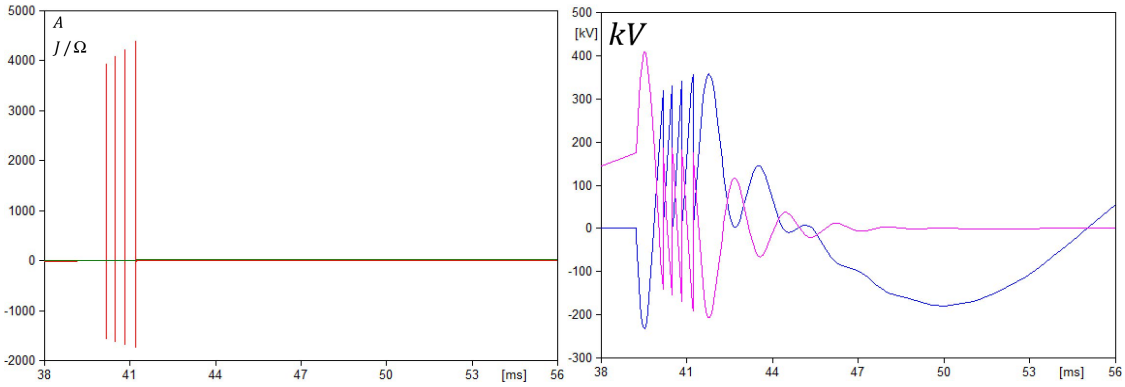

Figure 4.36: Arcing Time equals to $7ms$ at $10A$ Load Current (TG3)

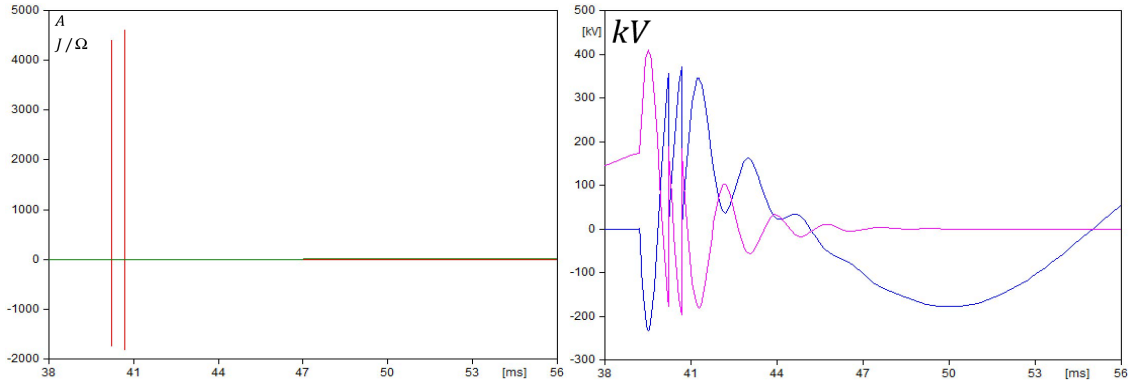

Figure 4.37: Arcing Time equals to $8ms$ at $10A$ Load Current (TG3)

Also, the maximum voltage amplitude at multiple re-ignitions and load current is about the same as in TG1.

Table 4.6 concludes the above results from Test 1, 2 and 3.

Table 4.6: Simulation Results for Test Group Three

Load Current (A)	**Arcing time (ms)**	**P (J/Ω)**	**U_{ma} (kV)**	**U_{CB_PK} (kV)**	**U_{load_PK} (kV)**
315	8	168.53	193.17	398.72	249.67
100	5	367.11	221.63	371.51	334.29
	6	241.87	221.63	375.35	291.83
	7	95.032	221.63	376.79	250.50
	8	19.989	221.63	357.99	193.04
10	0	77.701	227.04	271.04	316.79
	1	73.698	257.04	292.04	315.45
	2	66.846	296.03	306.73	297.29
	3	41.475	331.98	307.37	244.31
	4	37.351	358.49	323.19	236.53
	5	17.433	397.42	318.13	204.75
	6	25.804	409.34	361.74	231.54
	7	12.739	409.34	355.37	206.63
	8	7.447	409.34	371.81	196.33

Comparing Table 4.4 and 4.6, the result indicates that circuit-breaker model with reduced dielectric recovery rate needs a longer minimum arcing time to make a successful current interruption. From the heat energy producings point of view, circuit-breaker model with reduced dielectric recovery rate tends to generate much more energy with the same arcing time. This conclusion is quite obvious in those tests undertaken at $10A$ load current. From the peak voltage values point of view, the differences between Test Group One and Three are not that obvious as the first conclusion. For tests undertaken at $315A$ and $100A$ load current, lower dielectric recovery rate brings slightly lower peak voltage value. For $10A$ load current, on the other hand, the differences are very insignificant.

4.6.4 Test Group Four

In Test Group Four, parameters for high-frequency current quenching capability and dielectric recovery rate will be modified at the same time to make an overall comparison between vacuum circuit-breaker model and SF_6 breaker model.

(1) **Test results undertaken at** $315A$ **load current**

Circuit-breaker model with reduced high-frequency current quenching capability and reduced dielectric recovery rate is unable to interrupt such load current within one power frequency current loop. With an additional power frequency current loop, the circuit-breaker can interrupt the current without multiple re-ignitions.

(2) **Test results undertaken at** $100A$ **load current**

For $100A$ load current, the only suitable arcing time which makes a successful interruption within one power frequency current loop is $8ms$.

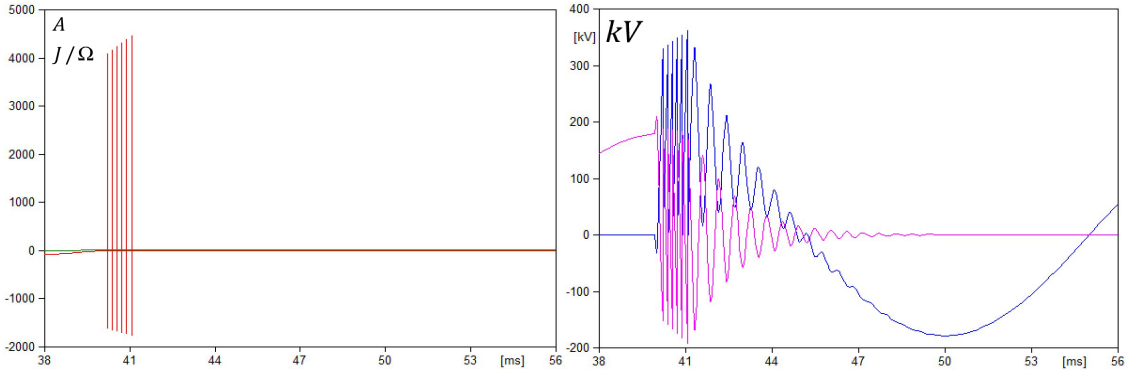

Figure 4.38: Arcing Time equals to $8ms$ at $100A$ Load Current (TG4)

(3) **Test results undertaken at** $10A$ **load current**

For $10A$ load current, the minimum arcing time that leads to a successful interrupting without another current loop is $2ms$ while the maximum arcing time that leads to a successful interrupting with at least one re-ignition is $8ms$.

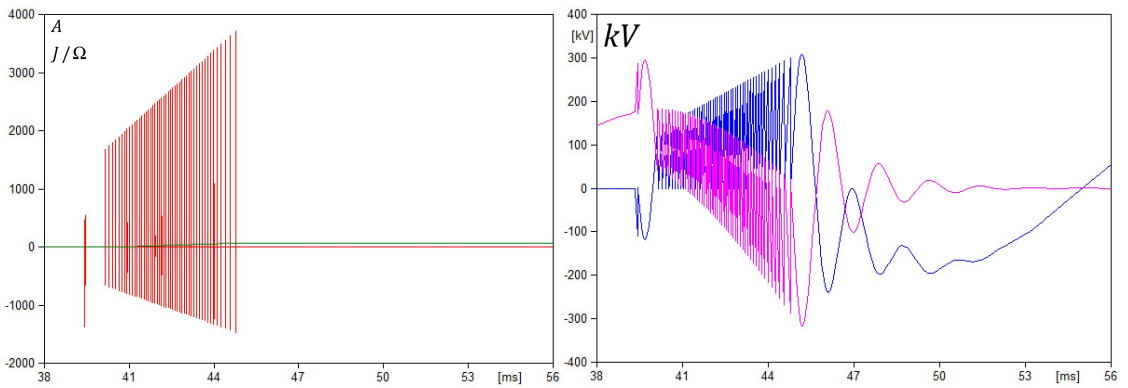

Figure 4.39: Arcing Time equals to $2ms$ at $10A$ Load Current (TG4)

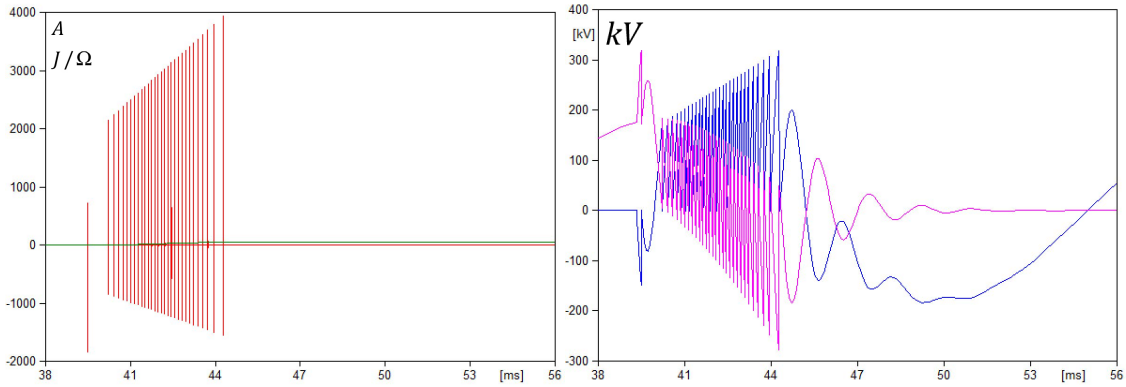

Figure 4.40: Arcing Time equals to $3ms$ at $10A$ Load Current (TG4)

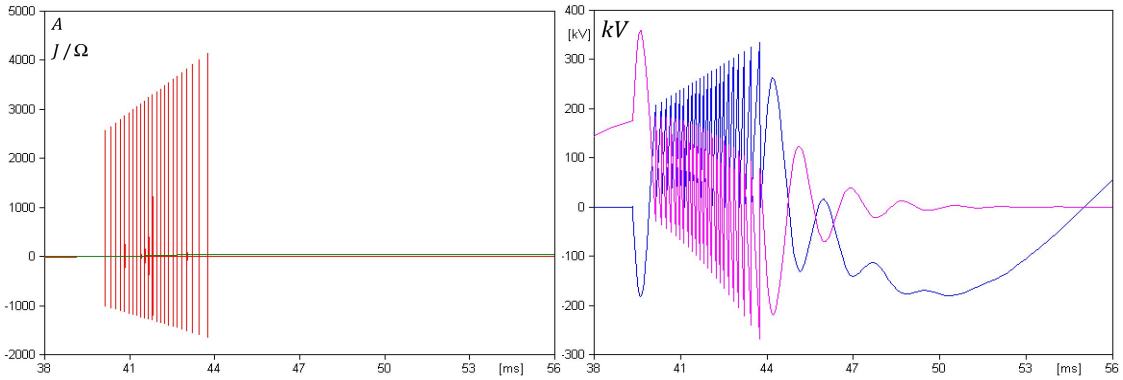

Figure 4.41: Arcing Time equals to $4ms$ at $10A$ Load Current (TG4)

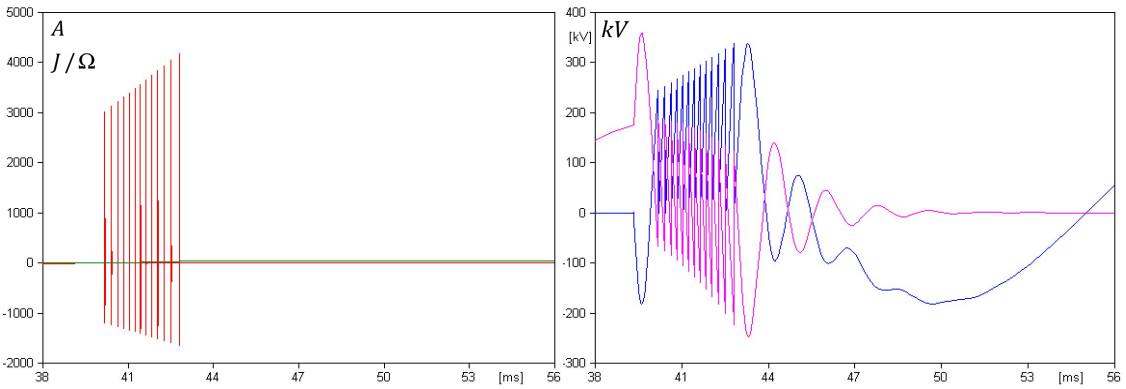

Figure 4.42: Arcing Time equals to $5ms$ at $10A$ Load Current (TG4)

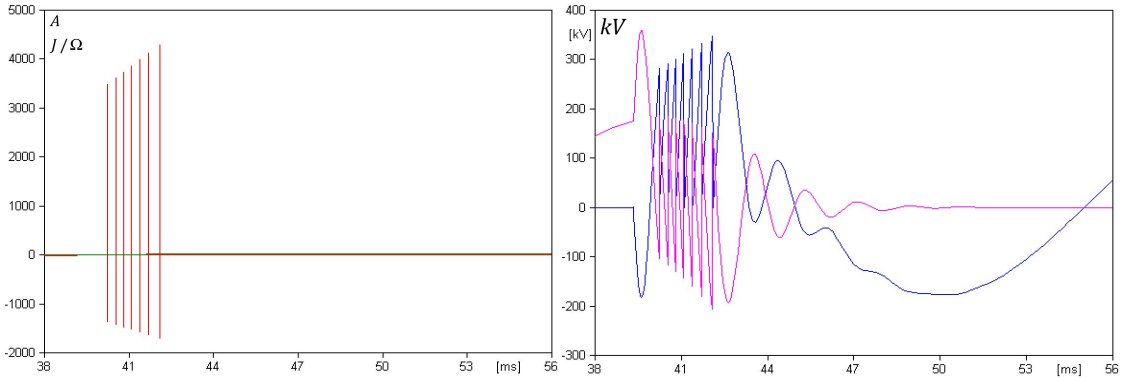

Figure 4.43: Arcing Time equals to $6ms$ at $10A$ Load Current (TG4)

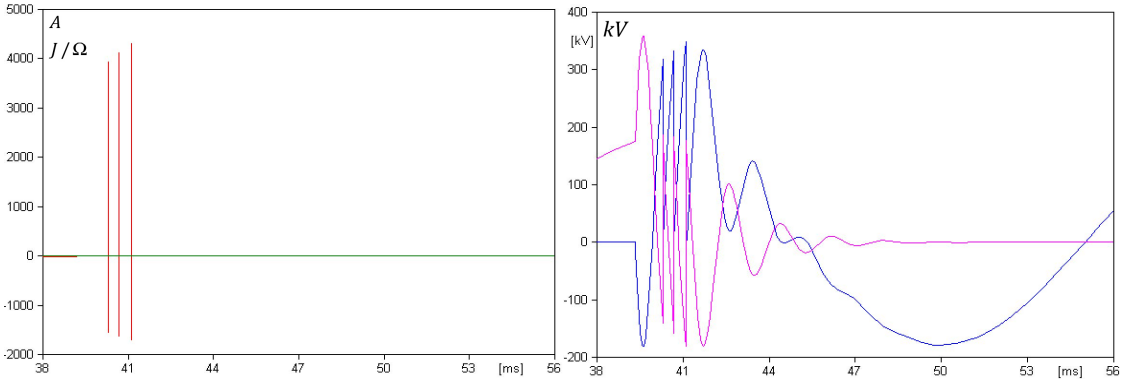

Figure 4.44: Arcing Time equals to $7ms$ at $10A$ Load Current (TG4)

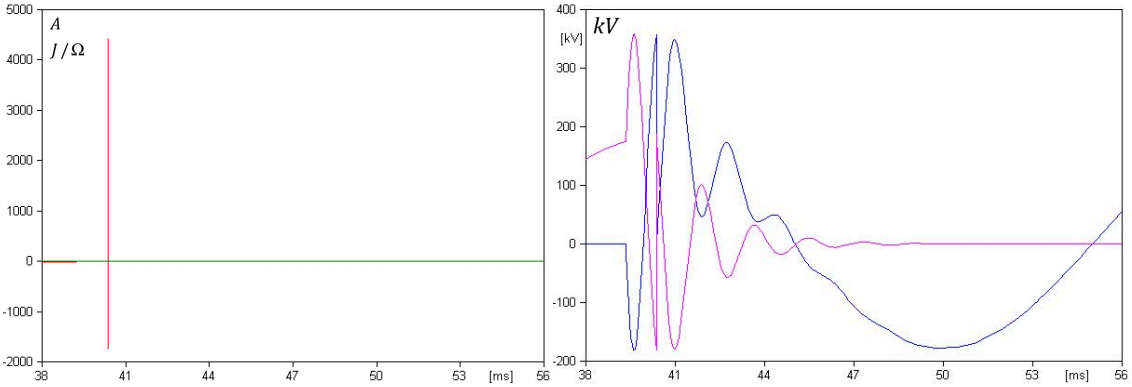

Figure 4.45: Arcing Time equals to $8ms$ at $10A$ Load Current (TG4)

Table 4.7 assembles the data from each of the single test and concludes the result as following:

Table 4.7: Simulation Results for Test Group Four

Load Current (A)	**Arcing time (ms)**	**P (J/Ω)**	**U_{ma} (kV)**	**U_{CB_PK} (kV)**	**U_{load_PK} (kV)**
100	8	20.131	209.38	360.56	190.98
10	2	66.066	295.83	307.32	190.98
	3	49.522	322.43	317.65	317.42
	4	47.038	358.47	334.03	273.09
	5	30.827	358.47	337.70	265.98
	6	19.319	358.47	346.56	246.94
	7	9.366	358.47	347.54	205.27
	8	3.588	358.47	354.23	177.14

Comparing the results obtained from Table 4.4 and 4.7, it shows that 85% off high-frequency current quenching capability makes much greater impact on heat energy generation during multiple re-ignitions than 40% off dielectric recovery rate. The overall heat energy generation in Test Group Four is higher than in Test Group One but still lower than the results in Test Group Three. From the peak voltage values point of view, again, they do not present very significant differences. Yet, slightly lower peak voltage values can be observed in Test Group Four.

4.7 Chapter Conclusions

In this chapter, four test groups have been carried out according to IEC 62271-110. The proposed vacuum and SF_6 circuit-breaker models have been compared under different inductive load conditions. By examining the test results, conclusions for this chapter can be conducted as following:

1. For the same circuit-breaker properties (same D and Q), the load current determines the minimum arcing time. Larger load current leads to longer minimum arcing time and brings more severe overvoltages during re-ignition.

2. At the same load current, shorter arcing time brings higher re-ignition voltage.

3. Solely reduced D or Q can make the minimum arcing time longer but makes no good to the load side re-ignition overvoltage.

4. Reduced D and Q together can lower the possibility of the current interruption within the first attempting, which is good from the prospective of load side voltage.

5. From the point of view of heat energy generation, the proposed vacuum circuit-breaker model would produce more heat during re-ignitions.

The last conclusion point also answers the question that re-ignitions with more number of sections, each section with shorter time duration cause more thermal stress on the contacts of the circuit-breaker.

Chapter 5

Capcitive Current Switching

5.1 Chapter Introduction

In Chapter 5, switching performances between vacuum and SF_6 circuit-breaker models have been compared in terms of small inductive load current breaking condition. In this chapter, similar comparisons will be carried out under capacitive load currents. Particularly on this occasion, both current making and breaking scenarios will be examined.

Strictly speaking, no circuit-breaker, even for class C2, in reality is re-strike free. One of the major objectives in this chapter is trying to figure out when re-strike happens, what reactions can be observed from both type of breaker models.

Pre-strike during capacitive load switching in can normally bring high magnitude and high-frequency inrush current. Another objective of this chapter is comparing the performances between vacuum and SF_6 during pre-strike phenomena happens.

The structure of this chapter is quite similar to Chapter 5.

5.2 IEC Standard Study

The standard which has been referred in this chapter is sub-clause 6.111, Capacitive current switching tests, IEC 62271-100(2008). In relation to this simulation work, the standard will be studied in the following aspects: (1) characteristics of supply circuit, (2) characteristic of the capacitive circuit to be switched, (3) test voltage, (4) test current and (5) criteria to pass the test.

5.2.1 Characteristics of Supply Circuit

According to sub-clause 6.111.3, the impedance of the supply circuit shall not be so low that its short-circuit current exceeds the rated short-circuit current of the circuit-breaker. Further more, for back-to-back capacitor bank breaking current, the capacitance of the supply circuit and the impedance between the capacitor on the supply and load sides shall be such as to give the rated back-to-back capacitor bank inrush making current when testing with 100% of the rated back-to-back capacitor bank breaking current. These two conditions will be ensured in the circuit parameters determination section later. For single-phase laboratory test in general, either terminal of the single-phase supply circuit can be earthed.

5.2.2 Characteristics of the Capacitive Circuit

Sub-clause 6.111.4 gives the possibility that in single-phase laboratory tests, where in case of line- or cable-charging current switching tests it is allowed to replace partly or fully the real lines or cables respectively by concentrated capacitor banks and to use any parallel connection of the conductors in the individual phases with the return current through earth or through a conductor. Therefore, in this chapter, only the capacitor/capacitor banks condition will be studied.

For rated voltage equal to or above $52kV$, the neutral of the capacitor can be earthed.

5.2.3 Test Voltage

The standard required test voltage is based on systems earthing condition. For direct single-phase laboratory tests, the test voltage measured at the circuit-breaker location immediately before the opening shall not be less than the product of $U_r/\sqrt{3}$ and the capacitive voltage factor 1.0 for tests corresponding to normal service in solidly earthed system without significant mutual influence of adjacent phases of the capacitive circuit, typically capacitor banks with earthed neutral.

5.2.4 Test Current

In terms of test current, the standard provides with a set of preferred values of rated capacitive currents. Be quoting Table 9 in IEC 62271-100[13], for circuit-breaker rated at 145kV, relevant data has been concluded in Table These values are chosen

Table 5.1: Preferred Values of Rated Capacitive Switching Currents

	Single capacitor bank	Back-to-back capacitor banks		
Rated voltage U_r(kV)	Rated capacitor bank breaking current $I_{sc}(A)$	Rated back-to -back capacitor bank breaking current $I_{bb}(A)$	Rated back-to-back bank inrush making current $I_{bi}(kA)$	Frequency of the inrush current $f_{bi}(Hz)$
145	400	400	20	4250

for standardisation purposes and cover the majority of typical applications. If different values are needed, any appropriate value, also different form the preferred ones, may be specified as rated value.

5.2.5 Criteria to Pass the Test

There is basically no passing criteria specified for simulation test. However, based on the statement of the related section of IEC standard, it is clear that during

capacitive breaking, no more than one re-strike leading to another loop of power frequency current is acceptable. Therefore, in the following simulation work, only on re-strike will be included in the current breaking operation as a pre-set condition.

5.3 Test Objectives and Grouping

Generally speaking, there are two objectives for this chapter: comparing switching behaviours between SF_6 and vacuum circuit-breakers during capacitive current breaking and making. To achieve this goal a set of tests are to be carried out by well structuralised grouping. In this section, detailed test grouping strategy will be explained from the perspective of the aforementioned two objectives.

5.3.1 Test Grouping for Capacitive Current Breaking

After contact separating and the first current zero, assume no thermal break down happens and no current chopping involves, voltage across the capacitor will keep at its maximum value. Voltage on the source side will oscillate sinusoidally with power frequency. The voltage across the contact gap after current zero, as a result, can be mathematically expressed as:

$$V_{gap} = U_m[\cos(\omega(t - t_0) - \pi)] + U_m, \tag{5.1}$$

where U_m is the peak value of the voltage source,t_0 is the time instance of the power frequency current has been interrupted and ω is the power frequency. The gap voltage, then, varies from 0 to $2U_m$. By performing the first order differential calculation, the changing rate of the gap voltage can be determined as:

$$\frac{dV_{gap}}{dt} = \omega \sin[\omega(t - t_0)]U_m \tag{5.2}$$

The maximum value of the voltage changing ratio can be achieved at the moment when $t - t_0 = 5ms$. (at 50Hz power frequency)

$$\left[\frac{dV_{gap}}{dt}\right]_{max} = \omega U_m = 100\pi \cdot \frac{145kV}{\sqrt{3}} \cdot \sqrt{2} = 37.189kV/ms \tag{5.3}$$

This voltage rising rate is way lower than the designed dielectric recovery rate of the VCB and is also lower than the SF_6 breaker before $t - t_0 = 5ms$. Therefore, dielectric breakdown happens before the first quarter of the voltage cycle (which is also known as re-ignition) will not be discussed here. Instead, study will be focused on dielectric breakdown which happens after the first quarter of the voltage cycle (which is known as re-strike).

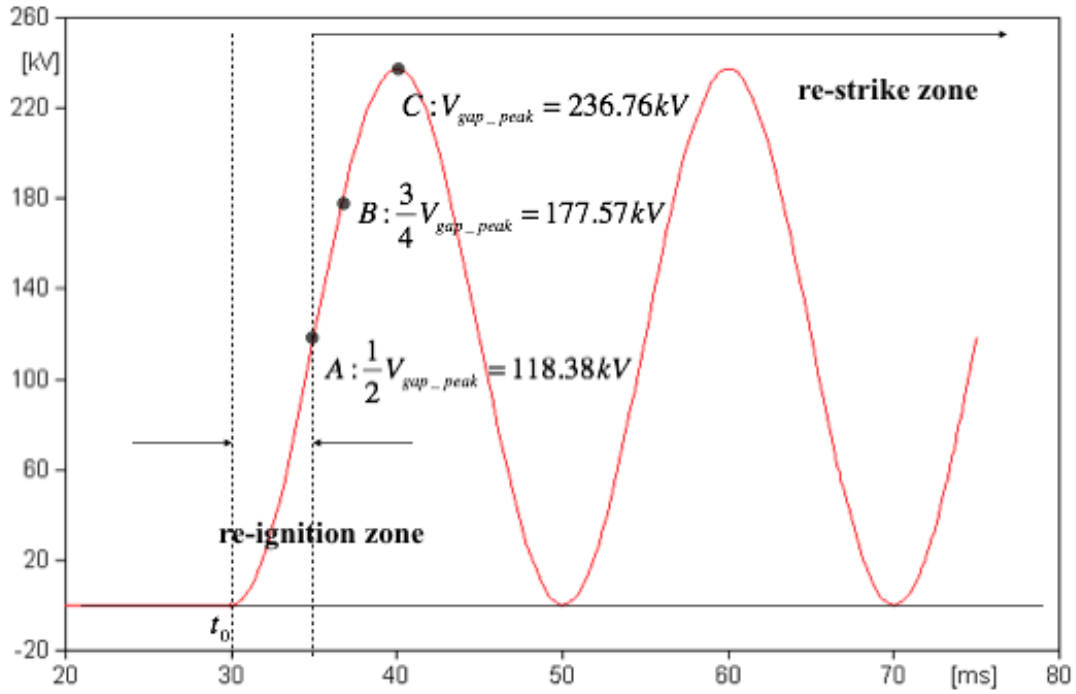

Figure 5.1: Typical Gap Voltage during capacitive current breaking

Dielectric breakdown happening after $5ms$ of the first current zero results in re-strike. Three dielectric breakdown points have been manually set up in the re-strike zone: point A at half of the maximum gap voltage; point B at three quarters of the maximum gap voltage; point C at the maximum gap voltage. To have a deep investigate of the performance comparison between vacuum and SF_6 circuit-breaker

during re-strike, four groups of test are to be carried out. Likewise in Chapter 5, the first test group will test the circuit-breaker switching behaviour in principle of the original vacuum circuit-breaker design. In the last test group, SF_6 breaker model will be tested. In the second and third test group, the breaker models are not physically realistic but have been introduced as intermediate assumptions for comparison purposes only. The same discipline applies to the current making discussion, Section 5.3.2, as well.

- **Test Group One**

Dielectric recovery rate (D), high-frequency current and quenching capability (Q) are assigned to the circuit-breaker logical control box according to the proposed VCB designs. Load side voltage peak value, peak voltage value across the contacts and the accumulated heat energy generated during re-strike at point A, B and C will be recorded. The objective to test group one is setting up a reference line for further comparisons.

- **Test Group Two**

Reduce Q to 15% of its original value while maintain D. Repeat testing procedures at re-strike point A, B and C. The objective to test group two is figuring out the solo influence caused by changing high-frequency current quenching capability.

- **Test Group Three**

In the third test group, dielectric recovery rate of the circuit-breaker will be reduced to 60% of its original value while maintain Q as the setups in test group one. Test procedures will be repeated at re-strike point A, B and C. The objective to test group three is figuring out the solo influence caused by changing dielectric recovery rate.

- **Test Group Four**

In the last test group, Q will be reduced to 15%, D will be reduced to 60% of its original value respectively. The objective is figuring out the overall influences cased by all three circuit-breaker parameters.

5.3.2 Test Grouping for Capacitive Current Making

When considering capacitor banks switching on, pre-strike, e.g., dielectric breakdown happens before contacts physically touching, instead of re-strike, is the major concern. This phenomenon is basically inevitable in every current making operation. The dielectric strength between the contacts gap decreases linearly with contacts closing distance. Because of the designing of the spring mechanism, closing velocity, for both type of circuit-breakers, is much slower than the velocity during opening. Therefore, a dielectric breakdown point can always be found.

According to the requirements made by IEC 62271-100, the maximum inrush current peak value for capacitive load testing is $20kA$ and the maximum frequency is $4,250Hz$. Therefore, it gives the theoretic maximum value of $^{di}/_{dt}$ as:

$$\left(\frac{di}{dt}\right)_{max} = \omega\hat{I} = 2\pi\hat{f}\hat{I} = 2\pi \times 4250 \times 20 \times 10^3 = 5.24 \times 10^8 A/s = 534A/\mu s \quad (5.4)$$

The maximum $^{dt}/_{dt}$ value is located at the first current zero point.

Pre-strike is not horrible but inevitable. Contact voltage is always constrained within the boundary of the decaying dielectric strength. However, question rises with respect to the over magnitude inrush current with different current interrupting media, the high-frequency arc burning between the contacts gap demonstrates different behaviours: for interrupting media with high current quenching capability, VCB for instance, high-frequency current could be interrupted for several times, each time with considerably higher current magnitude; for interrupting media with lower current quenching capability, SF_6 breakers for instance, high-frequency current cannot be interrupted but the arc keeps burning until it damps out to power frequency. Therefore, it is of great interest to investigate which technology causes stronger thermal stress on the contacts material. Another four groups of tests are to be carried out to give an answer to the aforementioned question.

- **Test Group Five**

In this test group, dielectric breakdown will be manipulated at the first voltage peak across the gap after contact starts moving. The contacts closing velocity is set up according to the standard designing, which is 1/4 of the separating velocity of the vacuum circuit-breaker in the small inductive current interrupting tests.

- **Test Group Six**

In the next test group, changes will be made to high-frequency quenching capability only: its value will be reduced from $1000A/\mu s$ down to $150A/\mu s$. All the other conditions remain the same. Repeat the testing procedures in Test Group Five.

- **Test Group Seven**

In the seventh test group, the dielectric decay rate will be reduced to 60% of the original value in test group five. Repeat the testing procedures in Test Group Five.

- **Test Group Eight**

In the last test group, both high-frequency current quenching capability and dielectric decay rate will be reduced to the standard SF_6 breaker level ($150A/\mu s$ and $31kV/ms$ respectively). Repeat the testing procedures in Test Group Five.

5.4 Circuit Arrangement

5.4.1 Typical 145kV Capacitive Switching Circuit

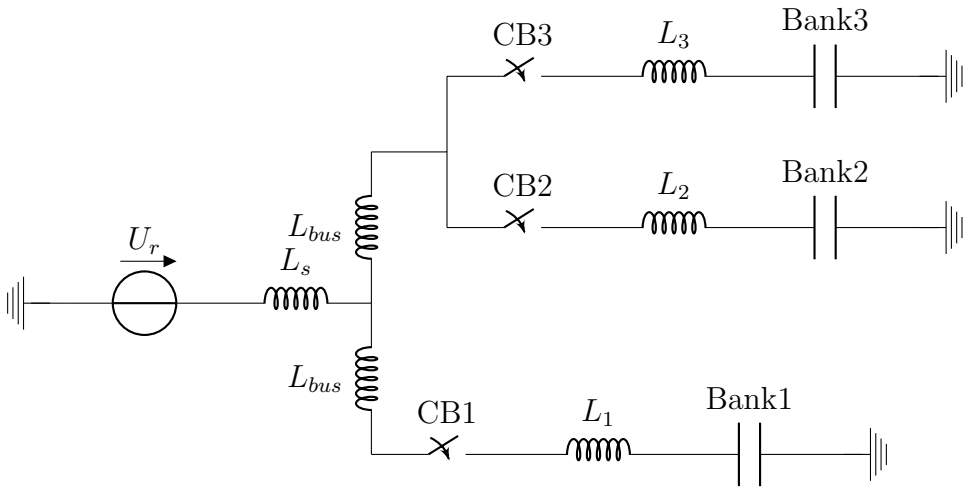

Figure 5.2: Typical 145kV Capacitive Loads Switching Circuit

A typical structure of a 145kV capacitive current breaking circuit composed the following components:

U_r	Single phase voltage source
L_s	Source inductance
L_1, L_2 and L_3	Inductance between circuit-breaker and capacitor bank, including inductance of capacitor bank
L_{bus}	Inductance of bus between switch devices
CB1, 2 and 3	Circuit-breakers
U_{drive}	The voltage of the power source in r.m.s
U_{source}	The voltage value measured immediately at the source side of the circuit-braeker

5.4.2 Test Circuit for Current Breaking

For capacitance current breaking tests, no specific requirement has been made to the source side capacitance and its associated resistance. As a matter of fact, their influence is quite insignificant to the test result. For simplification, these two components will not be included.

As has been discussed earlier in Section 5.2.3, for single phase testing, the multiplier of the source voltage is 1.0. Therefore, the voltage value immediately before opening at the circuit-breaker location is:

$$U_{source} = \frac{U_r}{\sqrt{3}} = \frac{145}{\sqrt{3}} = 83.72kV \tag{5.5}$$

The rated symmetrical short-circuit current for both of these two circuit-breaker types is $31.5kA$. As a result, the source impedance can be calculated as:

$$I_{sc} = \frac{U_{drive}}{\omega L_s} \tag{5.6}$$

For single capacitor bank testing, namely the branch Bank 2 and 3 is not connected, its normal current for circuit-breaker testing purpose is $400A$ in r.m.s. Therefore, the capacitance value of the capacitor bank can be calculated as:

$$\begin{aligned} I_c &= U_{source}\omega C \\ \Rightarrow C &= \frac{I}{\omega U_{source}} = \frac{I}{2\pi f U_{source}} = \frac{400}{100\pi \cdot 83.72 \times 10^3} = 15.2\mu F \end{aligned} \tag{5.7}$$

It is also known that:

$$\frac{U_{drive}}{X_L - X_C} = -I_c \tag{5.8}$$

$$\frac{U_{drive}}{X_L} = I_{sc} \tag{5.9}$$

Solve equation 5.6, 5.7, 5.8 and 5.9, we have the results:

$$X_L = 2.62\Omega \Rightarrow L_s + L_1 + L_{bus} = \frac{X_L}{\omega} = 8.34mH \tag{5.10}$$

$$U_{drive} = 82.652kV \tag{5.11}$$

The inductance associated with the capacitor bank L_1 and bus inductance L_{bus} are extremely small with a typical value of $40\mu H$ and $45\mu H$ respectively, which have very insignificant influence to the overall outcome of the test result. Table 5.2 concludes the parameters of the circuit for capacitive current breaking tests:

Table 5.2: Circuit Parameters for Current Breaking Tests

$U_{drive}(kV)$	$L_s(mH)$	$L_1(\mu H)$	$L_{bus}(\mu H)$	$C(\mu F)$
82.625	8.3	40	45	15.2

5.4.3 Test Circuit for Current Making

For capacitive current making test, the IEC 62271-100 gives detailed requirements for inrush current peak value and frequency.

- **Case One: Energising a bank with two others on the same bus**

$$i_{peak} = 13500\sqrt{\frac{U_r I_1 I_2}{f L_{eq}(I_1 + I_2)}} \tag{5.12}$$

$$f_i = 9.5\sqrt{\frac{f U_r (I_1 + I_2)}{L_{eq}(I_1 I_2)}} \tag{5.13}$$

U_r is the rated voltage (in kV), I_1 and I_2 are the currents (in A) of banks being switched and of banks already energised, respectively. Capacitor bank being switched is assumed uncharged, with closing at the voltage crest of the source voltage. The current used should include the effect of operating the capacitor bank at the effect of operating the capacitor bank at a voltage above nominal rating of

the capacitors and the effect of a positive tolerance of capacitance. In the absence of specific information, a multiplier of 1.15 times normal capacitor current would give conservative result. L_{eq} is the total equivalent inductance per phase between capacitor banks, which equals to $L_{bus} + L_1 + (L_2//L_3)$ in this scenario.

Assume bank 1, 2 and 3 are identical and 2 and 3 already have been connected to the system, working at steady-state. If each of the three capacitor banks has rated current at $400A$, we have:

$$I_1 = 400A \tag{5.14}$$

$$I_2 = 800A \tag{5.15}$$

$$L_{eq} = 45 + 40 + 20 = 115\mu H \tag{5.16}$$

Substituting the results from equation 5.14 to 5.16 back to equation 5.12 and 5.13, we have:

$$i_{peak} = 13500 \times \sqrt{\frac{83.72 \times 400 \times 800 \times 1.15^2}{50 \times 115 \times (400 + 800) \times 1.15}} = 28.53kA \tag{5.17}$$

$$f_i = 9.5 \times \sqrt{\frac{50 \times 83.72 \times (400 + 800) \times 1.15}{115 \times 400 \times 800 \times 1.15^2}} = 3.27kHz \tag{5.18}$$

The above results show that the frequency of the inrush current is within the required rating ($4.25kHz$) but current peak is exceeded ($20kA$). An additional inductance of $120\mu H$ is to be inserted between each banks to limit the peak current value.

$$i_{peak} = 13500 \times \sqrt{\frac{83.72 \times 400 \times 800 \times 1.15^2}{50 \times (115 + 120) \times (400 + 800) \times 1.15}} = 19.96kA \tag{5.19}$$

$$f_i = 9.5 \times \sqrt{\frac{50 \times 83.72 \times (400 + 800) \times 1.15}{(115 + 120) \times 400 \times 800 \times 1.15^2}} = 2.29kHz \tag{5.20}$$

Now, both the frequency and peak value of the inrush current are within the range of IEC standard. Therefore, $80\mu H$ additional inductance will be added to each of the capacitor branch.

• **Case Two: Energising a bank with an equal bank energised**

Using the same branch parameters, we can have the inrush current peak value and frequency as:

$$i_{peak} = 9545\sqrt{\frac{U_r I_1}{f L_{eq}}} = 9545 \times \sqrt{\frac{83.72 \times 400 \times 1.15}{50 \times [45 + 2 \times (40 + 80)]}} = 15.69kA \tag{5.21}$$

$$f_i = 13.5\sqrt{\frac{f U_r}{L_{eq} I_1}} = 13.5 \times \sqrt{\frac{50 \times 83.72}{285 \times 400 \times 1.15}} = 2.41kHz \tag{5.22}$$

The calculation results prove that both the peak value and the frequency of the inrush current are within the range of the IEC standard.

• **Case Three: Energising an isolated bank**

For isolated capacitor bank switching, its peak value and frequency of the inrush current can be obtained by the following equations:

$$i_{peak} = \sqrt{2 I_{sc} I_1} = \sqrt{2 \times 31500 \times 400 \times 1.15} = 5383A \tag{5.23}$$

$$f_i = f\sqrt{\frac{I_{sc}}{I_1}} = 50 \times \sqrt{\frac{31500}{400 \times 1.15}} = 413.8Hz \tag{5.24}$$

Obviously, both of these two values are safely within the required range. Table 5.2 concludes the parameters of the circuit for capacitive current making tests:

Table 5.3: Circuit Parameters for Current Making Tests

$U_{drive}(kV)$	$L_s(mH)$	$L_1(\mu H)$	$L_{additional}(\mu H)$	$L_{bus}(\mu H)$	$C(\mu F)$
82.625	8.3	40	80	45	15.2

5.5 Test Results and Analysis

5.5.1 Test Group One

In Test Group One, original vacuum circuit-breaker parameter set-ups will be tested at three manually determined dielectric breakdown points: point A at $119kV$, point B at $178kV$ and point C at $235kV$ as indicated in Figure 5.1. The heat energy produced in the re-strike process in terms of J/Ω, maximum voltage peck value during re-strike, the number of dielectric breakdowns and the load side voltage after re-strike will be recorded.

(1) **First dielectric breakdown occurs at Point A**

Point A was selected because it is slightly higher than the critical voltage value to cause re-strikes. At this point, it has the fastest voltage rising rate $^{du}/_{dt}$, which makes it the most vulnerable spot to cause a dielectric breakdown.

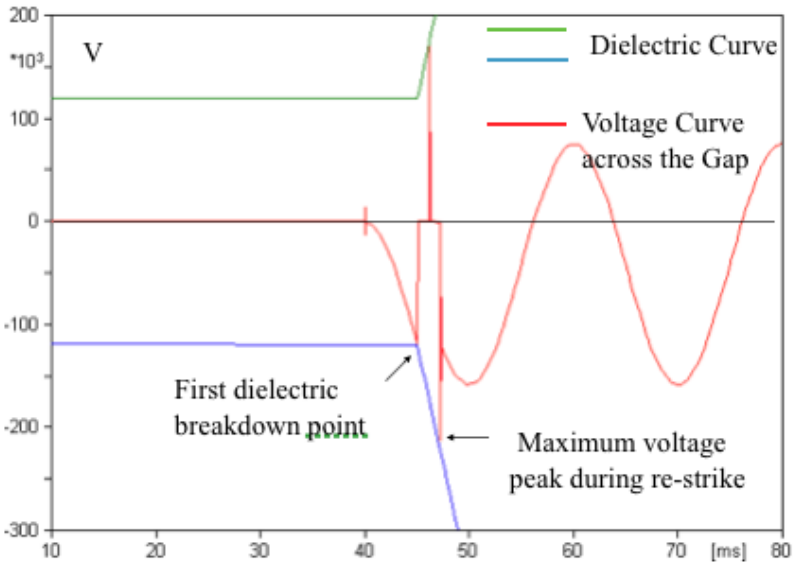

Figure 5.3: Voltage across the Gap with the 1st Dielectric Breakdown Occurs at Point A (TG1)

Figure 5.3 shows the voltage curve between the gap during the capacitive current interrupting process. The red curve represents the voltage wave, whereas the green and blue curves represent the dielectric strength from the perspective of

positive and negative polarities respectively. It can be found that after a small amplitude but high-frequency oscillation, which is caused by the stray capacitance and inductance associated with the circuit-breaker, the voltage experienced two dielectric breakdowns. The third potential dielectric breakdown has been prevented by the rapidly increased dielectric strength. Finally, the high-frequency oscillation has been damped out, oscillated at power frequency with a d.c. offset of $26.73kV$.

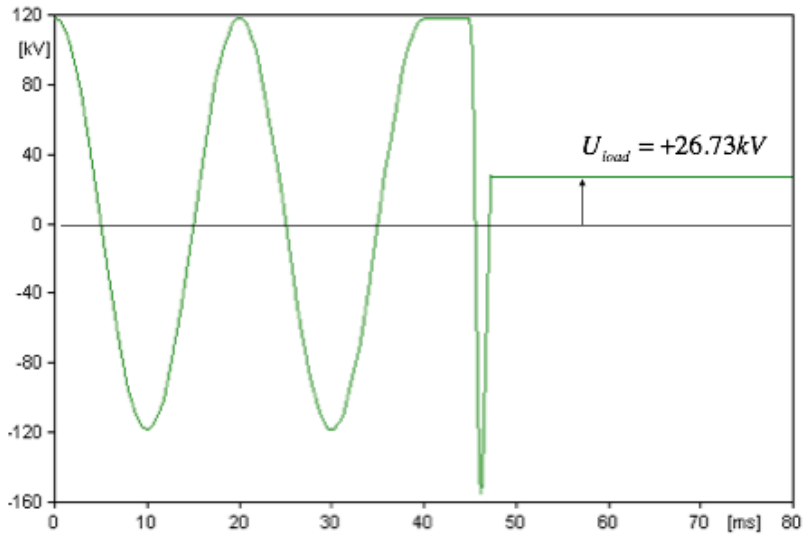

Figure 5.4: Voltage across the Load with the 1st Dielectric Breakdown Occurs at Point A (TG1)

Figure 5.4 shows the voltage curve across the load (including the inductance associated with the capacitor bank). The d.c. offset, which has been mentioned in Figure 5.3, is caused by the electrical charges held by the capacitor bank after current interrupting. The voltage across the load determines the maximum voltage value in the gap after interrupting.

Figure 5.5 shows the inrush current (blue curve) and the accumulated heat energy (purple curve) produced during re-strike. It can be found that although this capacitive inrush current has much lower frequency that the circuit-breaker is able to interrupt it at each of its current zero point, (Please note that at the second current zero, the circuit-breaker actually interrupted the current. However, almost immediately after the interruption another dielectric breakdown took place that

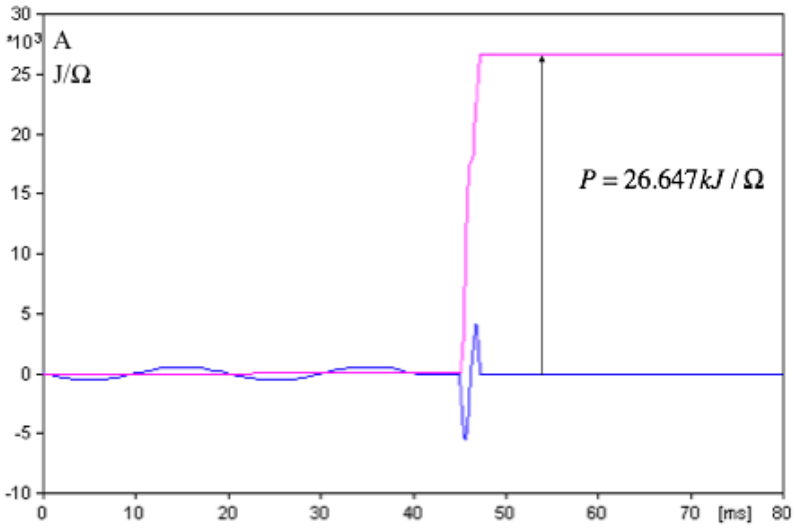

Figure 5.5: Current & Heat Energy Curves with the 1st Dielectric Breakdown Occurs at Point A (TG1)

makes the overall current curve "look like" successive.) the heat energy produced by it is much greater than which has been produced in small inductive multiple re-ignitions.

$U_{max\_peak} = 185.05kV, U_{load} = +26.73kV, P = 26.647kJ/\Omega$ (Please note the positive sign matters here.)

(2) **First dielectric breakdown occurs at Point B**

Point B was selected because it is the median value between the critical point A and the peak point C.

In this scenario, the circuit-breaker experienced two dielectric breakdowns. Because of that, the voltage held by the capacitor bank is still kept on the positive polarity, the voltage peak across the gap after re-strike is slightly higher than the previous case. More heat energy is produced at this circumstance.

$U_{max\_peak} = 277.76kV, U_{load} = +44.21kV, P = 59.015kJ/\Omega$

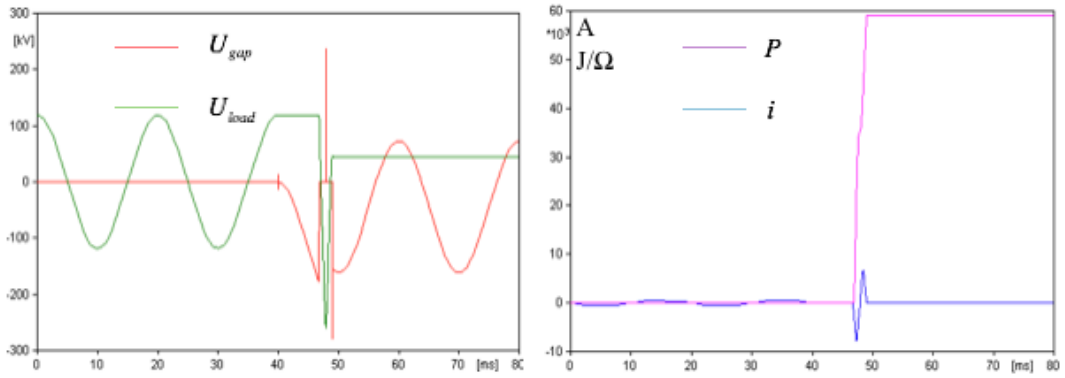

Figure 5.6: 1st Dielectric Breakdown Occurs at Point B (TG1)

(3) **First dielectric breakdown occurs at Point C**

Point C was selected because it is the crest value of the gap voltage after contacts separating, which in theory creates the most severe voltage and current stress on the contact material during re-strike.

$U_{max\_peak} = 348.17kV, U_{load} = -258.9kV, P = 138.17kJ/\Omega$

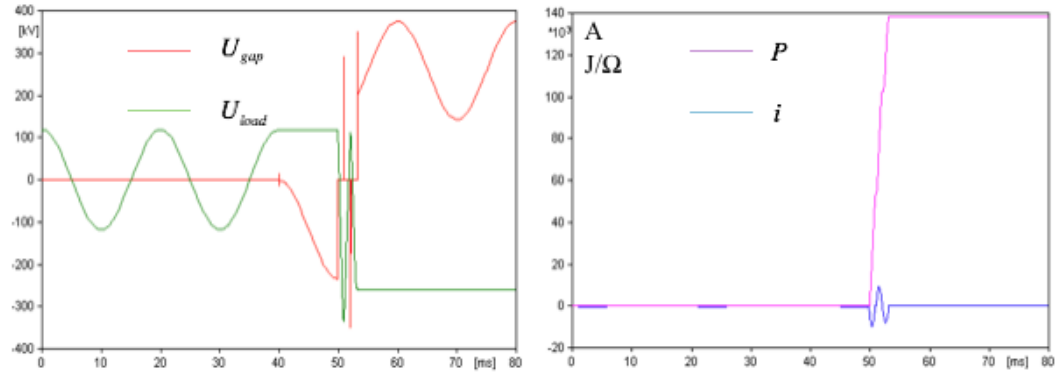

Figure 5.7: 1st Dielectric Breakdown Occurs at Point C (TG1)

As can be found in Figure 5.7, three times of dielectric breakdowns can be observed before the gap voltage damped to power frequency. The voltage held by the capacitor bank is kept at the negative polarity. Thus makes the d.c. offset of the power frequency gap voltage escalating to a higher level. The heat energy produced doubled the value in the previous case.

Table 5.4 concludes the results of Test Group One.

Table 5.4: Simulation Results for Test Group One

1st Dielectric Breakdown Point	Number of Dielectric Breakdowns	Maximum Re-Strike Voltage Peak (kV)	Load Voltage after Re-Strike (kV)	Heat Energy per Resistance (kJ/Ω)
A	2	185.05	+26.73	26.647
B	2	277.76	+44.21	59.015
C	3	348.17	-258.9	138.17

By analysing the above results, it is clear that the with increased first dielectric breakdown voltage level, the number of breakdowns afterwards, maximum re-strike voltage and the heat energy produced are all increased. Due to the limitation of the dielectric recovery rate, the load side voltage is restrained within an acceptable level. Thus makes the maximum voltage value between the gap not escalating extremely.

5.5.2 Test Group Two

In Test Group Two, the high-frequency current quenching capability of the circuit-breaker model will be reduced to 15% of its original value. Again, this circuit-breaker model does not exist in reality. It is introduced for comparison of the influence caused by different Q values purpose only.

$U_{max\_peak} = 185.05kV, U_{load} = +26.73kV, P = 26.647kJ/\Omega$

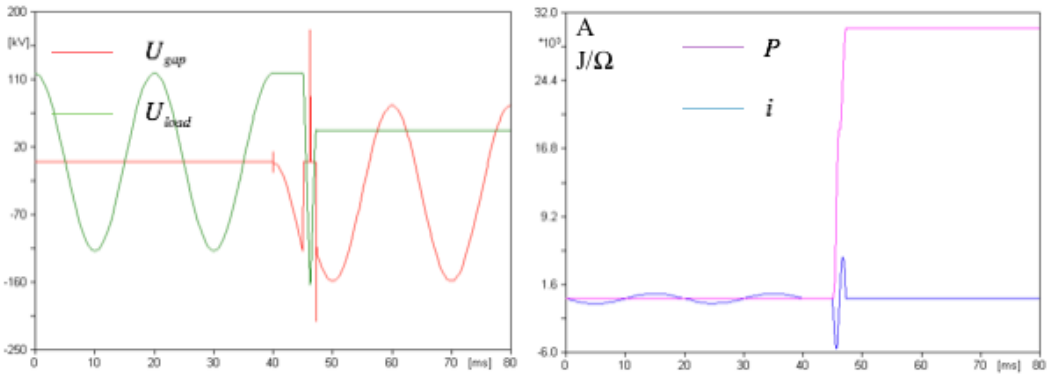

Figure 5.8: 1st Dielectric Breakdown Occurs at Point A (TG2)

$U_{max\_peak} = 277.76kV, U_{load} = +44.21kV, P = 59.015kJ/\Omega$

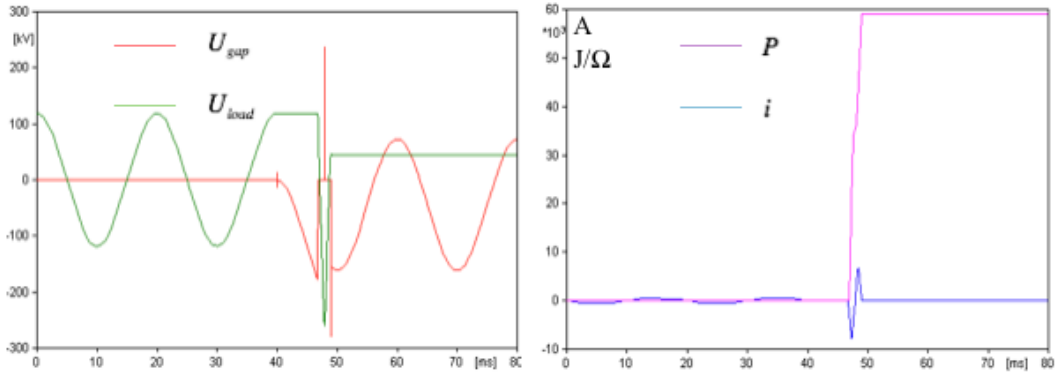

Figure 5.9: 1st Dielectric Breakdown Occurs at Point B (TG2)

$U_{max\_peak} = 348.17kV, U_{load} = -258.9kV, P = 138.17kJ/\Omega$

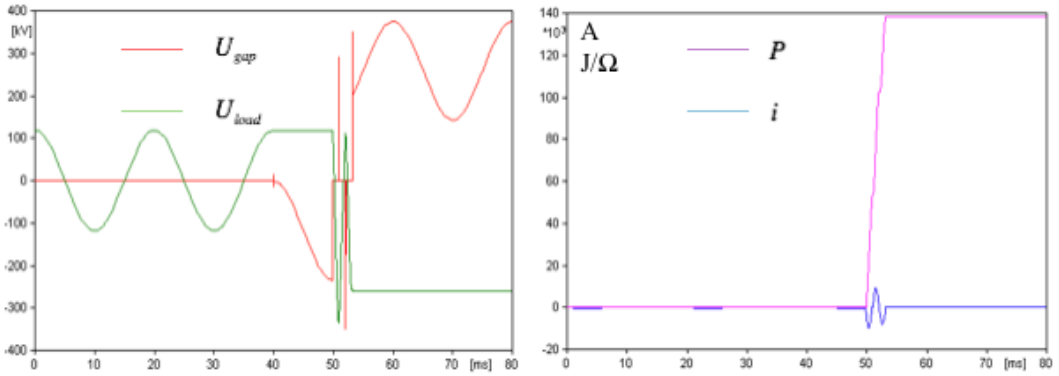

Figure 5.10: 1st Dielectric Breakdown Occurs at Point C (TG2)

Table 5.5 concludes the results of Test Group Two.

Table 5.5: Simulation Results for Test Group Two

1st Dielectric Breakdown Point	Number of Dielectric Breakdowns	Maximum Re-Strike Voltage Peak (kV)	Load Voltage after Re-Strike (kV)	Heat Energy per Resistance (kJ/Ω)
A	2	185.05	+26.73	26.647
B	2	277.76	+44.21	59.015
C	3	348.17	-258.9	138.17

There is no surprise that the results obtained in Test Group Two match the results from Test Group One. Because the value of $^{di}/_{dt}$ at the first current zero after re-strike is so low that even the Q parameter reduced circuit-breaker model can interrupt the current without any problems. According to this, we can safely draw the conclusion

that the high-frequency has no influence on the performance of capacitive load interrupting.

5.5.3 Test Group Three

In Test Group Three, similarly, only the dielectric recovery rate will be reduced to 60% of its original level to check its solo influence on the performance.

$U_{max\_peak} = 185.05kV, U_{load} = +26.73kV, P = 26.650kJ/\Omega$

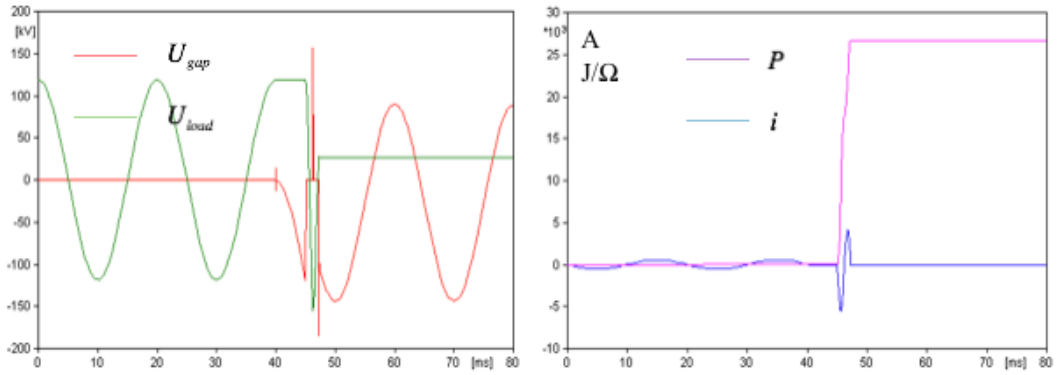

Figure 5.11: 1st Dielectric Breakdown Occurs at Point A (TG3)

$U_{max\_peak} = 264.88kV, U_{load} = -264.48kV, P = 83.239kJ/\Omega$

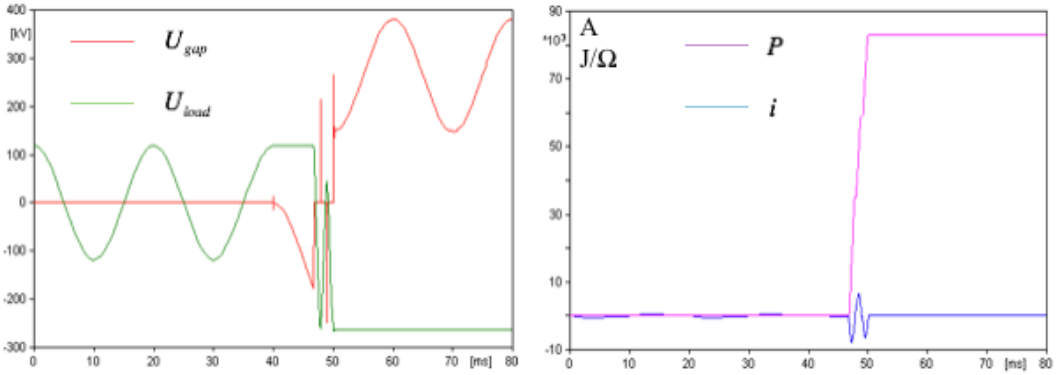

Figure 5.12: 1st Dielectric Breakdown Occurs at Point B (TG3)

$U_{max\_peak} = 321.66kV, U_{load} = +154.45kV, P = 180.01kJ/\Omega$

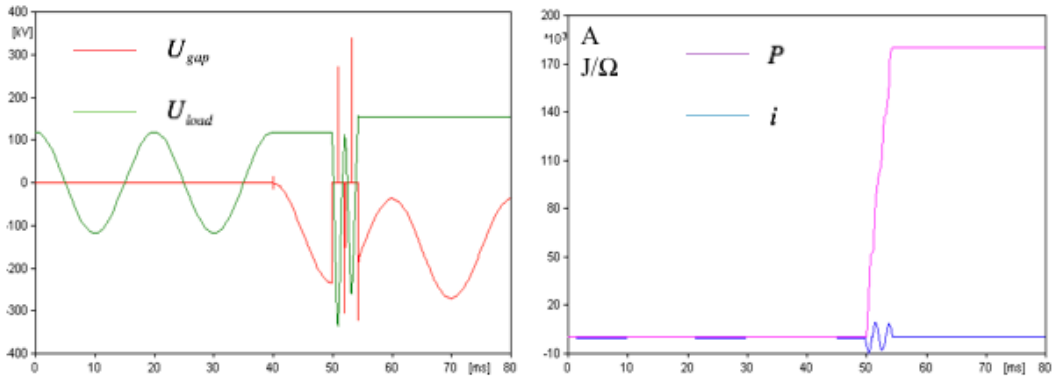

Figure 5.13: 1st Dielectric Breakdown Occurs at Point C (TG3)

Table 5.6 concludes the results of Test Group Three. Comparing the results obtained

Table 5.6: Simulation Results for Test Group Three

1st Dielectric Breakdown Point	Number of Dielectric Breakdowns	Maximum Re-Strike Voltage Peak (kV)	Load Voltage after Re-Strike (kV)	Heat Energy per Resistance (kJ/Ω)
A	2	185.05	+26.73	26.647
B	3	264.88	-264.48	83.239
C	4	321.66	+154.45	180.01

from Table 5.6 to those from Table 5.5 and 5.4, it can be found that when the first dielectric breakdown happens at the critical point, dielectric recovery rate makes very limited influence to the performance that the results are almost identical. When the first dielectric breakdown happens at a higher voltage level, say median value point B and crest point C, circuit-breaker model with lower dielectric recovery rate tends to have more numbers of re-strikes to achieve a voltage steady-state, which, consequently, leads to more pronounced heat energy generation. From the point of view of voltage, the maximum voltage peak between the gap is slightly lower in a circuit-breaker model with lower dielectric recovery rate at each of the testing points. The load steady-state voltage, however, depends on the parity of the total number of re-strikes. If the number is odd, the voltage on the capacitor bank will be kept on the opposite polarity of the original charge, which makes it stands at a higher place. On the other hand, if the number is even, the voltage will be kept on the same polarity, which makes it stands at a lower place. Nevertheless, in either

of the cases, the voltage is limited by the dielectric strength. In the worst case, the maximum voltage stress is as high as $3p.u.$ rated voltage crest.

5.5.4 Test Group Four and Conclusion

Similarly as what happened in Test Group Two, the test results obtain from Test Group Four match with those from Test Group Three for the same reason. To avoid redundancy, figures and tables will not be presented here again.

To sum up the first four tests groups, the comparison shows that in terms of voltage stress on the circuit-breaker contacts, the SF_6 technology is slightly superior over the vacuum technology. However, due to its slower dielectric recovery rate, it will need to experience more numbers of re-strikes to achieve a steady-state voltage. As a result, the heat energy produced by an SF_6 circuit-breaker in a capacitive load interrupting task is considerably larger than a vacuum circuit-breaker.

5.5.5 Test Group Five

From Test Group Five to Eight, focusing will be put on capacitor banks energising. Each test group contains three case studies, which are (1) energising a third capacitor bank while two banks with equal branch parameters are already energised and working at steady-state; (2) energising a second capacitor bank with another identical bank branch is energised and working at steady-state; (3) energising an isolated capacitor bank. In each of the case studies, dielectric breakdown caused by closing contacts gap will be manipulated at the power frequency voltage crest to simulate the worst scenario which brings the most severe inrush current. The total number of pre-strikes and accumulated heat energy produced in the energising process will be recorded and analysed.

In the first of the rear four test groups, original vacuum circuit-breaker parameter set-ups will be tested.

(1) **Energising a third bank when two identical branches are energised**

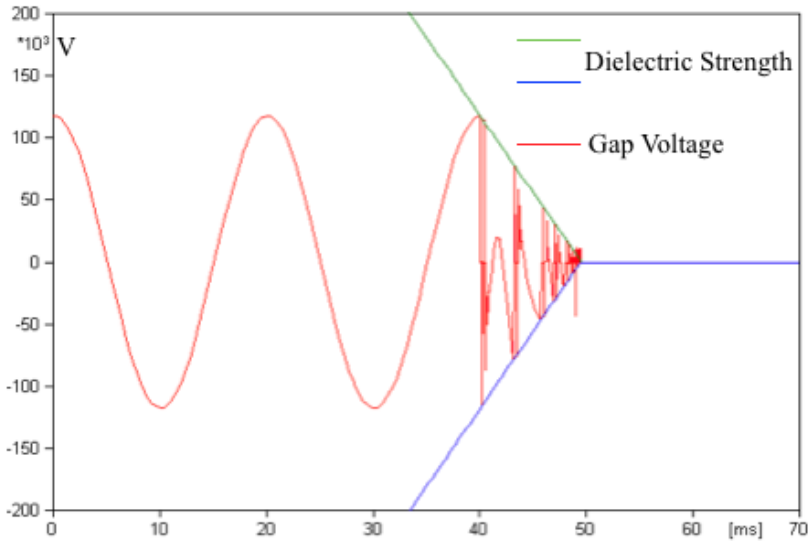

Figure 5.14: Voltage across the Gap when Energising a third Bank (TG5)

20 times of major pre-strikes can be observed in Figure 5.14. Due to the limitation of the reducing dielectric strength, no overvoltage is involved in this process.

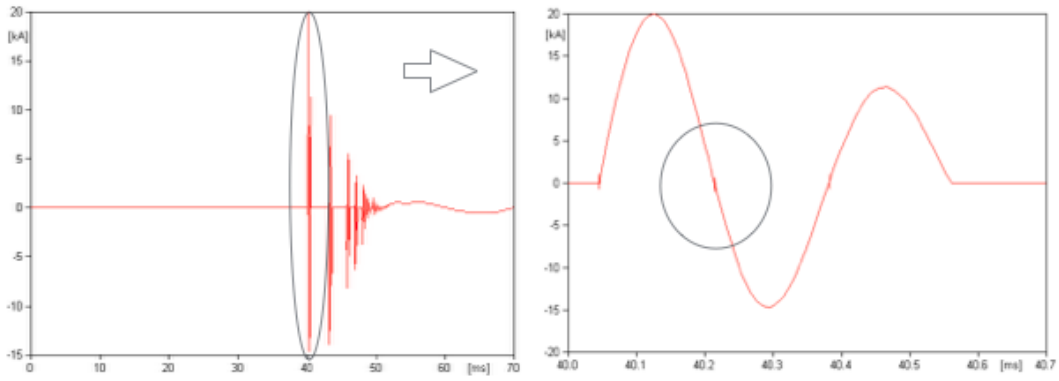

Figure 5.15: Inrush Current when Energising a third Bank (TG5)

On the left hand side of Figure 5.15, it shows the overall picture of the inrush current when experiencing multiple pre-strikes. On the right hand side, is the detailed waveform of such current at its first pre-strike. Small amplitude but high-frequency oscillations can be found at the first and second current zero in the right hand side

figure. It means that the vacuum circuit-breaker model is able to interrupt the most severe inrush current at its highest $^{di}/_{dt}$ point. (See the calculation in Chapter 5.3.2)

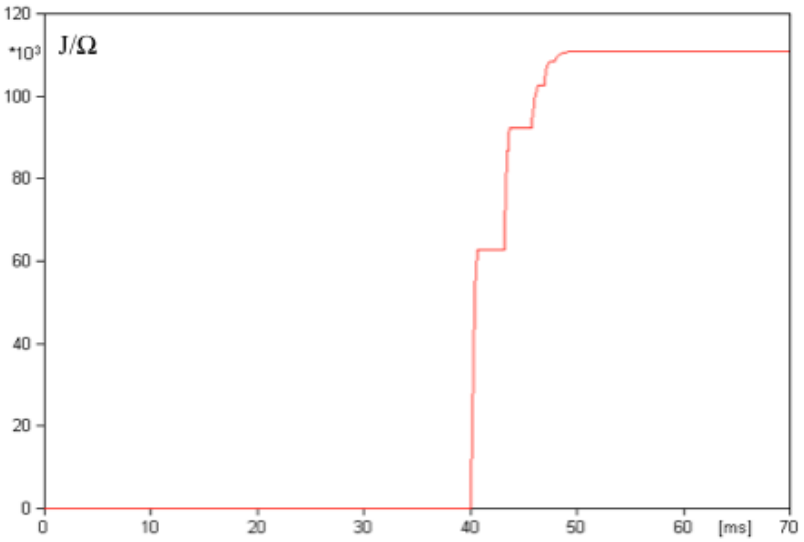

Figure 5.16: Accumulated Heat Energy produced when Energising a third Bank (TG5)

Figure 5.16 shows the accumulated heat energy in terms of Joule per Ohm. It is way larger than a small inductive current interrupting operation but in the same scale with capacitive load interrupting.

(2) **Energising a bank when another identical branch is energised**

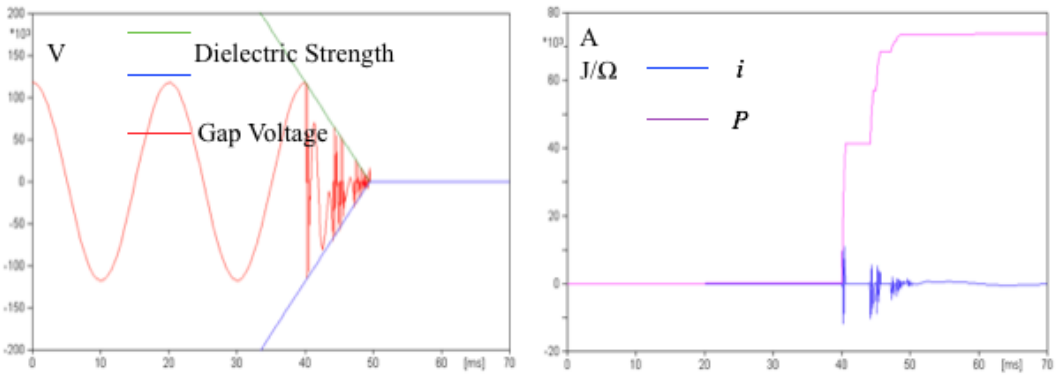

Figure 5.17: Energising a Bank when another Bank is energised (TG5)

When considering energising one capacitor bank with another identical branch is already energised, it can be found that the number of major pre-strikes increased.

However, because the amplitude of the inrush current is considerably lower than the pervious case, plus the time interval between the first two pre-strikes is prolonged, the overall heat energy is less produced.

(3) **Energising an isolated capacitor bank**

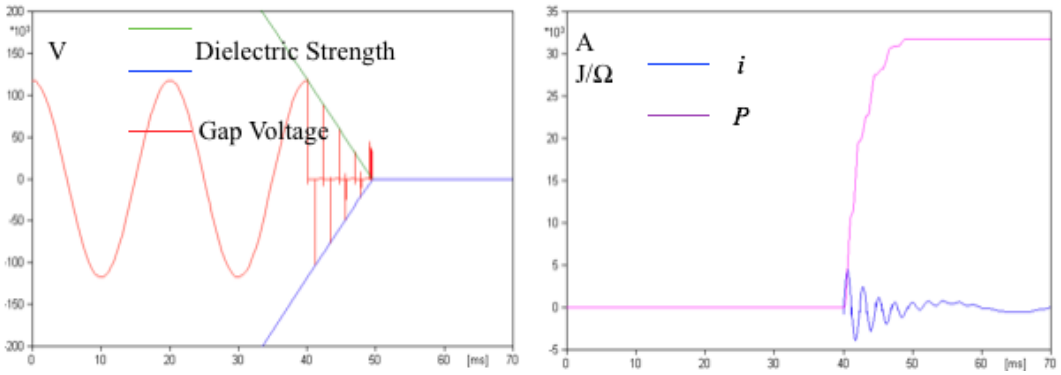

Figure 5.18: Energising an isolated capacitor bank (TG5)

As for energising an isolated capacitor bank, the total number of major pre-strikes is much lower than the last two cases. Correspondently, the overall heat energy produced is much lower as well.

Table 5.7: Simulation Results for Test Group Five

Number of Capacitor Banks Involved	Number of Major Pre-strikes	Accumulated Heat Energy (kJ/Ω)
3	20	110.75
2	22	71.358
1	9	31.785

Table 5.7 concludes the testing results obtained from Test Group Five. It is very clear that with more number of capacitor bank branches involved, it brings higher amplitude of inrush current, which consequently leads to higher heat energy producing. In terms of total number of major pre-strikes, there is no clear regular pattern. We can only tell that with a single capacitor bank involves, the total number reduced significantly.

5.5.6 Test Group Six

In this test group, circuit-breaker model with reduced high-frequency current quenching capability Q will be tested at the three aforementioned scenarios.

(1) **Energising a third bank when two identical branches are energised**

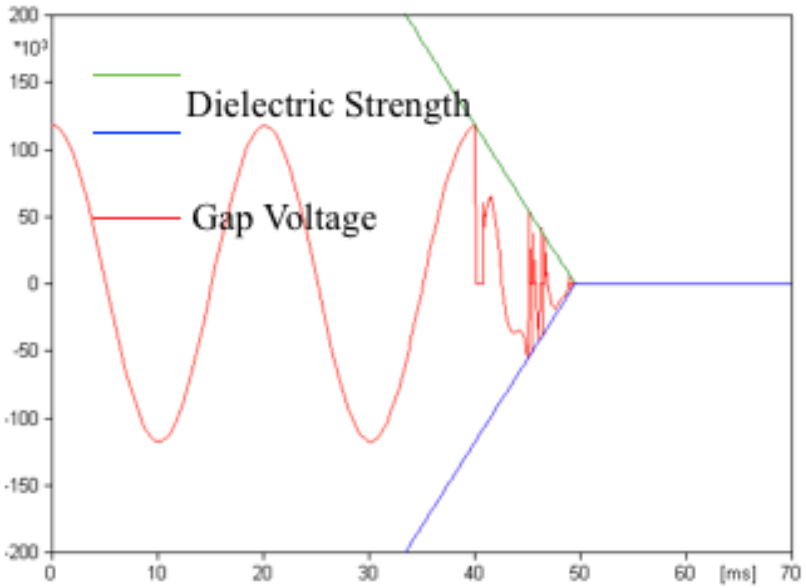

Figure 5.19: Voltage across the Gap when Energising a third Bank (TG6)

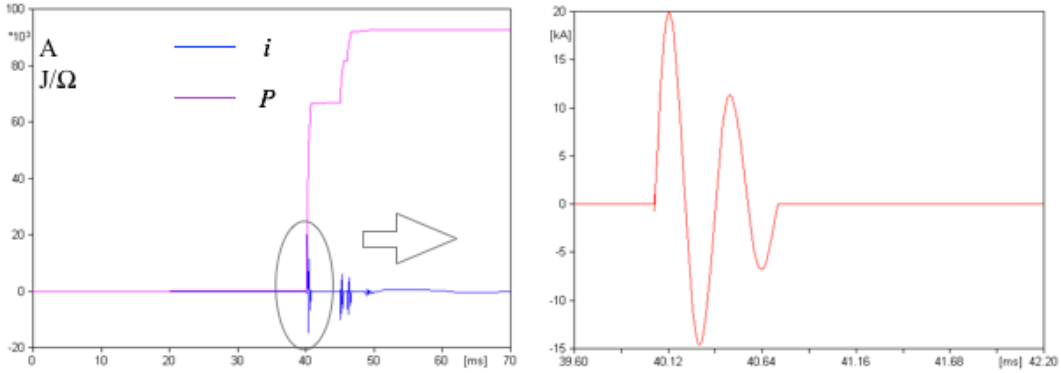

Figure 5.20: Inrush Current & Heat Energy when Energising a third Bank (TG6)

With reduced high-frequency current quenching capability Q, the circuit-breaker model is unable to interrupt the inrush current until the fourth current zero. (Figure 5.20, right hand side) However, because of the reducing of the dielectric

strength, the amplitude of each following per-strike voltages is getting lower and lower. Circuit-breaker model with reduced Q is still able to interrupt those currents with low $^{di}/_{dt}$. The number of major pre-strike, therefore, is reduced tremendously due to that change.

(2) **Energising a bank when another identical branch is energised**

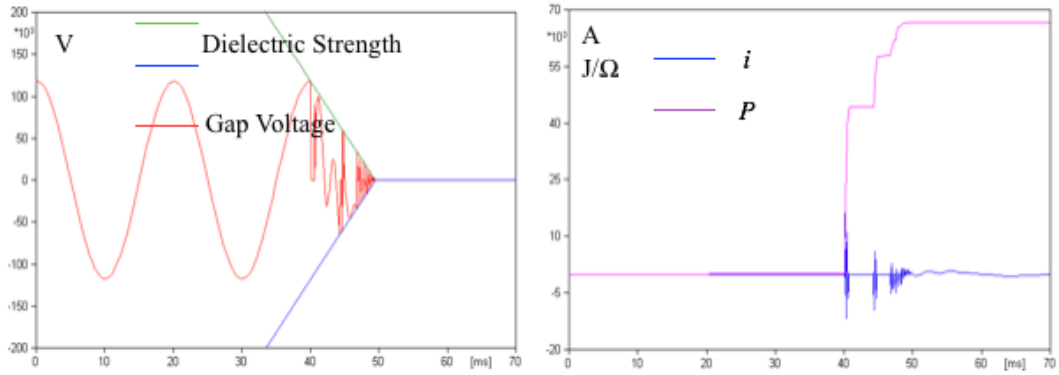

Figure 5.21: Energising a Bank when another Bank is energised (TG6)

(3) **Energising an isolated capacitor bank**

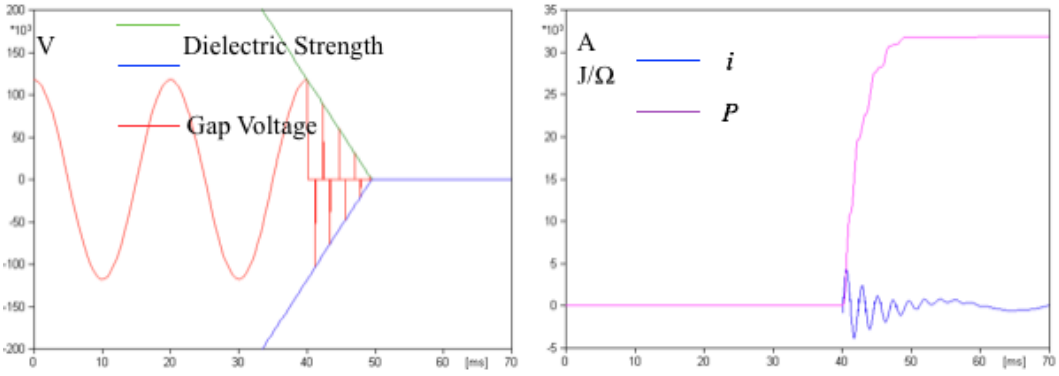

Figure 5.22: Energising an isolated Capacitor Bank (TG6)

Table 5.8 concludes the testing results obtained for Test Group Six. Comparing Table 5.8 to Table 5.7, it can be found that with three and two capacitor banks involved, circuit-breaker model with reduced Q produces less heat energy and fewer number of major per-strikes. As for isolated bank energising, because the $^{di}/_{dt}$ at the

Table 5.8: Simulation Results for Test Group Six

Number of Capacitor Banks Involved	Number of Major Pre-strikes	Accumulated Heat Energy (kJ/Ω)
3	10	92.586
2	15	66.716
1	9	31.773

first current zero of the inrush current is lower than the reduced Q, the test result from TG6 is almost identical as what has been acquired from TG5. The influenced solely caused by high-frequency current quenching capability is obvious: it reduces the heat energy producing.

5.5.7 Test Group Seven

In the seventh test group, the high-frequency current quenching capability Q will be restored to the original level while reducing the dielectric decreasing rate D to 60% of its original value. Repeat the three case studies again.

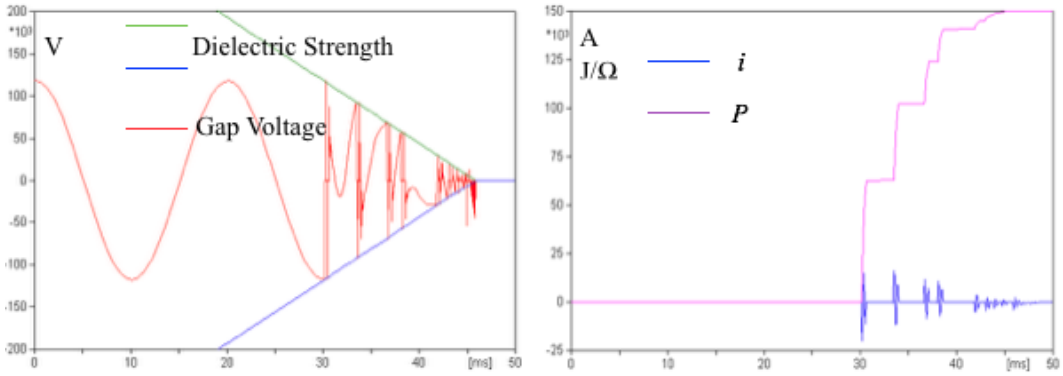

Figure 5.23: Energising a third Bank (TG7)

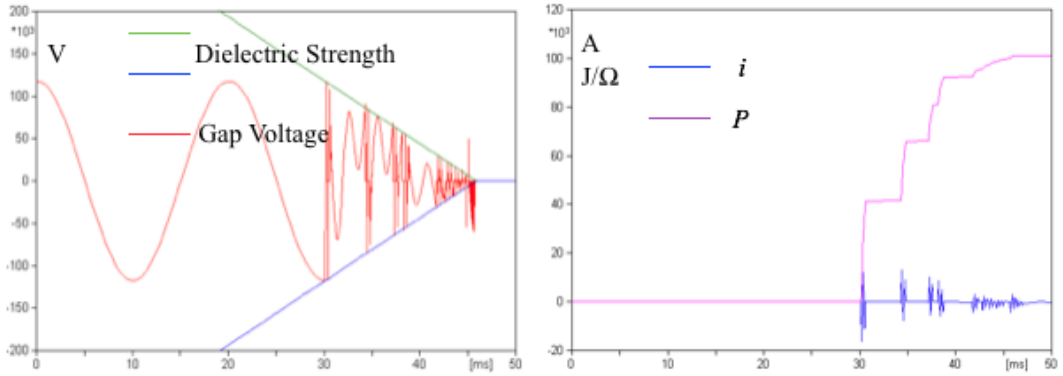

Figure 5.24: Energising a Bank when another Bank is energised (TG7)

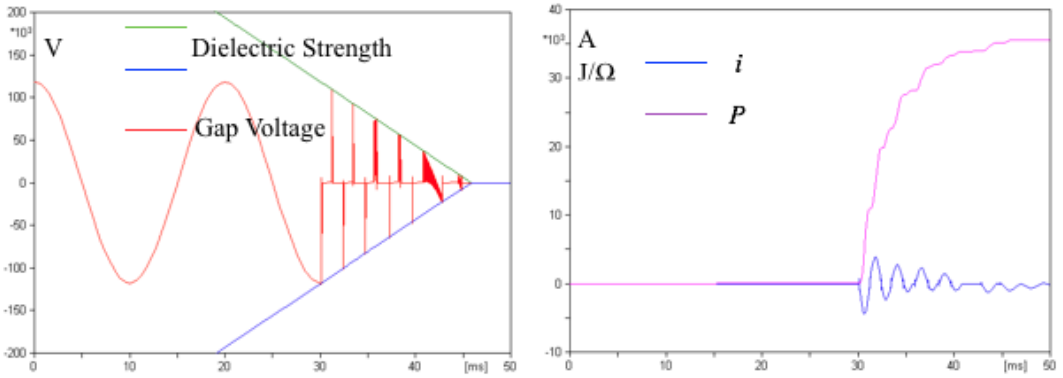

Figure 5.25: Energising an isolated Capacitor Bank (TG7)

Table 5.9 concludes the testing results obtained from Test Group Seven.

Table 5.9: Simulation Results for Test Group Seven

Number of Capacitor Banks Involved	Number of Major Pre-strikes	Accumulated Heat Energy (kJ/Ω)
3	20	149.88
2	26	101.07
1	11	35.608

Because the reduced dielectric decreasing rate prolonged the energising process, both of the number of major pre-strikes and heat energy are increased in all three cases. Circuit with more capacitor bank branches involved is more pronounced with this tendency. The sole influenced caused by reduced dielectric decreasing rate is it brings more heat energy.

5.5.8 Test Group Eight

In the last test group, both high-frequency current quenching capability Q and dielectric decreasing rate D will be reduced in order to simulate the standard SF_6 model and its performance.

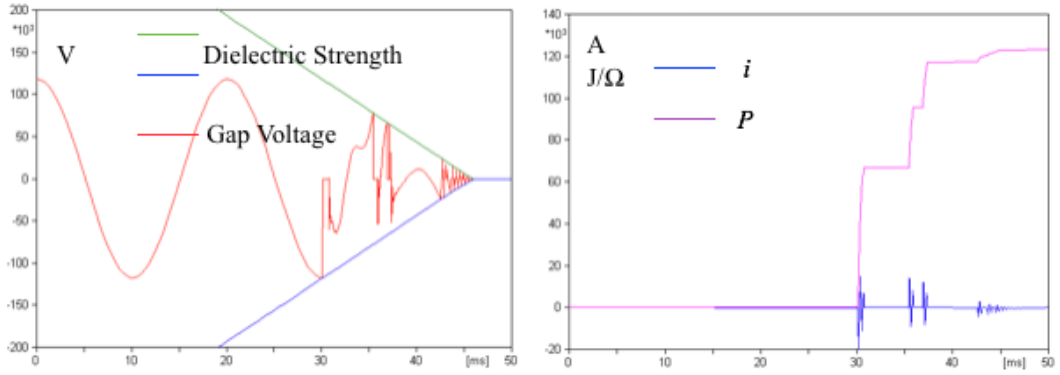

Figure 5.26: Energising a third Bank (TG8)

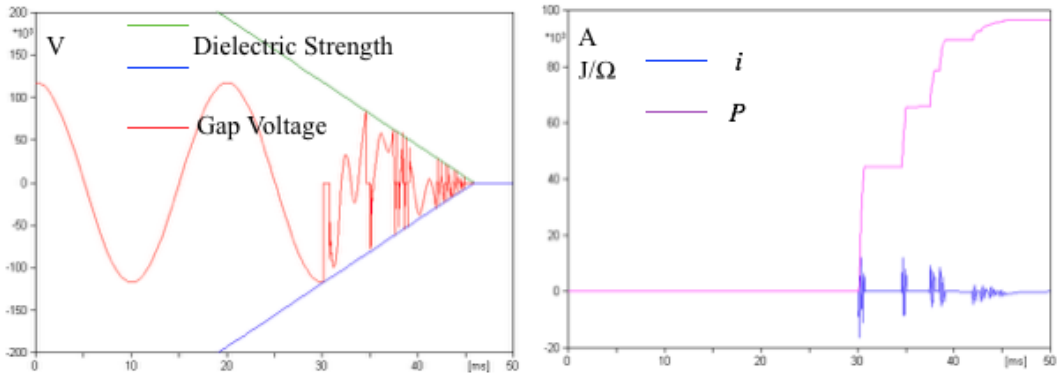

Figure 5.27: Energising an isolated Capacitor Bank (TG8)

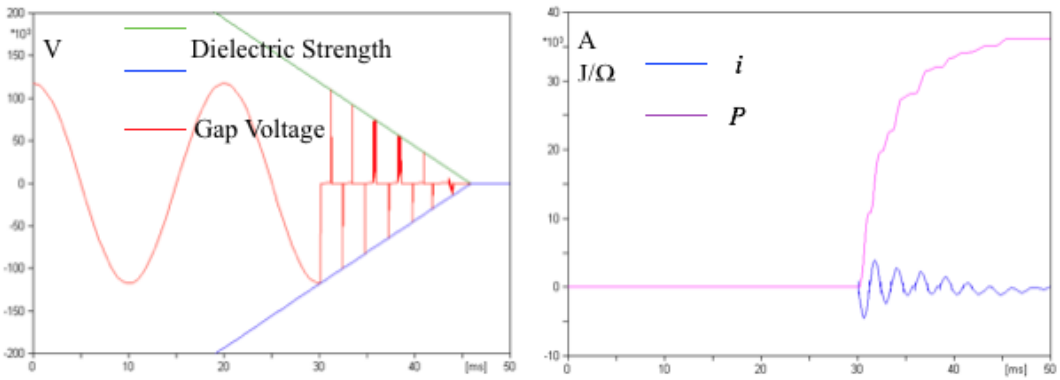

Figure 5.28: Energising an isolated Capacitor Bank (TG8)

Table 5.10 concludes the testing results obtained from Test Group Eight.

Table 5.10: Simulation Results for Test Group Eight

Number of Capacitor Banks Involved	Number of Major Pre-strikes	Accumulated Heat Energy (kJ/Ω)
3	12	123.16
2	22	96.654
1	12	35.171

By comparing Table 5.10 to Table tb5.7, we can have the conclusion that the influenced caused by 40% off dielectric decreasing rate is greater than the influenced caused by 85% off high-frequency current quenching capability. However, that does not mean vacuum circuit-breaker must have better performance than SF_6 breaker in reality. Because the high-frequency current quenching capability adopted in these tests is the same value which has been used in small inductive current interrupting. Actually, this parameter can be modified by adjusting the volume of gas blowing to the tube. In another word, if we can reduce the Q parameter in an SF_6 breaker to a much lower level, the influence caused by Q could be greater than D. Here is an example. Reducing Q to zero while keeping D at the same level as in TG8 and repeating the test with three capacitor bank branches involved, we have the following test result:

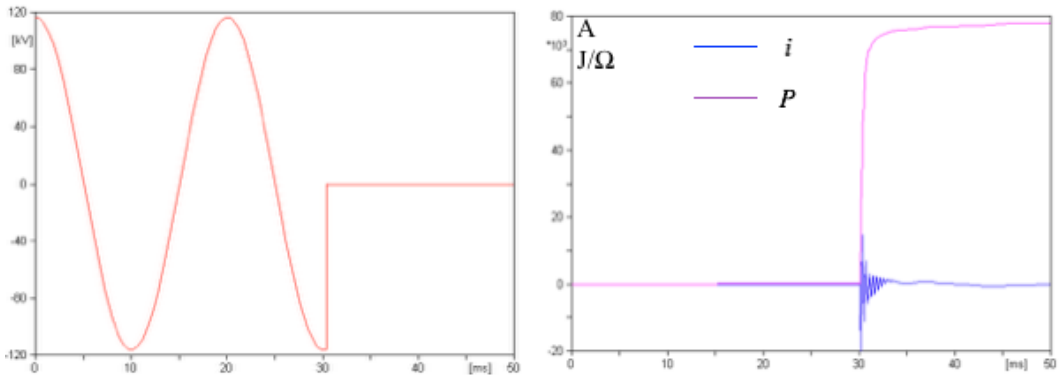

Figure 5.29: Simulation Result with Q completely removed

With Q completely removed, the circuit-breaker model is unable to interrupt any current during this process. Therefore, no multiple pre-strike can be observed and the high-frequency arcing current keeps burning until it damps out to power

frequency. The overall heat energy produced in this test is $77.942kJ/\Omega$, which is lower than the result obtained from TG5, $110.75kJ/\Omega$.

5.6 Chapter Conclusions

In this chapter, comparisons of capacitive current switching performances between vacuum and SF_6 circuit-breaker have been studied in two scenarios: current interrupting and current making. Test results tell us re-strike and pre-strike are the major concerns in each of the scenarios. By examining them carefully, conclusions for this chapter can be conducted as following:

1. Generally speaking, the thermal energy produced in a energising or de-energising capacitive loads operation is much pronounced than in an inductive load interrupting operation, usually in the order of 10^3.

2. For vacuum circuit-breakers, due to its rapid contacts separating velocity and outstanding dielectric strength vs. gap distance ratio, the possibility of re-strike is low. For SF_6 circuit-breakers, the possibility of re-strike is slightly higher.

3. In case re-strike takes place, no matter at which voltage level, one or more following up re-strikes are to be expected within the same power frequency current loop. This conclusion applies to both of the two breaker models.

4. In terms of capacitive load energising operations, circuit-breaker performance is highly dependent on its high-frequency current quenching capability. If the SF_6 circuit-breaker keeps its quenching capability at the same level as what has been assumed in an inductive load interrupting model, it would produce more thermal energy duo to its lower dielectric decaying rate. On the other hand, if the manufacture can design a new gas blowing mechanism that deletes its quenching capability in a capacitive load energising operation, the continuous burning arc would bring lower thermal stress on the contact material.

Chapter 6

Short-Line Fault Switching

6.1 Chapter Introduction

In Chapter 5 and 6, SF_6 and vacuum circuit-breakers have been studied when switching inductive and capacitive load duties. For both two cases, breakers are supposed to be working under normal conditions. The current level is in the order of up to hundreds of Amps. Therefore, breakdown caused by dielectric failure is the major concern after the first current zero. When considering faulty conditions, on the other hand, thermal breakdown is involved, which has the possibility to take place prior to the dielectric breakdown. In this chapter, circuit-breaker performances under faulty conditions, particularly shot-line fault (SLF), will be compared.

One of the objectives of this chapter is introducing the Mayr's arcing model to replace the high-frequency current quenching capability fixed circuit-breaker model in SF_6 breaker as what has been adopted in the previous two chapters in order to check its performance under thermal stress.

Transient recovery voltage (TRV) in SLF condition is much more severe than that in a terminal fault condition. Because of the wave reflection from the faulty spot of the transmission line, the initial transient recovery rate (ITRV) of the TRV, which

is the superposition TRV from the source side and faulty side of the circuit-breaker contacts, could be extremely high. Consequently, it is highly possible that a dielectric breakdown takes place at an even low transient recovery voltage level. The other objective of this chapter, therefore, is comparing the performance between SF_6 and vacuum circuit-breakers when experiencing early dielectric breakdowns.

The structure of this chapter is very similar to the previous two chapters.

6.2 IEC Standard Study

The standard which has been referred in this chapter is sub-clause 6.109, Short-line fault tests, and a part of sub-clause 6.104, Short-circuit test quantities, IEC 62271-100(2008). In relation to this simulation work, the standard will be studied in the following two aspects: (1) Applicability, (2) Test current, and (3) Test circuit.

6.2.1 Applicability

Applicability According to sub-clause 6.109.1 of IEC 62271-100, the short-line fault tests are applicable only to class S2 circuit-breakers designed for direct connection to overhead lines, irrespective of the type of network on the source side, having a rated voltage of 15kV and above and a rated short-circuit breaking current exceeding $12.5kA$.

In my case, the circuit-breaker models have been studied are rated at $145kV$ in voltage as a general setup and $31.5kA$ and $63kA$ in current for grouping purpose. Both of these parameters are within the required range of the specification of the standard.

6.2.2 Test Current

Sub-clause 6.109.2 states that the test current shall take into account the source and line side impedance. The source side impedance shall be that corresponding to approximately 100% rated short-circuit breaking current I_{sc} and the phase-to-earth value of the rated voltage U_r . In my case the rated short-circuit current will be studied at $31.5kA$ and $63kA$ respectively.

Standard values of the line side impedance are specified corresponding to a reduction of the a.c. component of the rated short-circuit breaking current to 90% (L_{90}) and 75% (L_{75}) for circuit-breakers with a rated voltage equal to or higher than $48.3kV$.

Because, in general, the RRRV generated by L_{90} is much more severe than L_{75}, only L_{90} will be included in the following context.

6.2.3 Test Circuit

The test circuit shall be single-phase and consists of a supply circuit and a line circuit. Sub-clause 6.109.3 gives three possible test circuits for short-line fault test. Regarding the time delays on the source side and on the line side and the ITRV, two main requirements are specified and shall be distinguished:

a) source side: with time delay (t_d) and without ITRV;
line side: with time delay(t_{dL})

b1) source side: with ITRV;
line side: with time delay(t_{dL})

b2) source side: with time delay (t_{dL});
line side: with insignificant time delay(t_{dL})

In Annex A of the standard, it gives a flowchart[1] for choosing the test circuit.

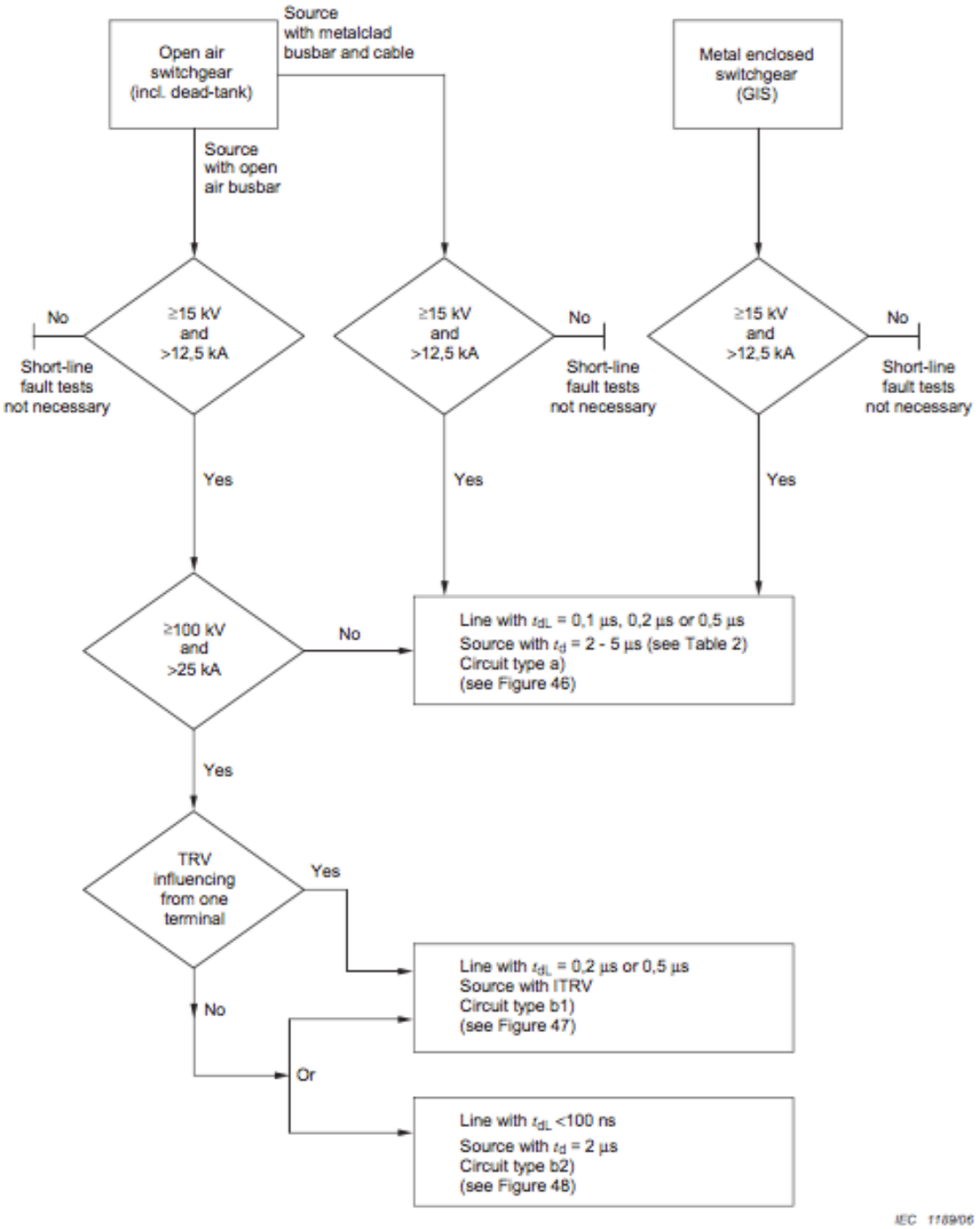

Figure 6.1: Flowchart for Test Circuit Choosing

Since the circuit-breakers are not GIS types, circuit b2) will be chosen for the study.

[1]This figure is directly cited from IEC 62271-100 and the label numbers inside of this flowchart refer to the original document.

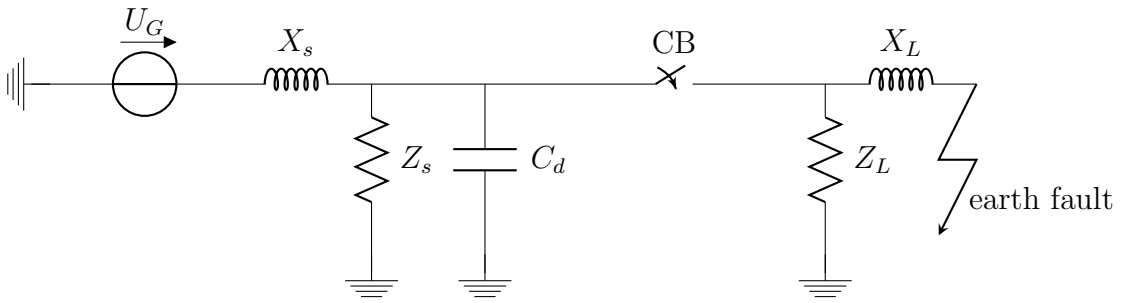

Figure 6.2: Proposed Test Circuit

Key

U_G: Supply voltage, phase to earth value
X_s: Power frequency source side reactance
Z_s: Source side TRV control components
C_d: Time delaying source capacitance
X_L: Power frequency line side reactance
Z_L: Line side TRV control components
CB: Circuit-breaker

6.2.4 Standard Study Summary

In summary, the IEC 62271-100 standard made specific requirements on the TRV on both of the source side and line side of the circuit-breaker.

Based on the guide line provided by Annex A, the TRV parameters for $31.5kA$ and $63kA$ rated short-circuit current testing at $145kV$ circuit-breakers are concluded in Table 6.1.

Table 6.1: Summary of Standard Required Circuit Parameters

	Unit	$31.5kA$	$63kA$
Power Frequency On the Source Side			
Rated voltage U_r	kV	145.00	145.00
Rated short-circuit current I_{sc}	kA	31.5	63
Rated frequency f_r	Hz	50	50
Driving supply voltage U_G	kV	83.72	83.72
Source reactance	Ω	2.66	1.33

Table 6.1 (continues)

	Unit	31.5kA	63kA
Source inductance	mH	8.46	4.23
Power Frequency On the Line Side			
Specified line setting	%	90	90
Short-line fault breaking current	kA	28.35	56.70
di/dt at the instant of current interruption	$A/\mu s$	12.60	25.19
Line side voltage U_L	kV	8.37	8.37
Line side reactance X_L	Ω	0.30	0.15
Line side inductance L_L	mH	0.94	0.47
TRV Parameters on the Line Side			
Voltage at the instant of current interruption U_0	kV	11.84	11.84
Peak factor k	$p.u.$	1.60	1.60
Peak value of the first line side TRV U_0	kV	11.84	11.84
Line side time delay t_{dL}	μs	0.20	0.20
RRRV line side du/dt	$kV/\mu s$	5.67	11.34
Specified line side impedance Z	Ω	450	450
Rise time t_L	μs	3.34	1.67
TRV Parameters in the Source Side			
Source side time delay t_d	μs	2.00	2.00
RRRV at rated terminal fault $(du/dt)_{TF}$	$kV/\mu s$	2.00	2.00
RRRV at rated short-line fault $(du/dt)_{SLF}$	$kV/\mu s$	1.8	1.5
Voltage at the instant of current interruption U_x	kV	106.55	106.55
Voltage $u_{1,test}$ at time t_1	kV	91.75	91.75
Time t_m to reach the voltage level U_m	μs	92.40	92.40
Transient peak voltage u_m	kV	214.04	214.04
Transident factor u_m/U_m	$p.u.$	4.8	4.8

Figure 6.3 gives the prospected waveform of the TRV in a short-line fault test that

indicates all key factors which have been calculated in Table 6.1.

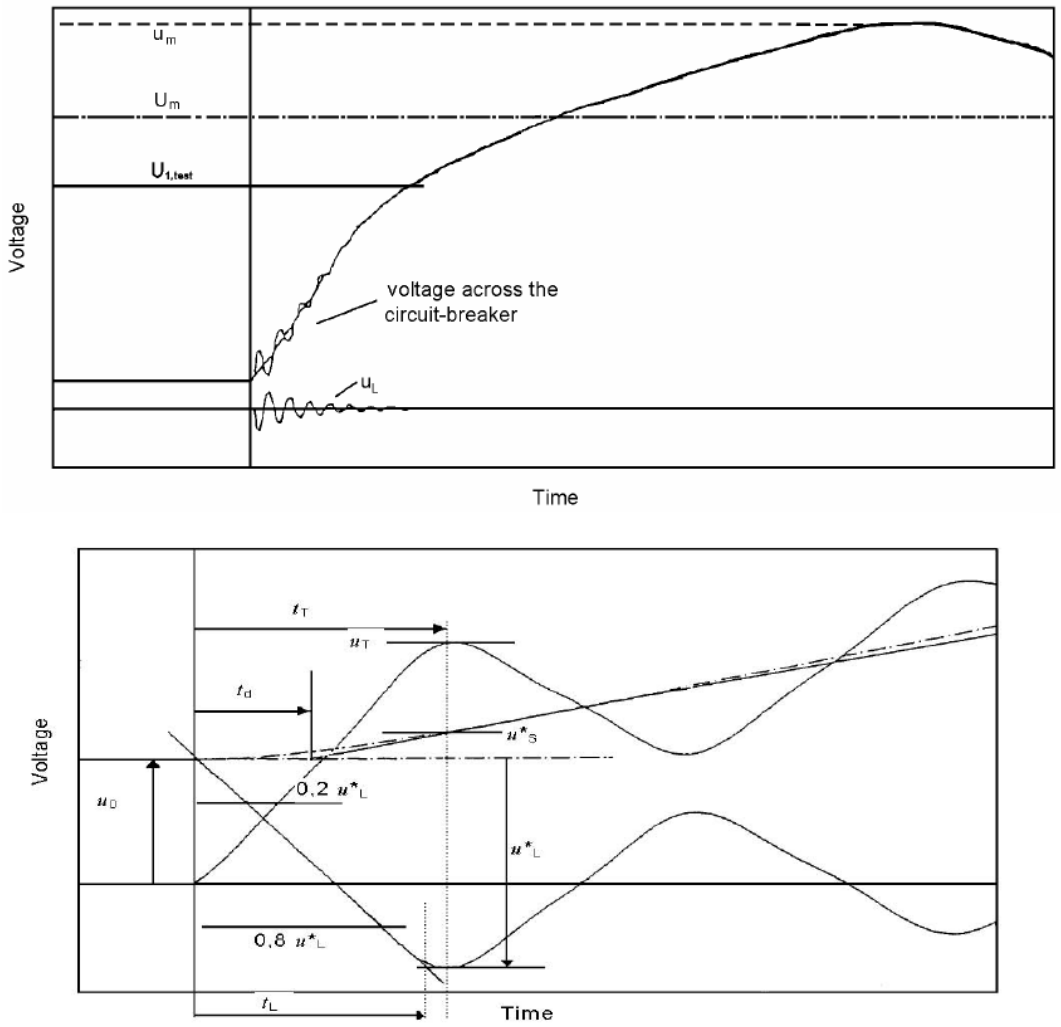

Figure 6.3: Prospected TRV Waveform

6.3 Test Circuit Arrangement

The parameters obtained in Table 6.1 gives an ideal guideline for type test. However, the source side TRV in reality is very dependent on the unpredictable magnetic-electrical field produced by the generator. Therefore, it is virtually impossible to keep every parameter within the standard specification in a computer simulation. On the other hand, the objective of this chapter is comparing switching performance between vacuum and SF_6 circuit-breakers when experiencing early

dielectric breakdowns. The TRV waveform after $1ms$ from its starting point is off concern. As a result, a new set of compromised source side TRV parameters are carried out in Table 6.2.

Table 6.2: Compromised Source Side TRV Parameters

	Unit	$31.5kA$	$63kA$
TRV Parameters on the Source Side			
Source side time delay t_d	μs	2.00	2.00
RRRV at rated short-line fault $(du/dt)_{SLF}$	$kV/\mu s$	1.8	1.8
Time t' to reach the reference voltage level u'	μs	24.00	24.00
Reference voltage level u'	kV	89	89
First reference voltage u_1	kV	89	89
Time t_1 to reach the first reference voltage level u_1	μs	44	44

Values in Table 6.2 are strictly complied with the requirements from Table 4, IEC 62271-100.

6.3.1 Source Side Parameters Calculation

As SLF tests are base on single-phase faults, the test voltage is equal to the phase to earth voltage i.e. the rated voltage divided by $\sqrt{3}$, with a first-pole-to-clear factor $k_{pp} = 1.0$. In my case, the voltage value for the power source, therefore, is:

$$U_r = 145/\sqrt{3} = 83.72kV \tag{6.1}$$

To give the right rated terminal fault short-circuit current, the source impedance is:

$X_{s1} = \dfrac{83.72kV}{31.5kA} = 2.66\Omega \Rightarrow L_{s1} = 8.46mH$ for the $31.5kA$ test circuit and

$X_{s2} = \dfrac{83.72kV}{63kA} = 1.33\Omega \Rightarrow L_{s2} = 4.23mH$ for the $63kA$ test circuit.

To give the right TRV and source side time delay, $R_{s1} = 200\Omega$ and $C_{d1} = 0.019\mu F$ have been added in parallel with the source impedance the for $31.5kA$ test circuit and $R_{s2} = 98\Omega$ and $C_{d2} = 0.038\mu F$ for the $63kA$ test circuit respectively.

6.3.2 Line Side Parameters Calculation

The standard gives no specification on what type of overhead line should be utilised in the test but required the surge impedance should be 450Ω. Therefore, a typical value of $1.2mH/km$, which stands for $0.377\Omega/km$ at $50Hz$, for the conductor inductance has been adopted as an assumption. To give the right surge impedance, the capacitance per kilometre can be calculated as:

$$Z = \sqrt{\frac{L_L}{C_L}} \Rightarrow C_L = \frac{L_L^2}{Z} = 5.93nF/km \tag{6.2}$$

For L_{90} test,

$$I_{90} = 90\% \cdot I_{sc} \Rightarrow \frac{U_r}{X_L + X_s} = 0.9 \cdot \frac{U_r}{X_s} \Rightarrow X_L = \frac{1}{9}X_s \tag{6.3}$$

Therefore, for the $31.5kA$ test circuit,

$X_{L1} = \frac{1}{9} \times 2.66 = 0.296\Omega$, which give the total length of the overhead line is $L_1 = \frac{0.296\Omega}{0.377\Omega/km} = 0.783$.

For the $63kA$ test circuit,

$X_{L2} = \frac{1}{9} \times 1.33 = 0.148\Omega$, which gives the total length of the overhead line is $L_2 = \frac{0.148\Omega}{0.377\Omega/km} = 0.392km$.

To give the right TRV and line side delay time, $R_{L1} = 2000\Omega$ has been added in parallel with the overhead line for $31.5kA$ test circuit and $R_{L2} = 2000\Omega$ for the $63kA$ test circuit as well.

6.3.3 Circuit Arrangement Summary

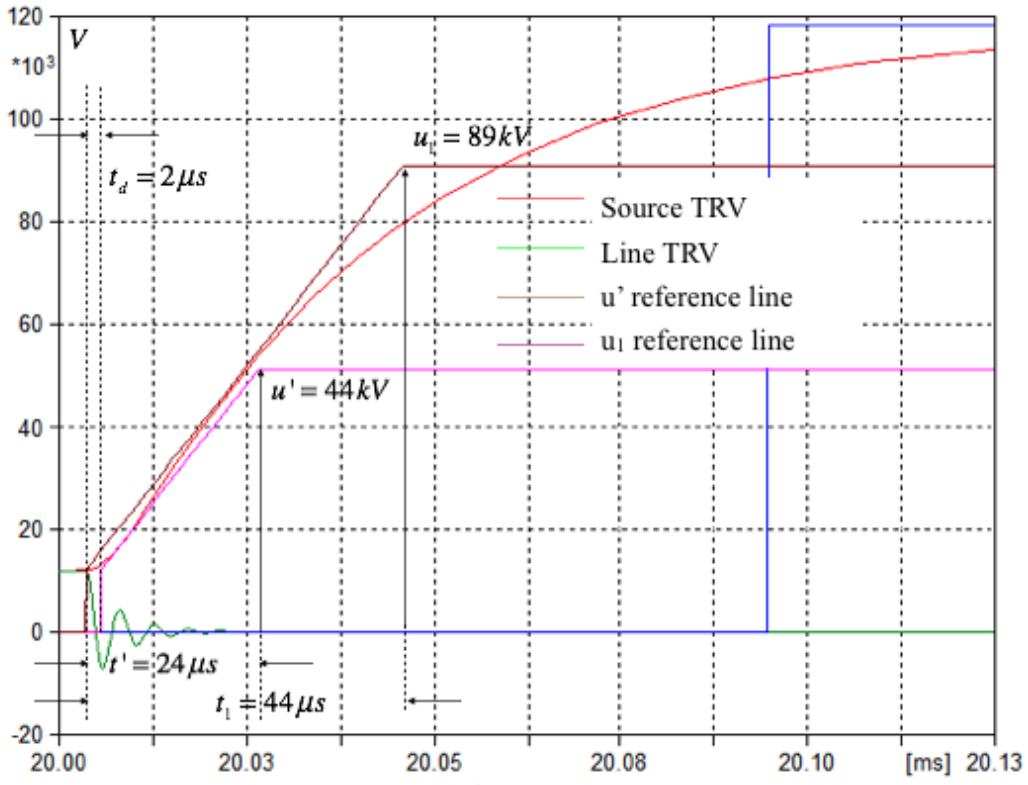

Figure 6.4: Source and Line Side TRV Curves for $31.5kA$ Test Circuit

With the aforementioned circuit parameters setup, Figure 6.4 shows the voltage curves on both source side and line side. The red curve represents the source side TRV. As can be found in the figure, after $2\mu s$ time delay, it rises up almost linearly. After $24\mu s$, it reaches the reference voltage $u' = 44kV$; after $44\mu s$ the TRV value is slightly lower than the First reference voltage $u_1 = 89kV$. This result shows that based on the circuit parameters setup, the TRV curve is perfectly restrained within the given reference envelop, which means for the first $24\mu s$ time duration, the result TRV complies the standard requirement. Figure 6.5 shows the TRV curves for $63kA$ test circuit.

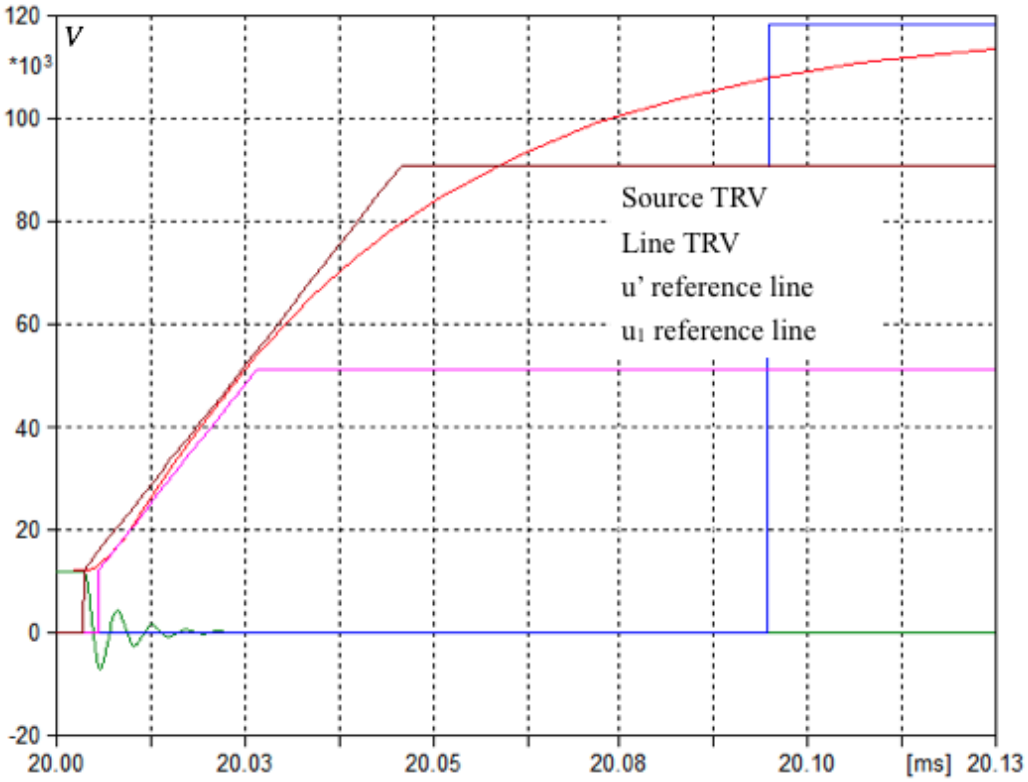

Figure 6.5: Source and Line Side TRV Curves for $63kA$ Test Circuit

In summary, Table 6.3 concludes the circuit parameters for both 31.5kA and 63kA test circuits to give the right TRV curves.

Table 6.3: Test Circuits Parameters

Test Circuit	Source voltage $U_r(kV)$	Source inductance $L_s(mH)$	Source TRV control Resistance $R_s(\Omega)$	Source time delaying control capacitance $C_s(\mu F)$
$31.5kA$	83.72	8.46	200	0.019
$63kA$	83.72	4.23	98	0.038
Test Circuit	Length of the line $L(km)$	Inductance per length $L_L(mH/km)$	Capacitance per length $C_L(nF/km)$	Line TRV control Resistance $R_L(\Omega)$
$31.5kA$	0.783	1.2	5.93	2000
$63kA$	0.392	1.2	5.93	2000

6.4 Test Objectives and Grouping

As has been discussed in the introduction section of this chapter, there are two major objectives for short-line fault switching study: (1) adopting Mayr's arc model into the SF_6 type circuit-breaker to have a deep understanding of its working performance under thermal stress; (2) comparing switching performance between SF_6 and vacuum circuit-breakers when experiencing early dielectric breakdowns. Therefore, two categories of test groups are designed to achieve this target.

6.4.1 Test Groups for SF_6 Circuit-Breaker under Thermal Stress

In the inductive and capacitive current switching tests, the power frequency current been interrupted is not very high in amplitude. Power frequency current can easily be interrupted by SF_6 and vacuum circuit-breakers without difficulties. When considering large amplitude faulty current interruption, vacuum circuit-breaker can, due to its excellent interrupting capacity, still withstand this challenge. SF_6 type circuit-breakers, however, may not be able to accomplish the same task.

As it has been covered in Section 2.2.4 and 2.3.2, Chapter 2 (page 12 and 22), whether an SF_6 circuit-breaker can interrupt a high-amplitude current is dependent upon two factors: arc time constant θ and heat energy removal factor N_0. These two factors are determined by circuit-breaker manufactures and can be obtained via a large number of field tests. Recall the classic Mayr's arc equation and its discrete format:

$$\begin{aligned} \frac{1}{R}\frac{dR}{dt} &= \frac{1}{\theta}(1 - \frac{V \cdot i}{N_0}) \\ R &= \frac{prevval(R)}{1 - \frac{\Delta t}{\theta}(1 - \frac{V \cdot i}{N_0})} \end{aligned} \tag{6.4}$$

If θ is very small and N_0 is very large, the present arc resistance value R is always higher than its previous value $prevval(R)$ in each of the simulation time-steps, which eventually leads to a continues decreasing of arc conductivity and, hence, a successful current interruption.(Please refer to the right hand slide, Figure 2.9, page 23.) Contrarily, if either θ is not small enough or N_0 is not large enough, R could be lower than $prevval(R)$ at a certain time instance. (For detailed explanation, please refer to Section 3.4, Chapter 3, page 36.) And if that happens, an avalanche of the arc resistance decreasing would follow, which eventually leads to a thermal breakdown. (left hand slide, Figure 2.9)

- **Test Group One**

Tests will be done first in $31.5kA$ test circuit. A typical value of the arc time constant θ for the modern designed SF_6 circuit-breaker is $0.3\mu s$. Therefore, circuit-breaker model with $\theta = 0.3\mu s$ will be tested with various N_0 value combinations in the first test to identify the minimum required heat removal factor which is able to interrupt the power frequency faulty current. In the second test, θ will be reduced to half of its original value ($0.15\mu s$) and the same test procedures will be repeated. Finally, θ will be increased to double of its original value ($0.6\mu s$) and the same test procedures will be repeated again. The purpose of this test arrangement is trying to figure out how the circuit-breaker performance would be influenced by the interaction of different θ and N_0 combinations.

- **Test Group Two**

Tests will then be done in $63kA$ test circuit. Likewise what has been proposed in Test Group One, tests will first be done with $\theta = 0.3\mu s$, then moves to $\theta = 0.15\mu s$. $\theta = 0.6\mu s$ will not be included in the $63kA$ test because with such arrangement, the minimum required N_0 will be unrealistically high which is far beyond the real technic boundary. The purpose of this test group is trying to figure out the influence caused by higher power frequency current to be interrupted.

6.4.2 Test Groups for Early Dielectric Breakdowns

In the first two test groups, focusing has been put to the SF_6 circuit-breaker when subjected to interrupt power frequency faulty current. But what makes short-line fault special from terminal fault is it causes very steep TRV across the contacts gap at its initial stage due to the superposition of the source side TRV and line side TRV. In the following test groups, focusing will turn to investigate the difference of switching performance between SF_6 and vacuum circuit-breakers when experiencing early dielectric breakdowns.

With the circuit parameters arrangement which has been state in Section 6.3, in a $145kV$ 90% rated short-circuit current SLF test circuit the surge impedance of the testing line is 450Ω with 1.6 overvoltage factor. As a result, the first peak value of the gap TRV is located at $24.561kV$.

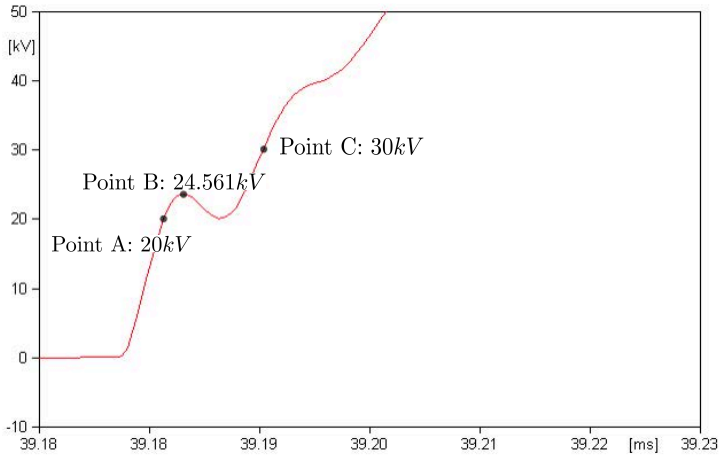

Figure 6.6: Gap TRV in an ideal Circuit-Breaker Switching

- **Test Group Three**

In the third test group, circuit-breaker with 10 times of minimum required N_0 and typical θ value will be subjected to dielectric stress at the $31.5kA$ test circuit. Manually controlled dielectric breakdowns at $20kV$ (Point A) which is a bit lower than the first peak of the contacts gap TRV, $24.561kV$ (Point B) which is exactly the first peak value of the gap TRV and $30kV$ (Point C) which is a bit lower than the second peak value will be tested.

- **Test Group Four**

In the fourth test group, the same test procedures will be repeated at $63kA$ test circuit.

- **Test Group Five**

In the last test group, vacuum circuit-breaker model will be used to replace the SF_6 circuit-breaker model. The same test procedures will be repeated at both $31.5kA$ and $63kA$ test circuits.

6.5 Test Results and Analysis

6.5.1 Test Group One

In Test Group One, the proposed SF_6 circuit-breaker model will be tested with different θ and N_0 combinations. N_0 with the minimum value which is able to interrupt the power frequency will be recorded.

(1) **Test results undertaken at** $\theta = 0.3\mu s$

Arc time constant $\theta = 0.3\mu s$ is a typical assumption. With numerous number of tests, the minimum N_0 which leads to a successful current interruption is identified as $5.285kW$.

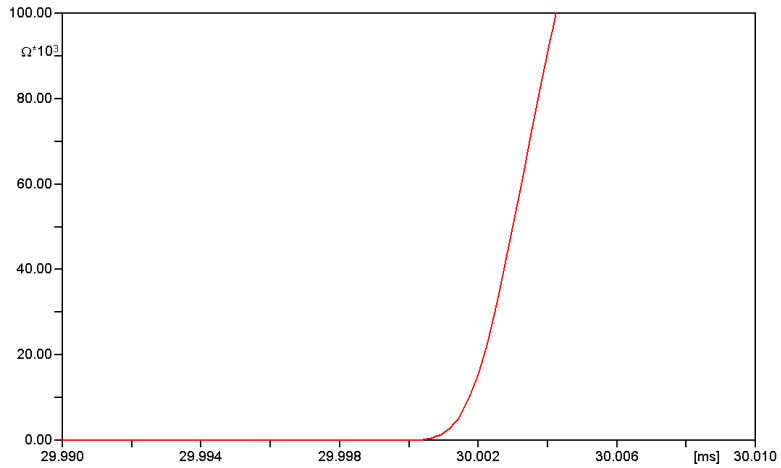

Figure 6.7: Arc Resistance Curve recorded at $\theta = 0.3\mu s$ ($31.5kA$ Circuit)

As can be found in Figure 6.7, the arc resistance continues increasing to, theoretically, infinity that converts the contact gap from conductor to dielectric.

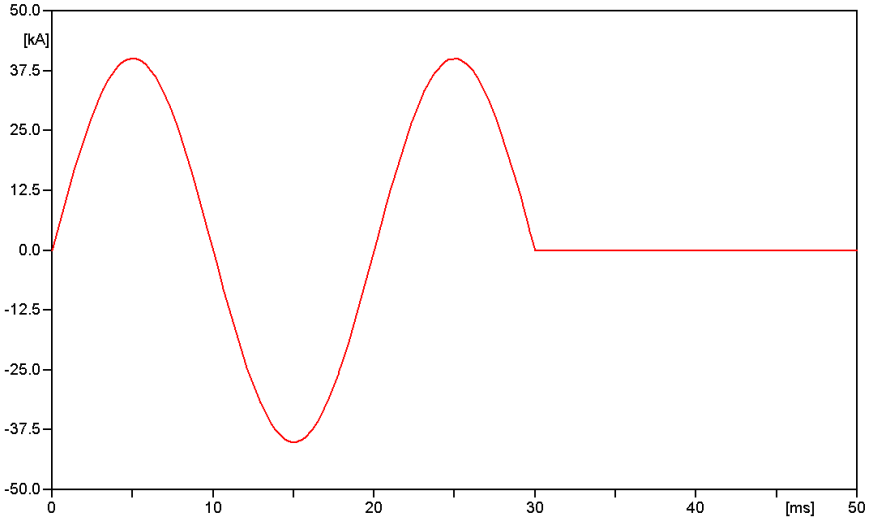

Figure 6.8a: Power Frequency Current Curve recorded at $\theta = 0.3\mu s$ ($31.5kA$ Circuit)

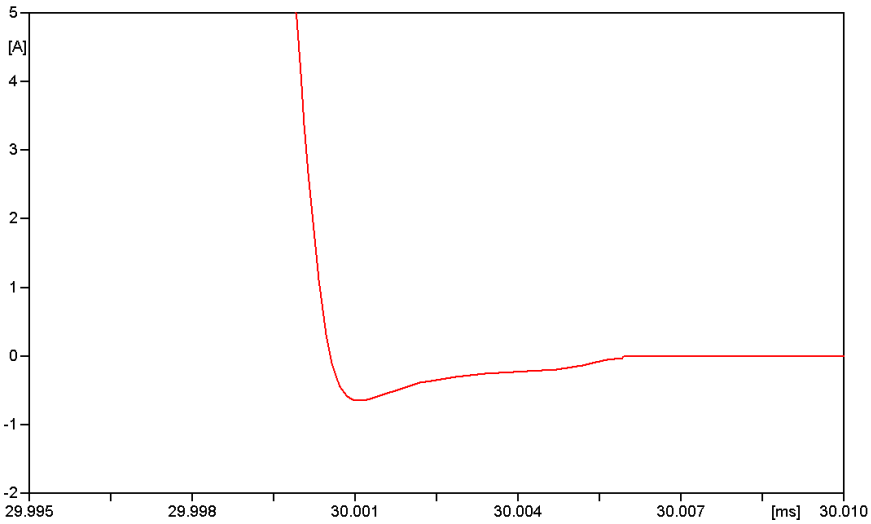

Figure 6.8b: Post-Arc Current Curve recorded at $\theta = 0.3\mu s$ ($31.5kA$ Circuit)

The upper trace in Figure 6.8a shows the overall current curve during the interrupting process while the lower trace in Figure 6.8b shows the zoom in details. The power frequency faulty current keeps decreasing from the positive polarity steeply. It does not cease when it reaches zero but continues its path to the negative polarity. This phenomenon is called post-arc. In a successful interruption, the post-arc current converges to zero.

If N_0 is not large enough, say lower than $5.285kW$ at this circumstance, the arc resistance will decrease after it reaches its peak value. Consequently, the post-arc current will not converge to zero and, hence, leads to a thermal breakdown.

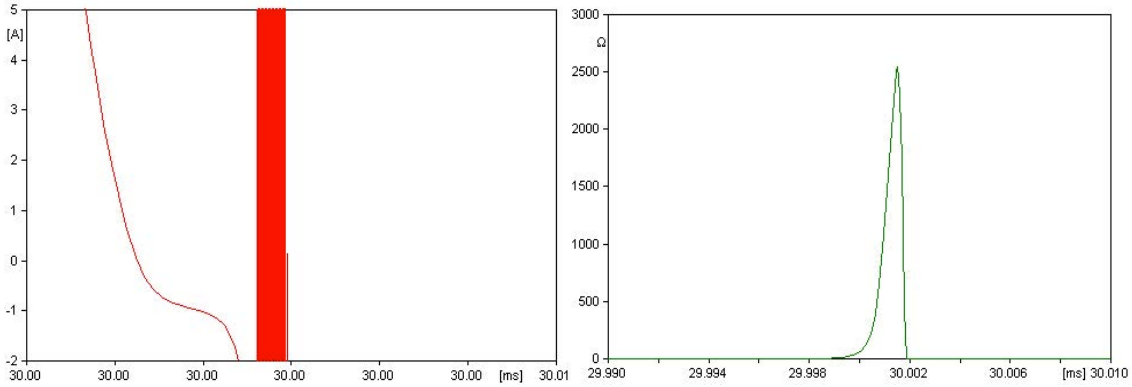

Figure 6.9: Test Result recored at $\theta = 0.3\mu s$ with $N_0 = 4kW$ ($31.5kA$ Circuit) Thermal Re-ignition

The red curve on the left slide of Figure 6.9 shows the current at post-arc zone while the green curve on the right slide shows the arc resistance. The arc resistance increases from 20Ω to approximately $2k\Omega$ sharply at first, then drops back to 20Ω with an even steeper slope. The post-arc current does not converge. Instead, it oscillates at very high frequency. This is a typical example for an unsuccessful interruption.

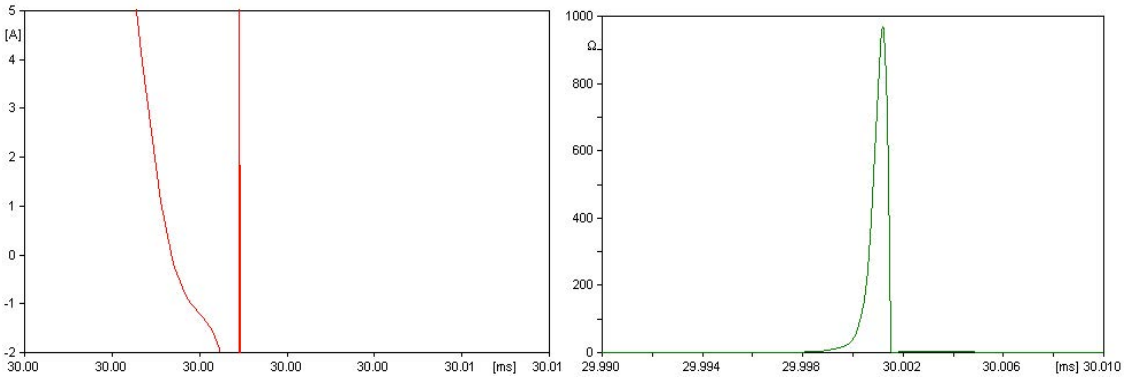

Figure 6.10: Test Result recored at $\theta = 0.3\mu s$ with $N_0 = 3kW$ ($31.5kA$ Circuit)

If reducing N_0 to a further level, say $3kW$, the arc resistance peak will be lower than the previous case.

(2) **Test results obtained at** $\theta = 0.15\mu s$

If the manufacture can produce a new type of SF_6 circuit-breaker with significantly reduced arc time constant, say $\theta = 0.15\mu s$, the minimum required heat removal factor can be reduced even further.

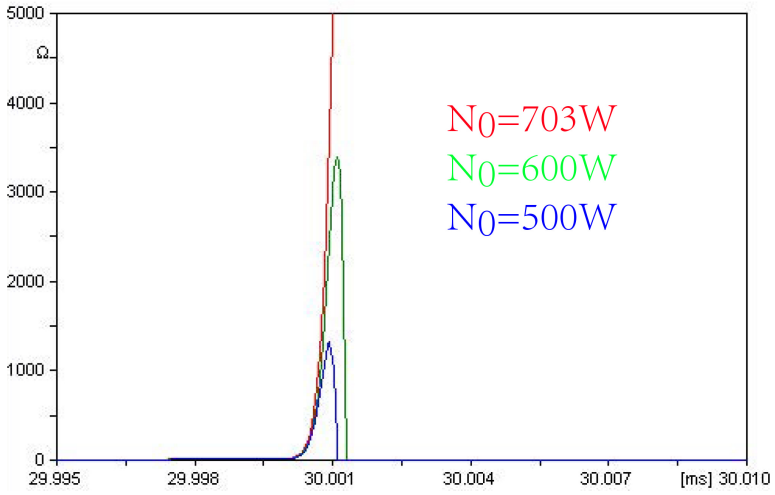

Figure 6.11: Test Result recored at $\theta = 0.15\mu s$ ($31.5kA$ Circuit)

With half reduced θ circuit-breaker model, the minimum required N_0 for a successful interruption has been reduced to $703W$.

(3) **Test results obtained at** $\theta = 60\mu s$

For comparison purpose, in the third test of Test Group One, the arc time constant θ has been unrealistically increased to double of its original value, i.e. $0.6\mu s$.

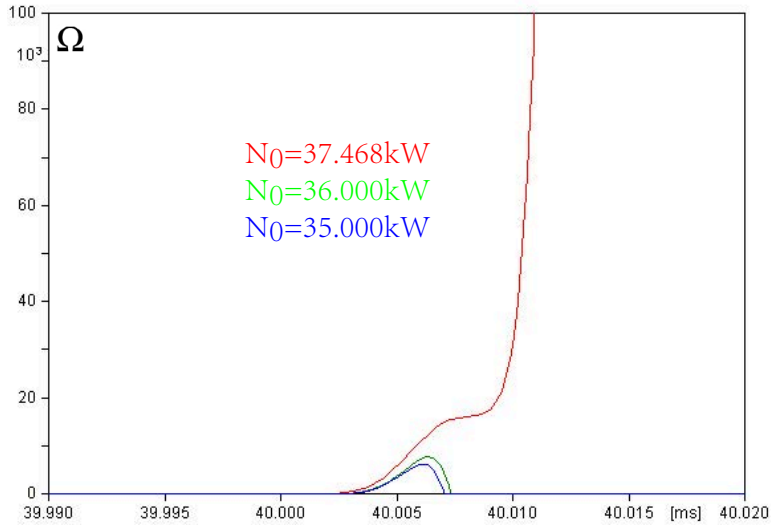

Figure 6.12: Test Result recored at $\theta = 0.6\mu s$ ($31.5kA$ Circuit)

The above test result shows that for doubled θ setup, the circuit-breaker would require seven times higher N_0 to make a successful interruption. In a short summary, test results obtained from Test Group One tell that the heat removal factor is very sensitive to even insignificant changes in arc time constant.

6.5.2 Test Group Two and Summary

(1) **Test results obtained at** $\theta = 0.3\mu s$

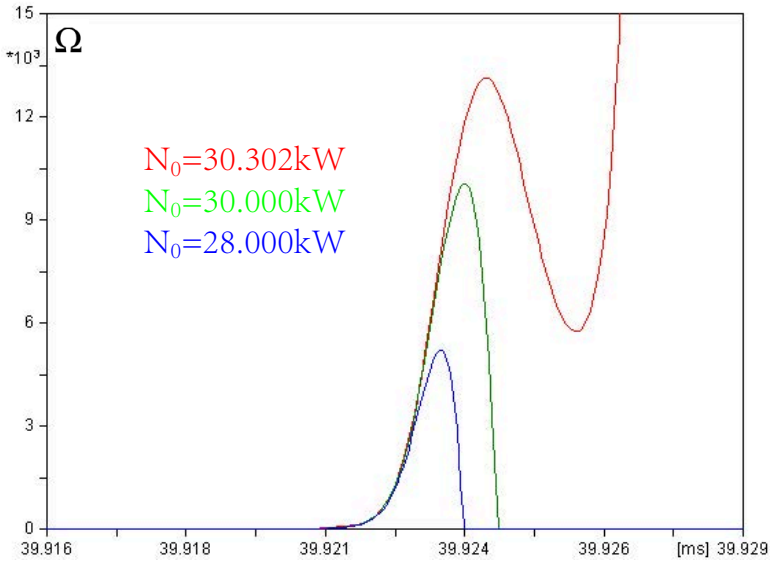

Figure 6.13: Test Result recored at $\theta = 0.3\mu s$ ($63A$ Circuit)

Test results demonstrated in Figure 6.13 indicate that when subject the circuit-breaker model into higher faulty current duty, with the same arc time constant, the minimum required heat removal factor has been increased approximately six times. It also can be found that in the successful interruption scenario (red curve with $N_0 = 30.302kW$) the arc resistance does not keep increasing as what has been found in the previous cases. Instead, an obvious decreasing can be observed after it reaches it first peak value. That is caused by the first reflection of the line side TRV wave which makes the gap TRV decreased in the meanwhile. This

is an unique phenomenon which can only be observed in short-line fault switching of short line segments.

(2) **Test results obtained at** $\theta = 0.15\mu s$

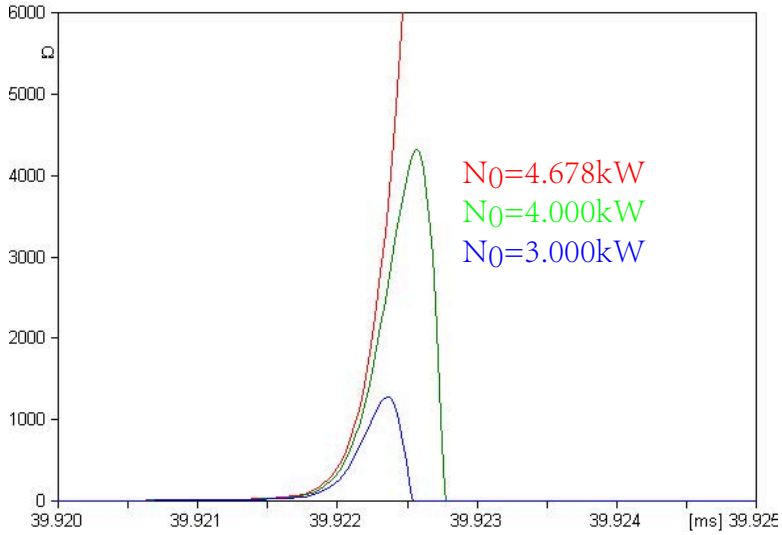

Figure 6.14: Test Result recored at $\theta = 0.15\mu s$ ($63A$ Circuit)

The minimum required N_0 measured in the second test of Test Group Two is $4.678kW$ as indicated in the red curve, Figure 6.14.

To sum up the test results obtained from Test Group One and Two, they have been concluded in Table 6.4.

Table 6.4: Simulation Results for Test Group One and Two

Arc time constant $\theta(\mu s)$	Minimum Required $N_0(kW)$	
	$31.5kA$ test circuit	$63kA$ test circuit
0.15	0.703	4.678
0.3	5.285	30.302
0.6	37.468	

Arc time constant and heat removal factor are key factor to evaluate the current interrupting capability of an SF_6 circuit-breaker. Breakers with lower arc time constant have higher current interrupting capability; breakers with higher heat

removal factor have higher interrupting capability as well. The di/dt of the current to be interrupted also plays an important role in this process. Higher faulty current level would require either lower arc time constant or much higher heat removal factor to deliver a successful interruption.

6.5.3 Test Group Three

In Test Group Three, tests will be done in $31.5kA$ test circuit. The heat removal factor N_0 will be increased to 10 times as the minimum required value which has been acquired from Test Group One at the typical arc time constant ($\theta = 0.3\mu s$).

(1) **Test results obtained at the first dielectric breakdown Point A**

What makes short-line fault special is due to its repid transient recovery voltage rising rate. The gap voltage can reach its first peak within $\leq 4\mu s$ after current zero. The first test of Test Group Three has been carried out at a manually created dielectric breakdown voltage level, $20kV$ (Point A) at this circumstance, which is a little bit lower than the first peak value $24.561kV$.

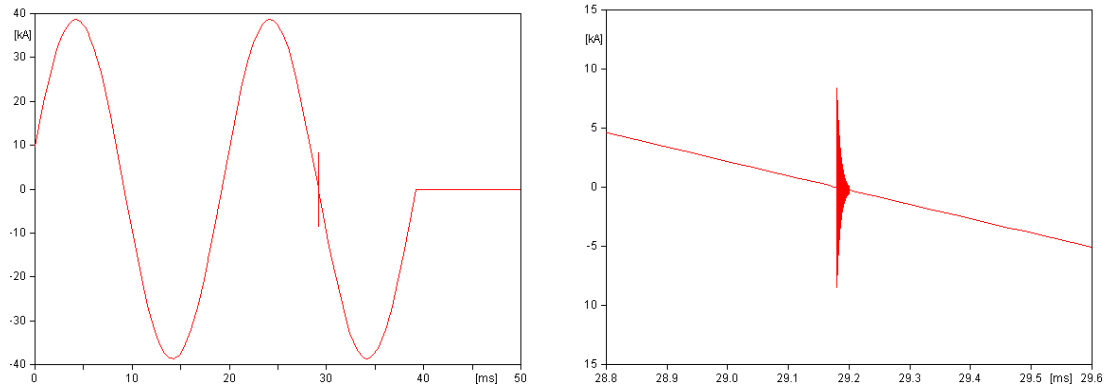

Figure 6.15: Current Curve recorded at Dielectric Breakdown Point A ($31.5kA$ Circuit)

The trace on the left hand side of Figure 6.15 shows the overall current curve during the current interrupting process. The right hand side trace gives zoom in details at the moment of first interrupting attempt. The test result indicates that if the first dielectric breakdown takes place at $20kV$ circuit-breaker with $\theta = 0.3\mu s$ and

$N_0 = 52.850kW$ is unable to interrupt the high-frequency re-ignition current. The maximum amplitude of the re-ignition current is measured as $8.329kA$.

(2) **Test results obtained at the first dielectric breakdown Point B**

Now if we increase the first dielectric breakdown voltage level from point A to B, $24.561kV$, which is exactly the first TRV peak value of the contacts gap, we can have the following test result:

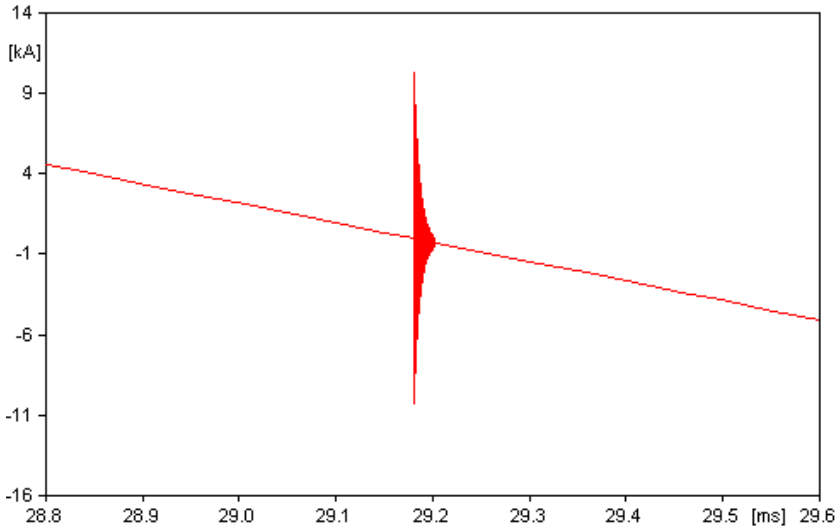

Figure 6.16: Current Curve recorded at Dielectric Breakdown Point B ($31.5kA$ Circuit)

Obviously, circuit-breaker model with the same θ and N_0 setups is unable to interrupt the high-frequency re-ignition current caused by early dielectric breakdown which takes place at $24.561kA$. The maximum amplitude of the re-ignition current is measured as $10.105kA$.

(3) **Test results obtained at the first dielectric breakdown Point C**

If we keep increasing the dielectric breakdown voltage level to a higher place, say $30kV$, we can have the following result:

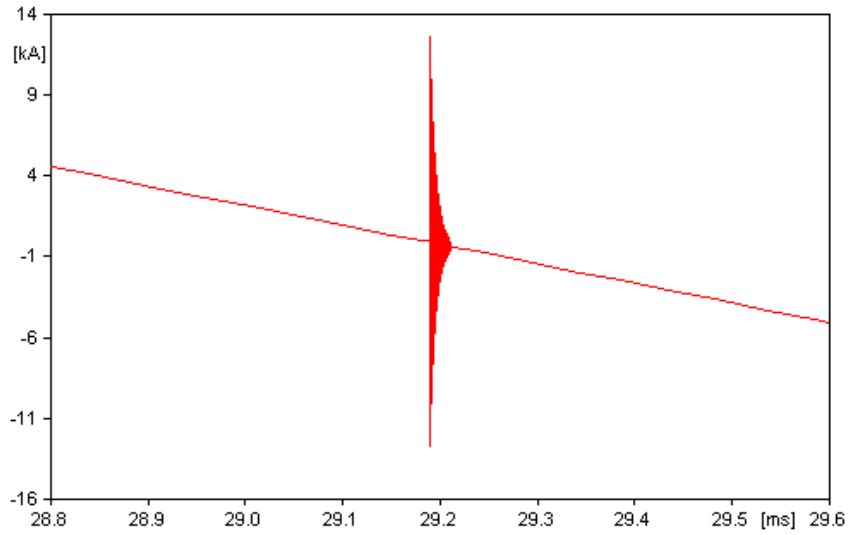

Figure 6.17: Current Curve recorded at Dielectric Breakdown Point C (31.5kA Circuit)

Again, circuit-breaker model with the same parameter setups is unable to interrupt the high-frequency re-ignition current. The maximum amplitude of the re-ignition current is measured as 12.543kA.

6.5.4 Test Group Four

Repeat the same tests at dielectric breakdown points A, B and C at the 63kA test circuit, results are demonstrated in Figure 6.18, 6.19 and 6.20.

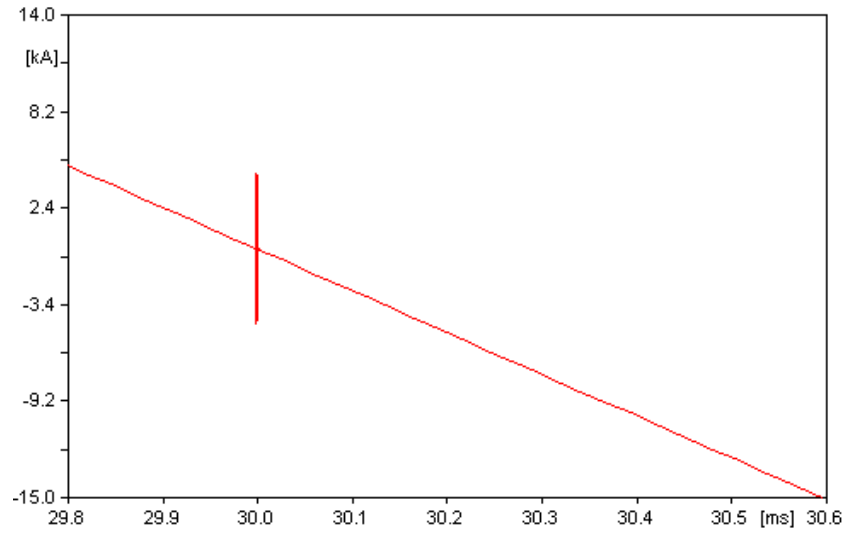

Figure 6.18: Current Curve recorded at Dielectric Breakdown Point A (63kA Circuit)

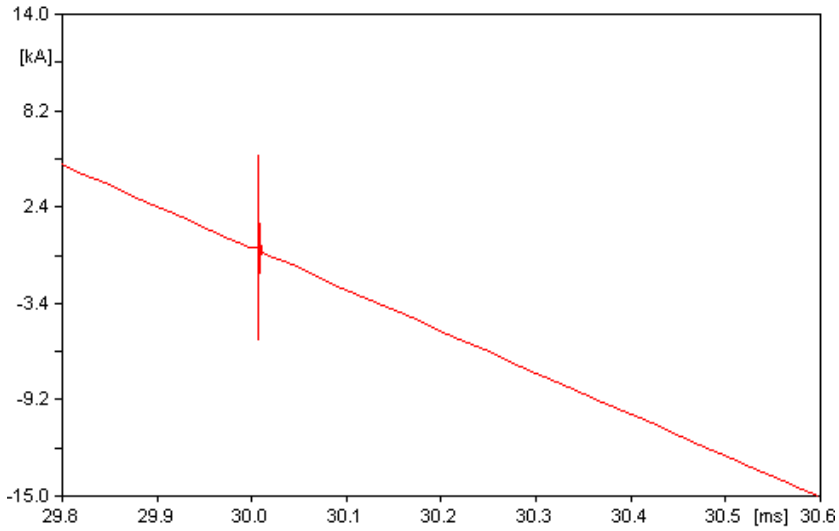

Figure 6.19: Current Curve recorded at Dielectric Breakdown Point B ($63kA$ Circuit)

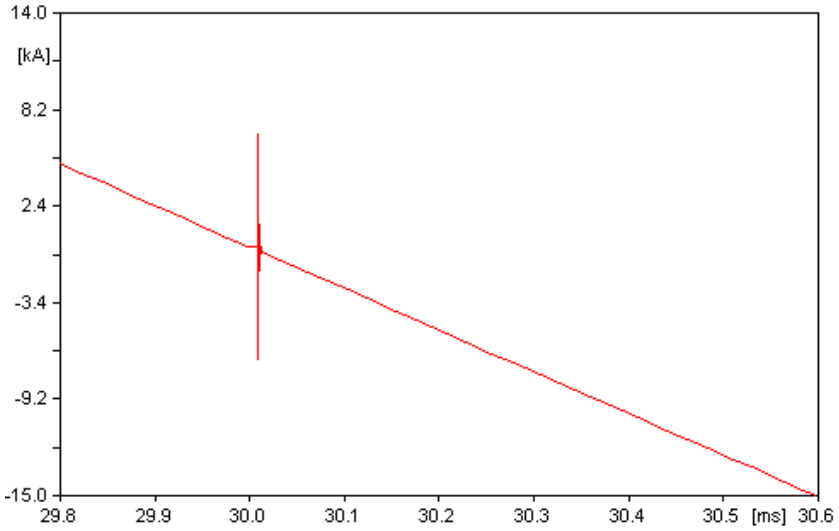

Figure 6.20: Current Curve recorded at Dielectric Breakdown Point C ($63kA$ Circuit)

The maximum re-ignition current amplitudes which have been measured in the above three tests are $4.39kA$, $5.016kA$ and $6.083kA$ for dielectric breakdown happens at Point A, B and C respectively.

The results obtained from Test Group Four proves that at $63kA$ test circuit, the circuit-breaker model with $\theta = 0.3\mu s$ and $N_0 = 303.020kW$ parameter setups is unable to interrupt the high-frequency current in either of the dielectric breakdown points. By comparing the results with those obtained from TG3, it also can be

found that at the same dielectric breakdown point, higher initial re-ignition current amplitude is observed in lower faulty level test circuit.

6.5.5 Test Group Five and Data Analysis

In the first three test group, the SF_6 circuit-breaker model which has been utilised is based on Mayr's arc model.Its high-frequency current quenching capability (Q) is determined by the dynamic arc current and arc resistance values. In the last test group, vacuum circuit-breaker model with a fixed $Q = 1000A/\mu s$ and $D = 51kV/ms$ (Table 4.3 in Chapter 4) will be tested in $31.5kA$ and $63kA$ test circuits.

(1) **Test results for VCB ($31.5kA$ Circuit)**

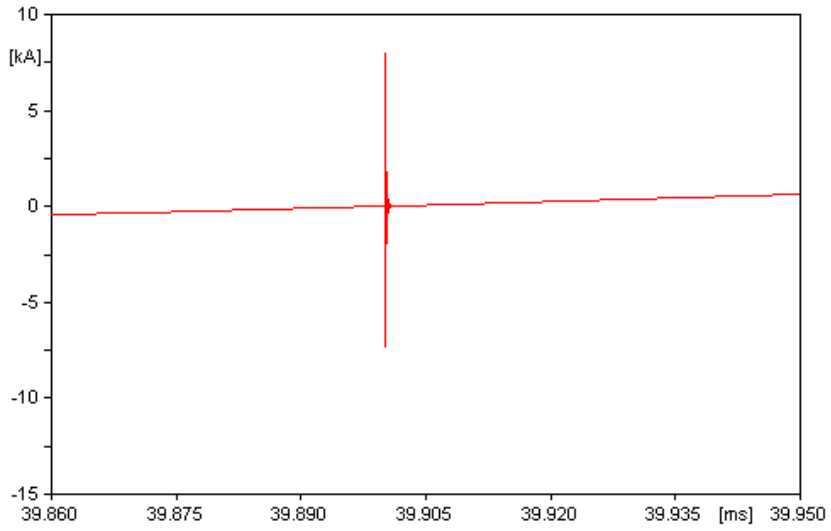

Figure 6.21: Current Curve recorded at Dielectric Breakdown Point A ($31.5kA$ Circuit)

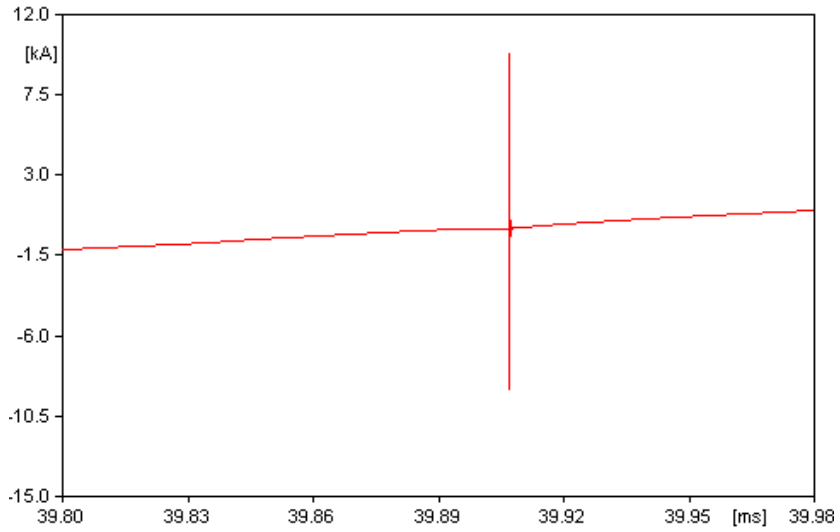

Figure 6.22: Current Curve recorded at Dielectric Breakdown Point B (31.5kA Circuit)

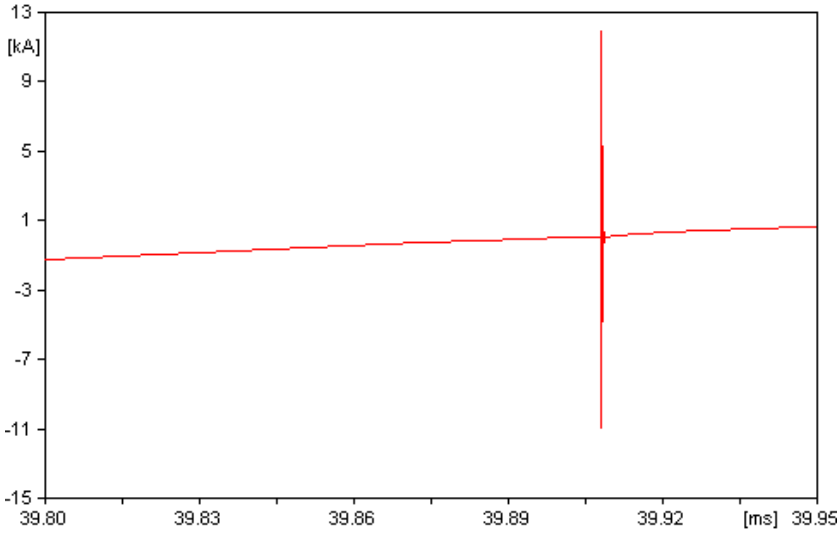

Figure 6.23: Current Curve recorded at Dielectric Breakdown Point C (31.5kA Circuit)

The maximum re-ignition current amplitudes which have been measured in the above three tests are 7.722kA, 9.788kA and 11.951kA for dielectric breakdown happens at Point A, B and C respectively.

(2) **Test results for VCB (63kA Circuit)**

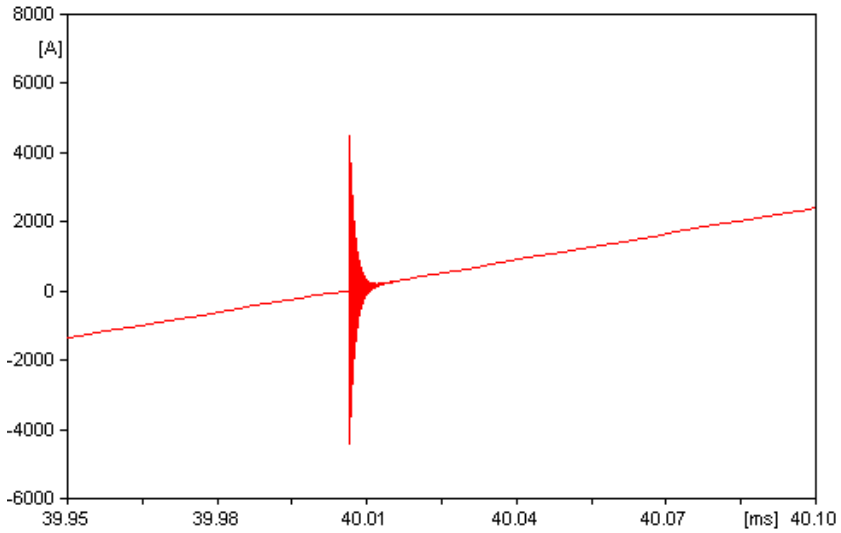

Figure 6.24: Current Curve recorded at Dielectric Breakdown Point A (63kA Circuit)

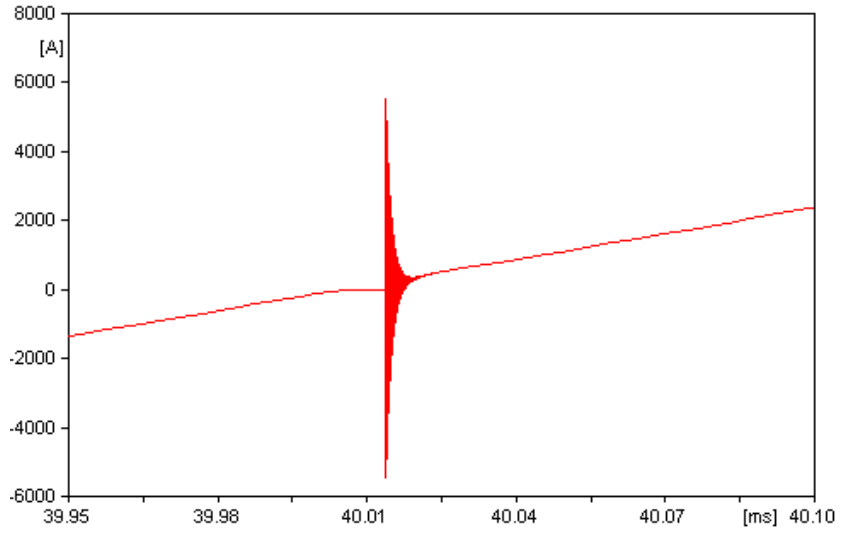

Figure 6.25: Current Curve recorded at Dielectric Breakdown Point B (63kA Circuit)

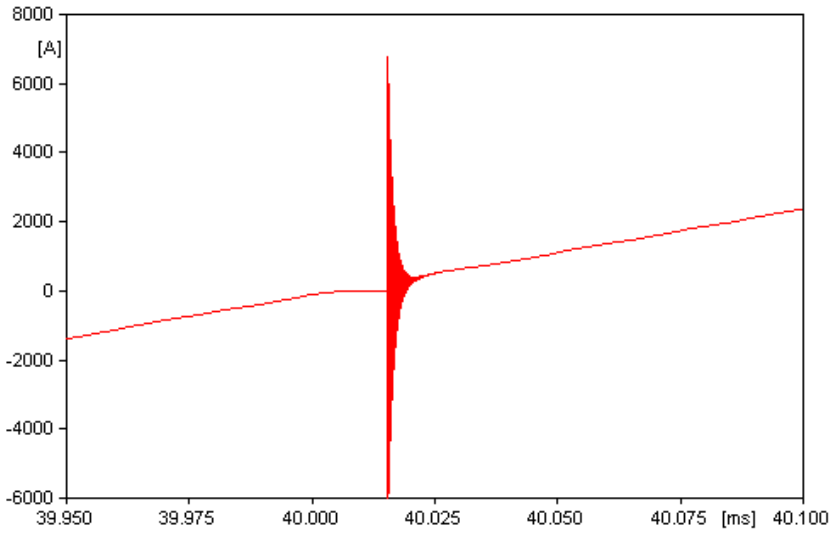

Figure 6.26: Current Curve recorded at Dielectric Breakdown Point C ($63kA$ Circuit)

The maximum re-ignition current amplitudes which have been measured in the above three tests are $4.433kA$, $5.526kA$ and $6.749kA$ for dielectric breakdown happens at Point A, B and C respectively.

There is no surprise that even the vacuum circuit-breaker is unable to interrupt the high-frequency re-ignition current, since the oscillation frequency which has been observed in the re-ignition proceeds exceeds hundreds of MHz. Test results obtained from Test Group Three, Four and Five prove that when an early dielectric breakdown takes place at a short-line fault, neither SF_6 nor vacuum circuit-breaker is able to interrupt the re-ignition current within one power frequency current loop. With an additional power frequency loop, neither of them would experience a dielectric breakdown again because the dielectric strength between the gap has already been built up.

Table 6.5 concludes Test Group Three to Five.

Table 6.5: Simulation Results for Test Group Three to Five

$31.5kA$ Test Circuit			
Circuit-breaker type	Maximum re-ignition current amplitude $I_{max}(kA)$		
	Pont A	Point B	Point C
SF_6	8.329	10.105	12.543
VCB	7.722	9.788	11.951
$63kA$ Test Circuit			
Circuit-breaker type	Maximum re-ignition current amplitude $I_{max}(kA)$		
	Point A	Point B	Point C
SF_6	4.39	5.016	6.083
VCB	4.433	5.526	6.749

By analysing the test results recorded in Table 6.5, it can be found that when early dielectric breakdown takes place, the maximum re-ignition current amplitude is irrelevant to the circuit-breaker type. Higher dielectric breakdown voltage level leads to higher re-ignition current amplitude. On the other hand, circuit with higher fault current level brings lower re-ignition current amplitude due to the total volume of the electrical charge transferring between source and load sides capacitors is different. Detailed explanation for this phenomenon has been concluded in Appendix I.

6.6 Chapter Conclusions

In this chapter, circuit-breaker models have been simulated under short-line fault scenarios. Based on the requirements specified by IEC 62271-100, two test circuit rated at $31.5kA$ and $63kA$ short circuit capacity have been developed in order to provide the correct $^{di}/_{dt}$ before current zero and $^{du}/_{dt}$ after current zero in the contact gap. To sum up the test results from this chapter, conclusions can be made as following:

1. SF_6 technology might have difficulties of handling power frequency short-line fault current due to its interrupting capacity is limited by two factors: the arc time constant θ and heat removal factor N_0. If θ is not small enough or N_0 is not large enough, potential thermal breakdown is expected. On the other hand, vacuum

technology has no problems regarding to the power frequency short-line fault current due to its superior thermal stress withstand capacity. Vacuum technology wins the first round.

2. Dielectric breakdown caused by extremely high $^{du}/_{dt}$ in short-line fault scenarios makes both vacuum and SF_6 technologies vulnerable. Although vacuum should have much better control of high-frequency re-ignition current theoretically, the actual re-ignition current we discussed in short-line fault is much more severe than its capability. As a result, vacuum and SF_6 technologies break even in the second round.

Chapter 7

Conclusion

7.1 Summary of Thesis Achievements

This PhD project started from one basic question: whether vacuum technology can be applied to $145kV$ electrical power system networks as a potential substitution to SF_6 technology which has been utilised for decades of practice, due to environment and economic concerns. Network data has been collected based on public information provided by two British electricity distribution companies. The study outlined the possible threats and challenges, which might cause problems for the proposed replacement, mainly in three areas: (1) small inductive current switching, (2) capacitive load current switching and (3) short-line fault switching.

SF_6 and vacuum technologies then have been studied from the physics in their arcs to the current and arc interruption mechanisms. At the end of the study, it is cleared that there are two key factors that determine a circuit-breaker's current interrupting capacity: (1) the maximum current slope $^{di}/_{dt}$ at current zero that can be interrupted; and (2) the rate of rise of the dielectric strength $^{du}/_{dt}$ that can be re-established after current zero. The former one stands for the thermal stress withstand capability of a breaker and the later one stands for the dielectric stress withstand capability. For vacuum technology, it is way superior in both of the two

judgement criteria. However, this superiority may not always bring advantages in different switching scenarios.

Three circuit-breaker programming models have been developed based on statistic data provided by breaker manufactures: (1) a maximum $^{di}/_{dt}$ fixed model which has been utilised for small inductive current switching tests and capacitive load current de-energising tests; (2) a dynamic $^{di}/_{dt}$ model adopting from Mayr's classic arc model which has been utilised for short-line fault tests; and (3) a current making model for capacitive load current energising tests.

In small inductive current switching study, multiple simulation tests have been grouped into four test groups. The outcome of the study proves that when undertaking small inductive current interrupting duties, vacuum technology has much higher possibility to interrupt it within one power frequency current loop while SF_6 normally would require another current loop to finish the same job. For that point of view, vacuum is superior than SF_6 . However, in case SF_6 interrupts the current within one current loop (depends on the time instant of contact separating which is totally random), it has better overvoltage control performance and generates less heat energy.

In capacitive load current switching study, eight test groups have been carried out. The result data obtained from the first four groups proves that when considering capacitive de-energising duties, the possibility of re-strike in a vacuum circuit-breaker is extremely low: only exists in theoretic. The possibility in an SF_6 circuit-breaker is, on the other hand, slightly higher. Nevertheless, if re-strike takes place, no significant difference can be observed from these two technologies. The result data collected from the later four groups proves that when considering energising duties, vacuum has better control of heat energy. But, the difference between them is insignificant.

And finally in short-line fault switching study, six test groups have been carried out. The outcome of the study proves that when considering short-line fault switching

duties, vacuum technology has decisively better control of the post-arc due to its superior maximum $^{di}/_{dt}$ interrupting capacity. The possibility of dielectric breakdown in a vacuum circuit-breaker is much lower than in an SF_6 circuit-breaker. However, in case it takes place (again, depends on the time instant of contact separating), the differences of switching performance which have been found between these two are negligible.

In a general conclusion, vacuum technology shows its superiority in most of the switching duties although in some rare cases, SF_6 technology still stands a chance to break it even. But if we take the environment and economic factors into consideration, vacuum is definitely worth investigating in the future market.

7.2 Future Work

So far, the comparisons of switching performance between SF_6 and vacuum circuit-breakers have been done via computer simulations. However, gaps between theoretical calculation and practical experiment must exist. There are many parameters in the simulation work, including circuit-breaker models and test circuit models, which are based on statistic records and assumptions. To make the new vacuum circuit-breaker products practically profitable in the market, field tests with proper arrangements are to be expected in the future works.

Appendix A

Amplitude of Re-Ignition Current in SLF Dielectric Breakdowns

A.1 Basic Idea

When dielectric break down happens in a SLF switching test, the initial amplitude of the re-ignition current is determined by the electrical charge transferring between the source side capacitance and the load side capacitance. Here we define C_{a1} and C_{b1} as the source side capacitance for the $31.5kA$ and $63kA$ circuits respectively; C_{a2} and C_{b2} as the load side capacitance; V_{a1} and V_{b1} as the voltage across the source side capacitance at the moment prior to the dielectric break down; V_{a2} and V_{b2} as the voltage across the load side capacitance at the moment prior to the dielectric break down; Q_{a1} and Q_{b1} as the electrical charge stored in C_{a1} and C_{b1} at the same moment as we are taking about; Q_{a2} and Q_{b2} as the electrical charge stored in C_{a2} and C_{b2}; V_a' and V_b' as the new voltage level after dielectric break down happens; ΔQ_a and ΔQ_b as the transferring electrical charge. In short, the footnotes "a" and "b" indicate the $31.5kA$ and $63kA$ circuit; "1" and "2" indicate the source side capacitance and load side capacitance; the headnote "prime" indicates the new status after dielectric break down happens.

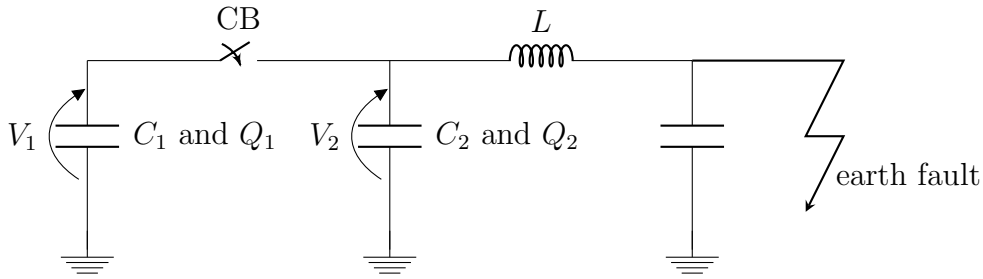

Figure A.1: Basic Circuit

If we disregard the difference between these two circuits and just focus on the electrical charge transferring, at the moment prior to the dielectric break down, we have:

$$Q_1 = C_1 V_1 \tag{A.1}$$

$$Q_2 = C_2 V_2 \tag{A.2}$$

And after the dielectric break down:

$$Q_1' = Q_1 - \Delta Q = C_1 V' \tag{A.3}$$

$$Q_2' = Q_2 + \Delta Q = C_2 V' \tag{A.4}$$

By solving equation A.3 and A.4 together, we have:

$$Q_1 + Q_2 = (C_1 + C_2) V' \tag{A.5}$$

Then the new voltage level across the capacitance on both sides of the circuit breaker can be achieved:

$$V' = \frac{Q_1 + Q_2}{C_1 + C_2} \tag{A.6}$$

By substituting equation A.1 and A.2 to equation A.6,

$$V' = \frac{C_1 V_1 + C_2 V_2}{C_1 + C_2} \tag{A.7}$$

Finally, the transferring electrical charge can be obtained by either of the following ways:

$$\Delta Q = Q_1 - C_1 \frac{C_1 V_1 + C_2 V_2}{C_1 + C_2} \tag{A.8}$$

or

$$\Delta Q = C_2 \frac{C_1 V_1 + C_2 V_2}{C_1 + C_2} - Q_2 \tag{A.9}$$

In summary, we can determine the amplitude of the re-ignition current by measuring the voltage level across the capacitors prior to the dielectric break down and comparing the transferring electrical charge based on the above calculations.

A.2 Actual Calculations

A.2.1 For $31.5kA$ Circuit

In order to create the appropriate time delay and RRRV of the TRV on the source side, the capacitance is selected as $C_{a1} = 0.019\mu F$; for the same reason, the capacitance per length of the transmission line is $5.93 \times 10^{-6}\mu F/m$ with a total length of $783.14m$, which gives $C_{a2} = 2.322 \times 10^{-3}\mu F$. (For simplification reason, the distributed line model has been modified as a single π junction model)

As indicated in Figure A.2, at the moment prior to the dielectric break down, the voltage across the source side capacitance $V_{a1} = -13.788kV$ (red number) and the voltage across the load side capacitor $V_{a2} = 1.2752kV$ (green number).

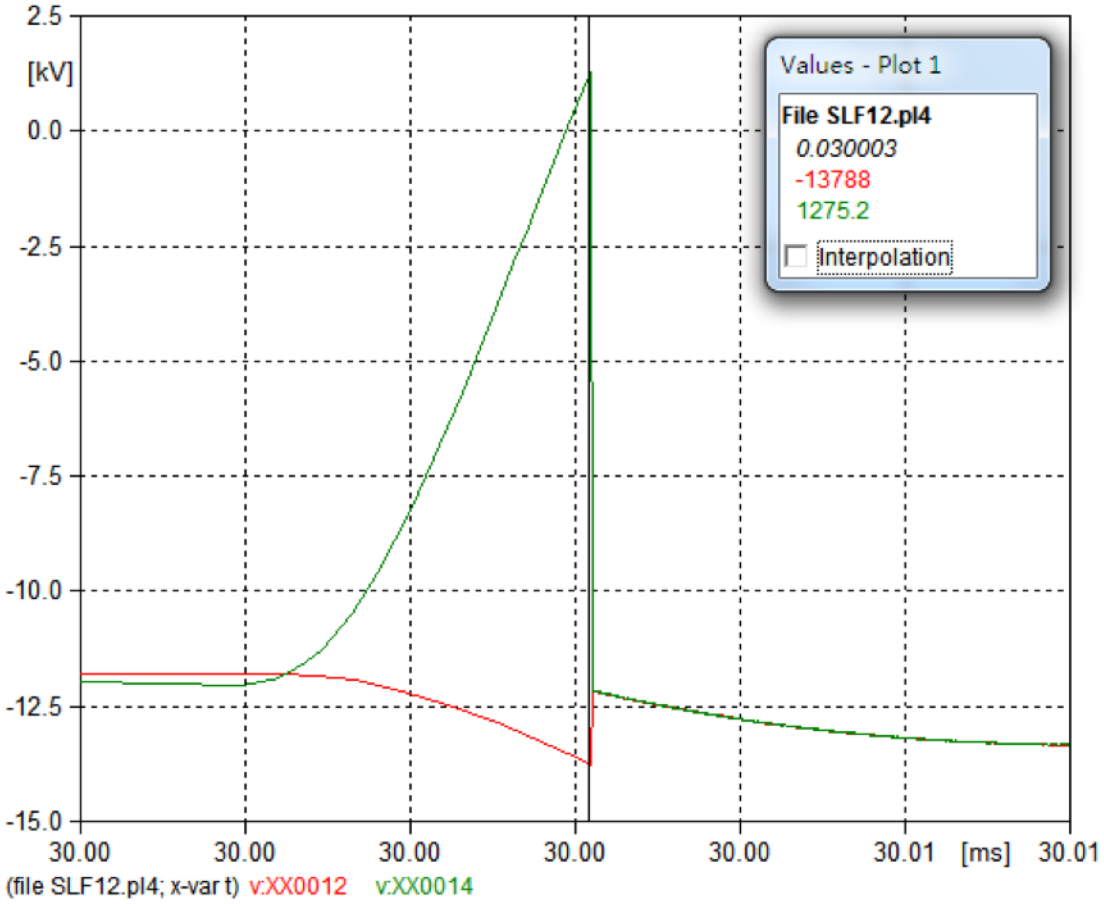

Figure A.2: Voltage Values at the Moment prior to the Dielectric Breakdown

By substituting these four values to equation A.7, we have:

$$\begin{aligned} V_a' &= \frac{C_{a1}V_{a1} + C_{a2}V_{a2}}{C_{a1} + C_{a2}} \\ &= \frac{-19 \times 13.788 \times 10^{-6} + 2.322 \times 1.2752 \times 10^{-6}}{(19 + 2.322) \times 10^{-9}} \\ &= -12.147kV \end{aligned} \tag{A.10}$$

The result matches the new voltage value as indicated in Figure A.3 perfectly.

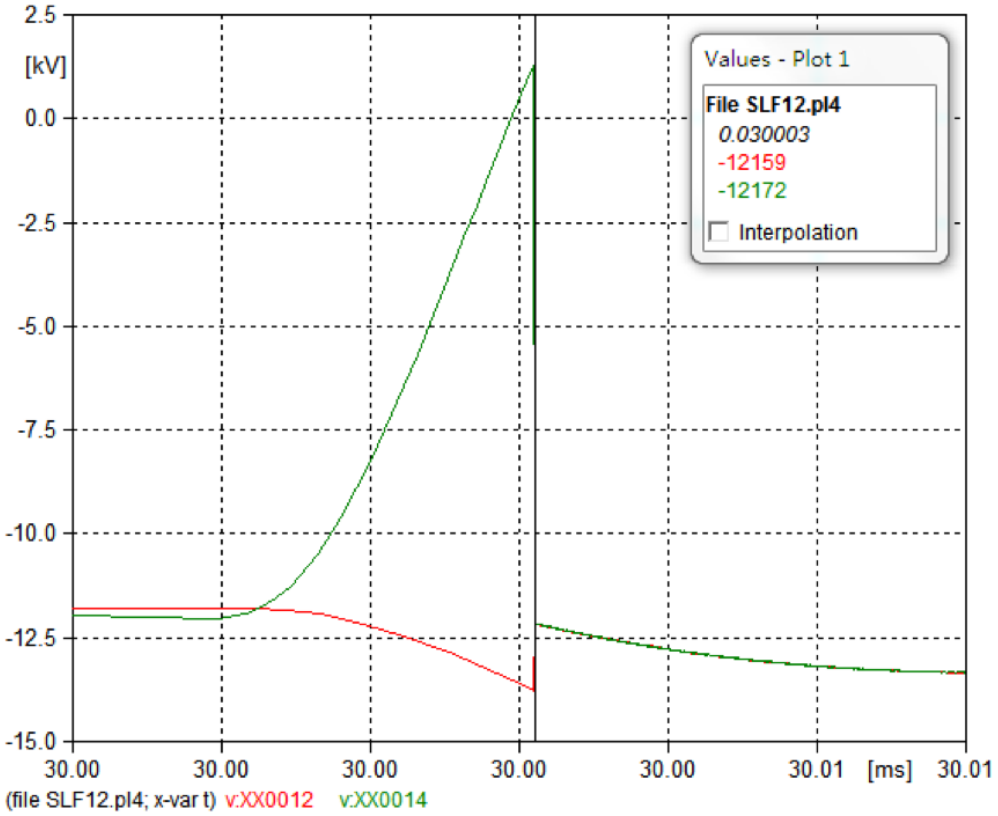

Figure A.3: New Voltage Value at the very first Moment after Dielectric Breakdown

By substituting the result obtained from equation A.10 to equation A.8, the transferring electrical charge is:

$$\begin{aligned} \Delta Q_a &= Q_{a1} - C_{a1} V_a' \\ &= -3.12 \times 10^{-5} C \end{aligned} \tag{A.11}$$

A.2.2 For $63kA$ Circuit

In this case, the source side capacitance has been doubled to create the appropriate time delay and RRRV of the TRV, which gives us $C_{b1} = 0.038\mu F$; with the same capacitance value per length but half of the original total length to give the appropriate short line current, the load side capacitance becomes $C_{b2} = 1.162 \times 10^{-3}\mu F$.

Similarly, as indicated in Figure A.3, voltage levels across the capacitance on each side of the circuit are $V_{b1} = -12.446kV$ and $V_{b2} = 2.5671kV$.

By using the same method, the new voltage level can be obtained as:

$$\begin{aligned} V_b' &= \frac{C_{b1}V_{b1} + C_{b2}V_{b2}}{C_{b1} + C_{b2}} \\ &= -12.00kV \end{aligned} \tag{A.12}$$

Therefore, the transferring of the electrical charge is:

$$\Delta Q_b = Q_{b1} - C_{b1}V_b' = -1.69 \times 10^{-5}C \tag{A.13}$$

which is nearly half of the pervious result we got in equation A.11. And the amplitude of the current in each case shows the same rate.

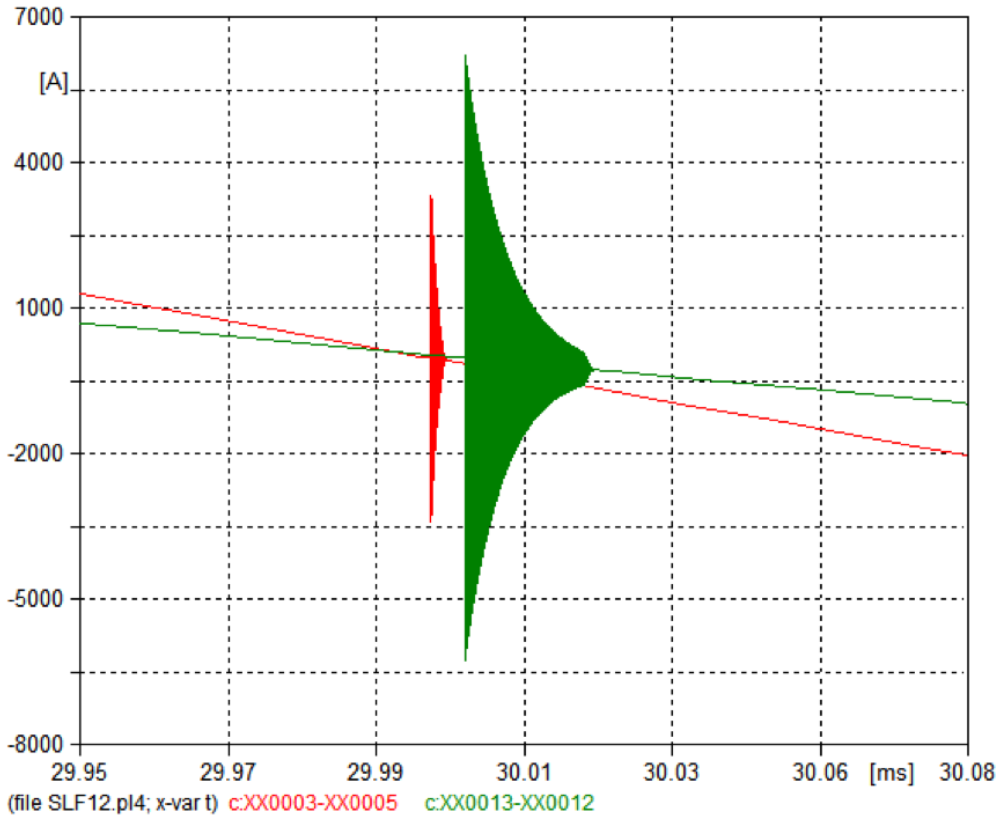

Figure A.4: Current Comparison between $31.5kA$ (Green) and $63kA$ (Red) Circuits

A.3 Conclusion

Because in SLF, at the same voltage level but with different fault current level, the TRV on the source side would not change much but the TRV on the load side rises up much quicker in a higher fault current level circuit. As a result, with the same dielectric break down level, V_{a1} is higher than V_{b1} but V_{a2} is lower than V_{b2} (See Figure A.5)

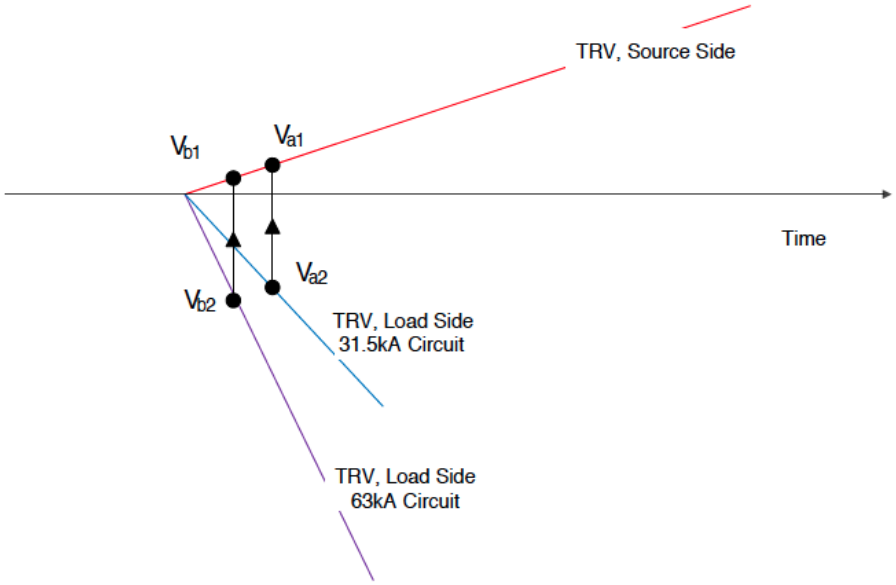

Figure A.5: Simplified TRV Diagram

On the other hand, the $63kA$ circuit has larger source side capacitance while lower load capacitance ($C_{a1} < C_{b1}$, $C_{a2} > C_{b2}$).

Together, they make the resulting transferring of the electrical charge in a circuit with lower fault current level has a higher amplitude of re-ignition current than in a higher fault current circuit.

Bibliography

[1] R. Garzon, *High Voltage Circuit Breakers: Design and Applications*. Electrical and Computer Engineering, Taylor & Francis, 2002.

[2] D. F. Amer, C. A. Fawdrey, F. C. H., S. M. Gonek, M. N. John, and M. W. Kennedy, *Power Circuit Breaker Theory and Design*. Energy Engineering, Institution of Engineering and Technology, 1982.

[3] P. T. D. Siemens AG, Energy Sector, "High-voltage circuit breakers," Nonnendammallee 104, 13629 Berlin, Germany, 2012.

[4] O. Mayr, "Beiträge zur theorie des statischen und des dynamischen lichtbogens," *Archiv für Elektrotechnik*, vol. 37, no. 12, pp. 588–608, 1943.

[5] A. Greenwood, *Vacuum Switchgear*. IET Power Engineering Series, Institution of Electrical Engineers, 1994.

[6] S. Berneryd, "Interruption of small inductive currents simple phsical model and interaction with network," *Abstracts, Symposium on Circuit Breaker Interruption and Power Testing*, May 1976.

[7] W. G. 13.02, *Interruption of Small Inductive Currents*. cigré, 1995.

[8] J. D. Cobine and G. A. Farrall, "Experimental study of arc stability. i," *Journal of Applied Physics*, vol. 31, pp. 2296–2304, dec 1960.

[9] J. M. Lafferty, J. D. Cobine, and G. E. Company., *Vacuum arcs : theory and application / J. M. Lafferty, editor (corporate Research and Development*

Center, General Electric Company) ; contributors, James D. Cobine ... [et al.]. Wiley New York, 1980.

[10] M. T. Glinkowski, M. R. Gutierrez, and D. Braun, "Voltage escalation and reignition behavior of vacuum generator circuit breakers during load shedding," *Power Delivery, IEEE Transactions on*, vol. 12, no. 1, pp. 219–226, Jan 1997.

[11] S. M. Wong, L. A. Snider, and E. W. C. Lo, "Overvoltages and reignition behavior of vacuum circuit breaker," *Advances in Power System Control, Operation and Management, 2003. ASDCOM 2003. Sixth International Conference on (Conf. Publ. No. 497)*, vol. 2, pp. 653–658, 11-14 Nov. 2003.

[12] IEC, "High-voltage switchgear and controlgear part110: Inductive load switching," *IEC 62271-110*, 2009.

[13] IEC, "High-voltage switchgear and controlgear part100: Alternating-current circuit-breakers," *IEC 62271-100*, 2008.